[American Journal of Science, Vol. 306, May, 2006, P. 303–366, DOI 10.2475/05.2006.02]

# GEOLOGY, AGE AND ORIGIN OF SUPRACRUSTAL ROCKS AT AKILIA, WEST GREENLAND

CRAIG E. MANNING*, STEPHEN J. MOJZSIS**, and T. MARK HARRISON*,***,‡

**ABSTRACT. New mapping, geochronology, and geochemistry of the supracrustal enclave and associated orthogneisses at Akilia, West Greenland, support a ≥3825 ± 6 Ma age for the sequence and a chemical sedimentary origin for the controversial Fe-rich quartz-pyroxene gneisses. Lithologies of the enclave comprise laterally continuous, mappable units of mafic amphibolite, ultramafic rocks, and two Fe-rich quartz-pyroxene units. A minor anthophyllite-garnet rock with chemical characteristics suggesting a sedimentary protolith was identified. The earliest foliation parallels lithologic contacts. This foliation was isoclinally folded about a steep hinge surface, and then tightly refolded about a steep NS hinge plane. The latest folding produced limbs exhibiting contrasting strains. The full deformation history is shared by all lithologies of the enclave. Two previously unidentified orthogneiss sheets preserve deformed magmatic crosscutting relations with amphibolite and ultramafic units in the low-strain limb.**

**The supracrustal anthophyllite-garnet rock experienced zircon growth at ~3600 and ~2700 Ma, in common with amphibolites. These ages are interpreted to reflect metamorphism at granulite and amphibolite facies, respectively, consistent with independent regional evidence. The crosscutting orthogneiss sheets preserve a complex history of zircon growth, but only earliest cores indicate Th/U exchange equilibrium with the bulk rock at magmatic conditions. Weighted-mean $^{207}Pb/^{206}Pb$ ages of cores of 3730 ± 7 Ma and 3825 ± 6 Ma date the crystallization ages of the sheets, indicating that the Akilia supracrustal rocks were deposited ≥3819 Ma.**

**Quartz-pyroxene rocks on Akilia have been interpreted as metamorphosed chemical sediments that may preserve carbon-isotope evidence for life at the time of their formation. An alternative proposal is an origin by metasomatic alteration. Our results show that these rocks experienced a history of deformation and zircon growth identical to other lithologies of the supracrustal body. Metamorphic zircons give a minimum $^{207}Pb/^{206}Pb$ age of 3589 ± 13 Ma regardless of origin. The two models of formation of quartz-pyroxene rocks were evaluated using field, petrologic and geochemical tests. The distribution of the units, the absence of field or petrologic indicators of metasomatism, and geochemistry (oxygen and nontraditional stable isotopes, immobile elements and REE) together support a sedimentary, but not a metasomatic, origin. Because their protolith was sedimentary, the quartz-pyroxene rocks are a primary part of the supracrustal sequence and have the same minimum age. Despite strong deformation and polymetamorphism, the Akilia supracrustal enclave contains information about terrestrial surficial processes at ≥3819 Ma.**

## INTRODUCTION

Supracrustal rocks from the Nuuk region of West Greenland preserve a record of surficial processes in the early Archean (≥3600 Ma). The identification of $^{13}C$-depleted graphite in lithologies interepreted to be metasedimentary rocks in this area (Schidlowski, 1988; Mojzsis and others, 1996; Rosing, 1999; Ueno and others, 2002), suggests that supracrustal lithologies may also contain evidence for the earliest life on Earth. However, the geologic relations are complex: the supracrustal rocks occur as discontinuous, multiply deformed and metamorphosed enclaves in complex orthog-

*Department of Earth and Space Sciences, University of California, Los Angeles, California 90095 U.S.A.; manning@ess.ucla.edu

**Department of Geological Sciences, University of Colorado, Boulder, Colorado 80309 U.S.A.

***Research School of Earth Sciences, Australian National University, Canberra ACT 0200 Australia

‡Institute of Geophysics and Planetary Physics, University of California, Los Angeles, California 90095 U.S.A.

neisses. Most studies have therefore focused on the best preserved and largest body of supracrustal rocks, the Isua Supracrustal Belt. Yet many other exposures throughout the region could give additional insights, provided that their geologic history can be established with confidence.

An example is the supracrustal enclave exposed on Akilia (fig. 1), in which it has been proposed that >3800 Ma metamorphosed sedimentary rocks preserve isotopic indicators of an early biosphere (Mojzsis and others, 1996; Nutman and others, 1997). If correct, Akilia lithologies and others in the region provide important information about surface processes, ocean chemistry, and biology in the early Archean. However, the rocks are strongly deformed and metamorphosed, which complicates their use as windows into Earth's early history. Indeed, the proposals have generated significant debate, arising in part from three contested geologic and geochronologic relationships, including (1) whether the host rocks have sedimentary protoliths (Mojzsis and others, 1996; Nutman and others, 1997; Mojzsis and Harrison, 2000, 2002b; Friend and others, 2002a; Palin, 2002; Fedo and Whitehouse, 2002a, 2002b, 2000c; Bolhar and others, 2004; Dauphas and others, 2004); (2) the nature of crosscutting relations that nominally constrain the age of the enclave (Nutman and others, 1996, 1997, 1999, 2000; Myers and Crowley, 2000; Whitehouse and Fedo, 2003); and (3) the origin of zircons used in the dating (Nutman and others, 1996, 1997, 1999, 2002; Whitehouse and others, 1999; McGregor, 2000; Mojzsis and Harrison, 2002a; Krogh and others, 2002; Kamber and others, 2003). Such substantial disagreement about the geology, geochronology, and geochemistry of Akilia raises concerns about the possibility of augmenting the limited record of early Archean surficial environments.

A significant problem with the work on Akilia is that the geologic foundation for the interpretations rests chiefly on low-precision sketch maps of the exposure (Nutman and others, 1997; Myers and Crowley, 2000; Fedo and Whitehouse, 2002a; Friend and others, 2002a; Nutman and others, 2002). We carried out detailed geologic mapping of the supracrustal enclave, and used the results to guide new studies of zircon geochronology and whole-rock chemistry. The combined data sets lead to an internally consistent model for the origin and evolution of the Akilia supracrustal rocks. In addition to the disparate geologic, geochronologic and geochemical interpretations that are addressed in this study, the origin of graphite which may preserve a biological signal in Akilia supracrustal rocks is also under discussion (Mojzsis and others, 1996; van Zuilen and others, 2002; Lepland and others, 2002, 2005) and is the subject of separate communications (for example, Mojzsis and others, 2005).

## GEOLOGIC BACKGROUND

The geology of early Archean rocks in the area of figure 1 is complex because of multiple intense metamorphic and deformation events that affected the terranes before, during and after their juxtaposition in the late Archean (Friend and others, 1987, 1988; McGregor and others, 1991; Nutman and others, 2004a; Friend and Nutman, 2005a, 2005b). Along the coast southwest of Nuuk, exposures on and near Akilia are part of the Færingehavn Terrane (Friend and others, 1988; Friend and Nutman, 2005b), in which supracrustal lithologies occur as enclaves in early Archean, polygenetic orthogneisses. In early descriptions, the two units were respectively termed the "Akilia Association" (McGregor and Mason, 1977) and the "Amîtsoq Gneisses" (McGregor, 1973). The units are now referred to collectively as the "Itsaq Gneiss Complex" (Nutman and others, 1996), chiefly because the gneisses appear to be a heterogeneous package of metaigneous lithologies of varying age and parentage (McGregor, 2000; Friend and Nutman, 2005b). The orthogneisses range widely in texture and include quartzofeldspathic tonalitic, granodioritic and granitic compositions. Ion-microprobe zircon geochronology of the orthogneisses reveals a complicated early history of zircon growth based on age zones that range from ~3850 Ma to

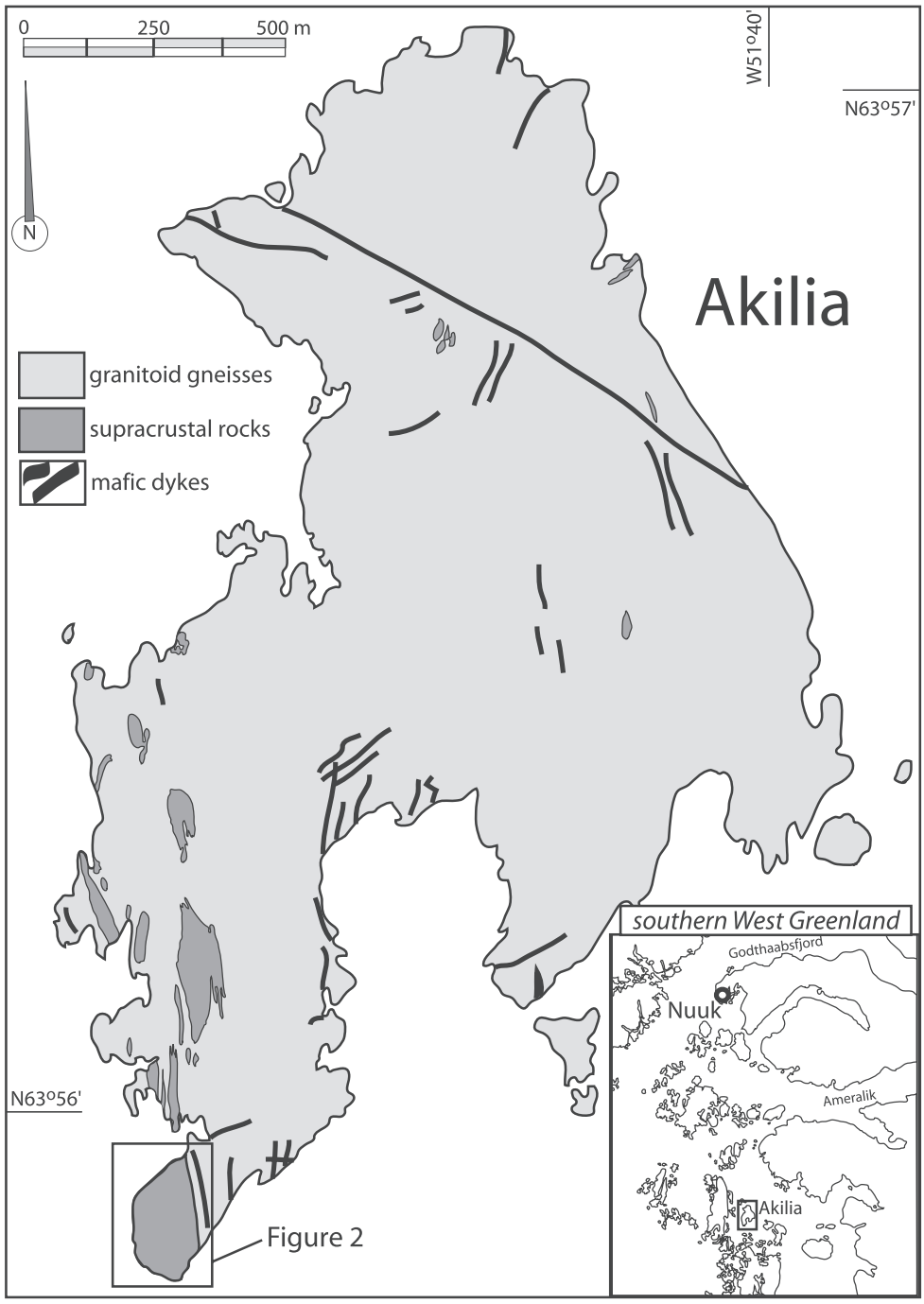


Fig. 1. Map showing location of Akilia and area of investigation.

~3500 Ma, as well as ~2700 Ma (Baadsgaard and others, 1984; Kinny, 1986; Nutman and others, 1996, 2000, 2002; Friend and Nutman, 2005a). Nutman and co-workers interpret the oldest zircon core-ages as emplacement ages, and propose that their wide range indicates that orthogneisses were emplaced during multiple intrusive events spanning ~300 Ma. This has been challenged by Kamber and Moorbath (1998, 2000), Whitehouse and others (1999, 2001) and Whitehouse and Kamber (2005), who suggest a shorter-lived magmatic event at ~3650 ± 50 Ma. In their model, zircon cores older than ~3650 Ma represent inherited grains.

The supracrustal rocks in the region comprise meter to km-sized bodies of chiefly mafic, ultramafic, and Fe-rich rocks of possible metasedimentary protolith (Bridgwater and others, 1976; McGregor and Mason, 1977; McLennan and others, 1984; Nutman and others, 1996, 1997). They occur as enclaves in Amîtsoq Gneisses, but contact relations are typically ambiguous. Early Archean metamorphism of the supracrustal lithologies was associated with strong deformation (Chadwick and Nutman, 1979) and local partial melting (Friend and Nutman, 2005a) at amphibolite to granulite facies (Griffin and others, 1980). Because supracrustal lithologies typically lack igneous or detrital zircons (Nutman and others, 2000; Friend and Nutman, 2005a), a minimum age for Akilia-type supracrustal rocks is established by metamorphic zircons of 3670 to 3500 Ma (Schiøtte and Compston, 1990; Friend and Nutman, 2005a). Older minimum ages have been suggested based on the interpretation that Amîtsoq Gneiss bodies crosscut the supracrustal enclaves at numerous localities, including Akilia (Nutman and others, 1997, 2000, 2002), though the Akilia relation has been challenged (Myers and Crowley, 2000). As with the Amîtsoq Gneisses in general, the crosscutting bodies give ages as old as ~3850 Ma if the oldest zircon cores are taken to be intrusive ages, but no older than ~3650 Ma if it is assumed that the cores are inherited.

The Itsaq Gneiss Complex was crosscut by younger mafic dikes ("Ameralik dikes," McGregor, 1973). Field evidence (Coe and others, 1976; Chadwick, 1981; Chadwick and Coe, 1983) and geochronologic studies (White and others, 2000; Nutman and others, 2004b) indicate multiple intrusive episodes over some 250 million years (~3510 – 3260 Ma). The Ameralik dikes are important time markers that permit distinction between the older rocks of the Itsaq Gneiss Complex, which they crosscut, and younger paragneissic and amphibolitic supracrustals and granodioritic orthogneisses, in which the dikes are absent (McGregor, 1973). These younger lithologies do not occur on Akilia, but exposures elsewhere in the region provide additional insight into the Middle and Late Archean history of the area.

Younger paragneisses ("Malene Supracrustals," McGregor, 1973) contain detrital zircons ranging from ~3230 to 2830 Ma (Schiøtte and others, 1988; Friend and others, 1996; Nutman and others, 2004a). Granodioritic Ikkatoq Gneisses (formerly "Nuuk Gneisses," McGregor and others, 1991) intruded the supracrustals at ~2800 Ma (Friend and others, 1996; Crowley, 2002; Nutman and others, 2004a). The younger gneisses were tectonically interleaved with the Itsaq Gneiss Complex during a major event at ~2700 Ma, during which all lithologies of the region were strongly deformed and metamorphosed to amphibolite facies (Friend and others, 1996; Friend and Nutman, 2005b). Widespread post-tectonic granitoid magmatism ("Qôrqut granites," McGregor, 1973; Brown and others, 1981) occurred at ~2520 Ma (Baadsgaard, 1976; Moorbath and Pankhurst, 1976). This marked the last major event to affect the region.

## GEOLOGY OF THE AKILIA SUPRACRUSTAL ROCKS

The Akilia supracrustal enclave occurs on the southwesternmost peninsula of the island (fig. 1). We mapped the exposure at 1:250 scale (fig. 2) by constructing an oriented grid using triangulation points at 25 m spacings. Topography was estimated by hand leveling. Isolated blocks and lenses of supracrustal lithologies occur to the

# Fig. 2
# Geologic Map of the Southwest Peninsula Akilia, West Greenland

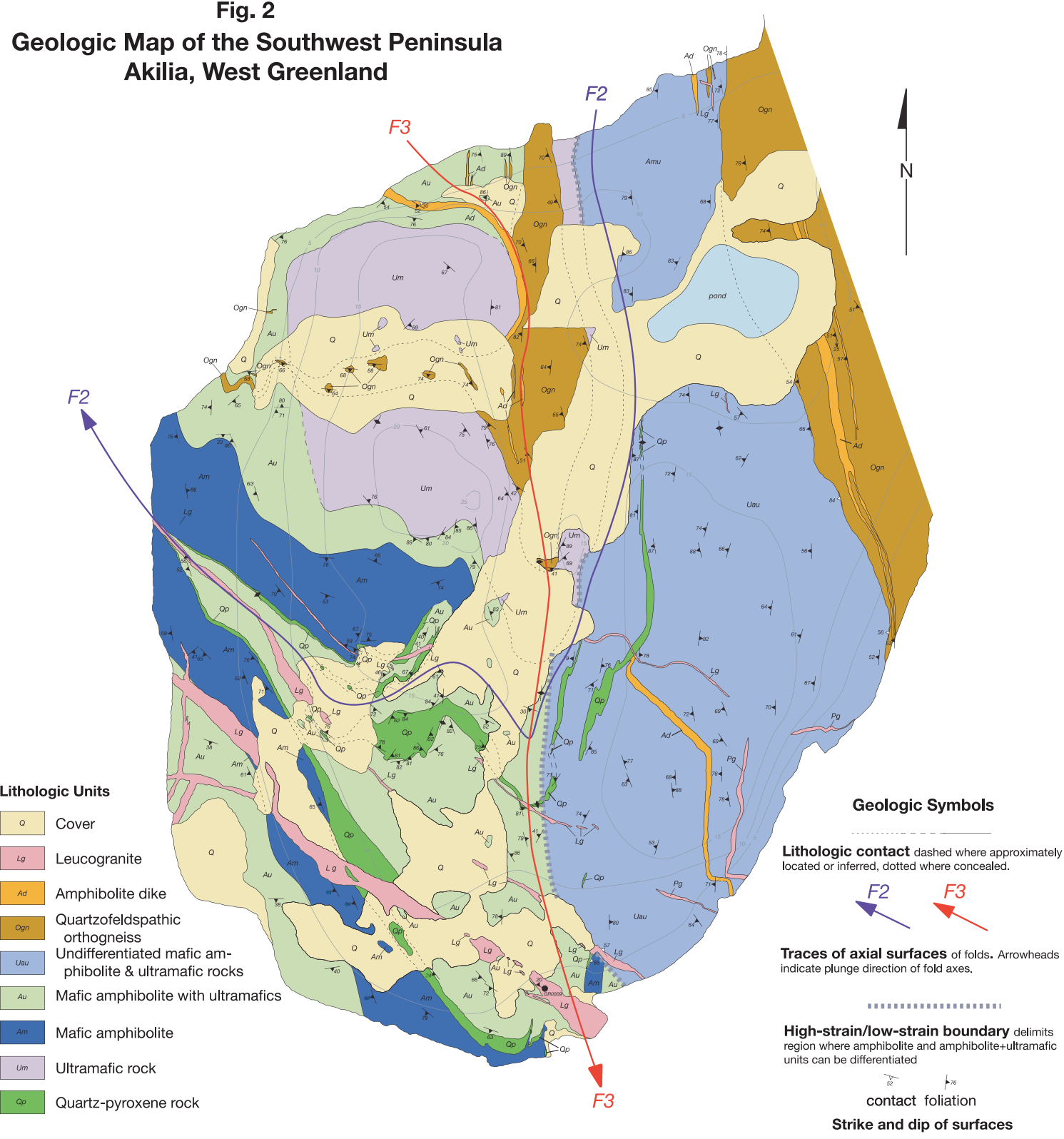


**Lithologic Units**

- Q — Cover
- Lg — Leucogranite
- Ad — Amphibolite dike
- Ogn — Quartzofeldspathic orthogneiss
- Uau — Undifferentiated mafic amphibolite & ultramafic rocks
- Au — Mafic amphibolite with ultramafics
- Am — Mafic amphibolite
- Um — Ultramafic rock
- Qp — Quartz-pyroxene rock

**Geologic Symbols**

**Lithologic contact** dashed where approximately located or inferred, dotted where concealed.

F2 F3

**Traces of axial surfaces** of folds. Arrowheads indicate plunge direction of fold axes.

**High-strain/low-strain boundary** delimits region where amphibolite and amphibolite+ultramafic units can be differentiated

52 76

contact foliation

**Strike and dip of surfaces**

0 10 20 30 40 50 meters

contour interval: 5 m

# Fig. 3
# Interpretive Bedrock and Form-Surface Map Southwest Peninsula Akilia, Greenland

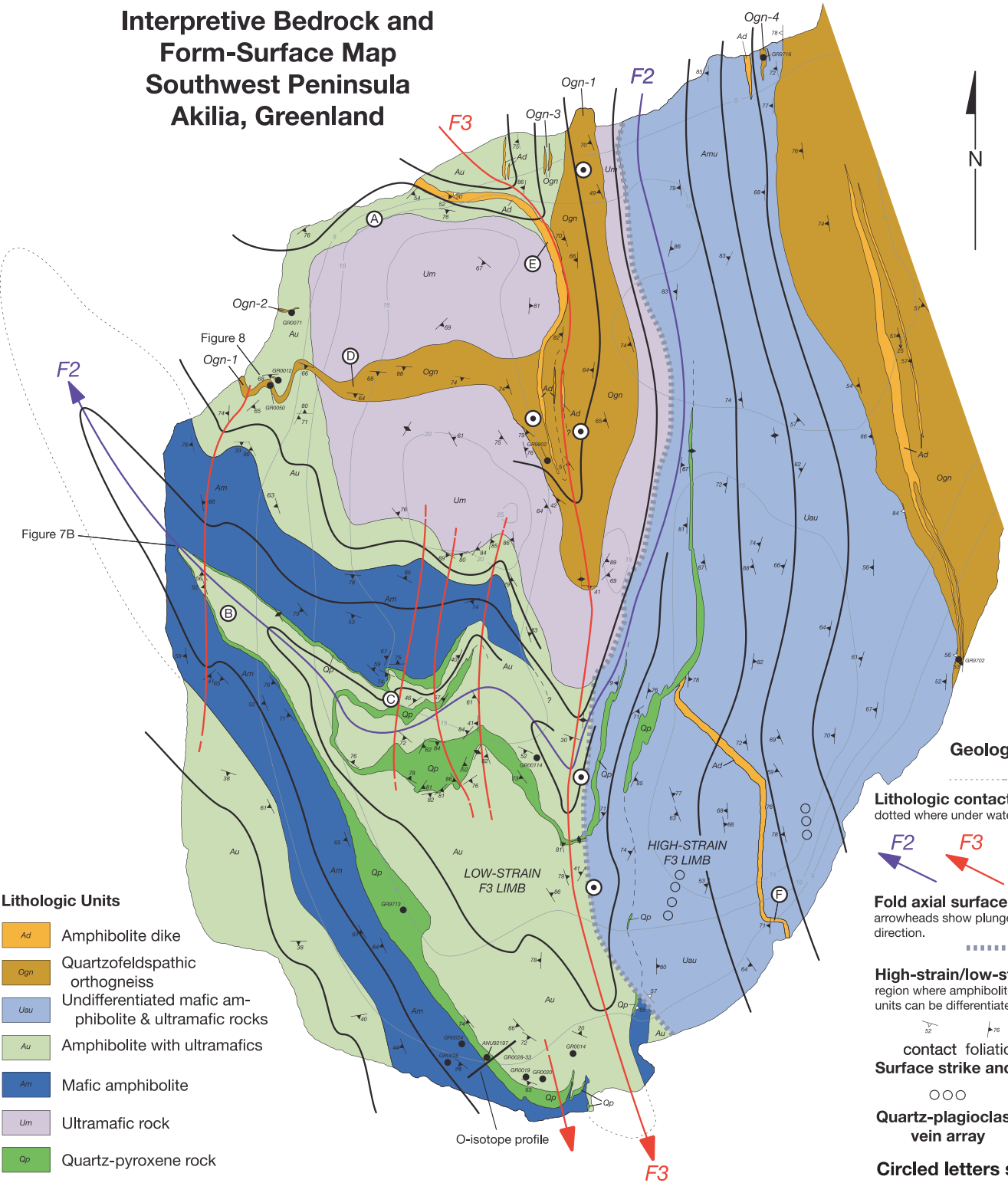


## Lithologic Units

- Ad — Amphibolite dike
- Ogn — Quartzofeldspathic orthogneiss
- Uau — Undifferentiated mafic amphibolite & ultramafic rocks
- Au — Amphibolite with ultramafics
- Am — Mafic amphibolite
- Um — Ultramafic rock
- Qp — Quartz-pyroxene rock

0 10 20 30 40 50 meters
contour interval: 5 m

## Geologic Symbols

**Lithologic contact** dashed where unit is attenuated, dotted where under water.

**Fold axial surfaces** arrowheads show plunge direction.

**S1 surfaces** (interpretive).

**High-strain/low-strain boundary** delimits region where amphibolite and amphibolite+ultramafic units can be differentiated

**Surface strike and dip** (contact, foliation)

**Sample location**

**Quartz-plagioclase vein array**

**Rootless fold hinges**

**Circled letters show postions of key localities discussed in text. Figure shows all sample locations, except Gr0009, which is shown in figure 2.**

north along the western coast of the island (Myers and Crowley, 2000) but were not mapped in detail.

Exposure of the main supracrustal package at the map scale is generally excellent except in the central portion of the peninsula. Variations in exposure quality lead to differing levels of confidence in contact locations. In figure 2, we use solid lines to depict contacts in areas of good exposure (~50% or more), long dashed lines in areas of moderate exposure (~20 – 50%) and short dashed lines in areas of poor exposure (~20% or less). Areas of poor exposure are indicated as cover (*Q*), with key outcrops indicated. Figure 3 is a simplified, interpretive map of bedrock geology omitting cover and late leucocratic granitoid bodies, with sample localities and positions of features discussed in the text.

The only exposed contact between the supracrustal package and the main body of the quartzofeldspathic gneisses is along the eastern edge of the map area. To the west, a small skerry of Amîtsoq Gneiss exposed at low tide ~50 m suggests that the enclave does not extend far offshore. The supracrustal rocks break up into a train of progressively smaller enclaves in Amîtsoq Geniesses to the north (fig. 1; Nutman and others, 1997; Myers and Crowley, 2000).

### *Lithologic Units*

*Mafic amphibolite gneiss and ultramafics.*—The dominant lithology in the Akilia supracrustal rocks is mafic amphibolite gneiss. Two mafic amphibolite units can be distinguished: a mafic gneiss with abundant ultramafic blocks (*Au;* fig. 4A) and a homogeneous, amphibolite gneiss largely free of ultramafic blocks (*Am;* fig. 4B). Amphibolite gneiss in both units consists of hornblende + plagioclase + biotite + ilmenite ± quartz, clinopyroxene, garnet and sphene. Compositional banding is variably developed. Rare patches of garnet + plagioclase + clinopyroxene may be relicts of an earlier, granulite-facies metamorphic event (Griffin and others, 1980).

The *Am* unit can be traced around a fold hinge (fig. 2) and is in contact with quartz-pyroxene rocks on one side and *Au* on the other. The presence of abundant ultramafic bodies (fig. 4A) distinguishes *Au* from *Am.* These are irregular blocks to oblate lenses, <1 m to several m in size, and massive to weakly foliated. Metamorphic minerals are Fe-Mg amphibole, hornblende, talc, Fe-oxide, clinopyroxene and rare olivine. Fe-Mg amphibole in ultramafic blocks sporadically occurs as polycrystalline aggregates that appear to pseudomorph earlier clusters of cm-sized prisms (fig. 4C), probably reflecting amphibolite-facies replacement of jackstraw-textured granulite-grade metamorphic olivine (Snoke and Calk, 1978).

A weakly foliated ultramafic body in *Au* occupies the topographic high of the peninsula (figs. 2 and 4D) and is sufficiently large to be mapped as a separate unit (*Um*). Disruption of this and similar ultramafic bodies along contacts with mafic rocks likely produced the mixed amphibolite and ultramafic unit (*Au*). This can be seen at locality A (fig. 3), where *Um* is disaggregated into phacoidal blocks hosted by amphibolite.

As discussed below, strain increases significantly from west to east. In the eastern half of figure 2, distinctions between *Am* and *Au* could not be made with confidence. We assigned these lithologies to an undifferentiated amphibolite and ultramafic unit (*Uau*).

*Quartz-pyroxene rock.*—Exposures of a lithology rich in quartz and Fe-rich ferromagnesian minerals (figs. 2, 3 and 5A) has been termed banded iron-formation (BIF), metachert, quartz-rich rock, or quartz-pyroxene rock (McGregor and Mason, 1977; Nutman and others, 1996, 1997; Myers and Crowley, 2000; Mojzsis and Harrison, 2000, 2002b; Fedo and Whitehouse, 2002a, 2000b, 2000c; Whitehouse and Fedo, 2003). We refer to this lithology as "quartz-pyroxene" rock or gneiss (*Qp*). *Qp* rocks exhibit strong gneissic layering defined by cm-scale bands dominated by quartz or pyroxene ±

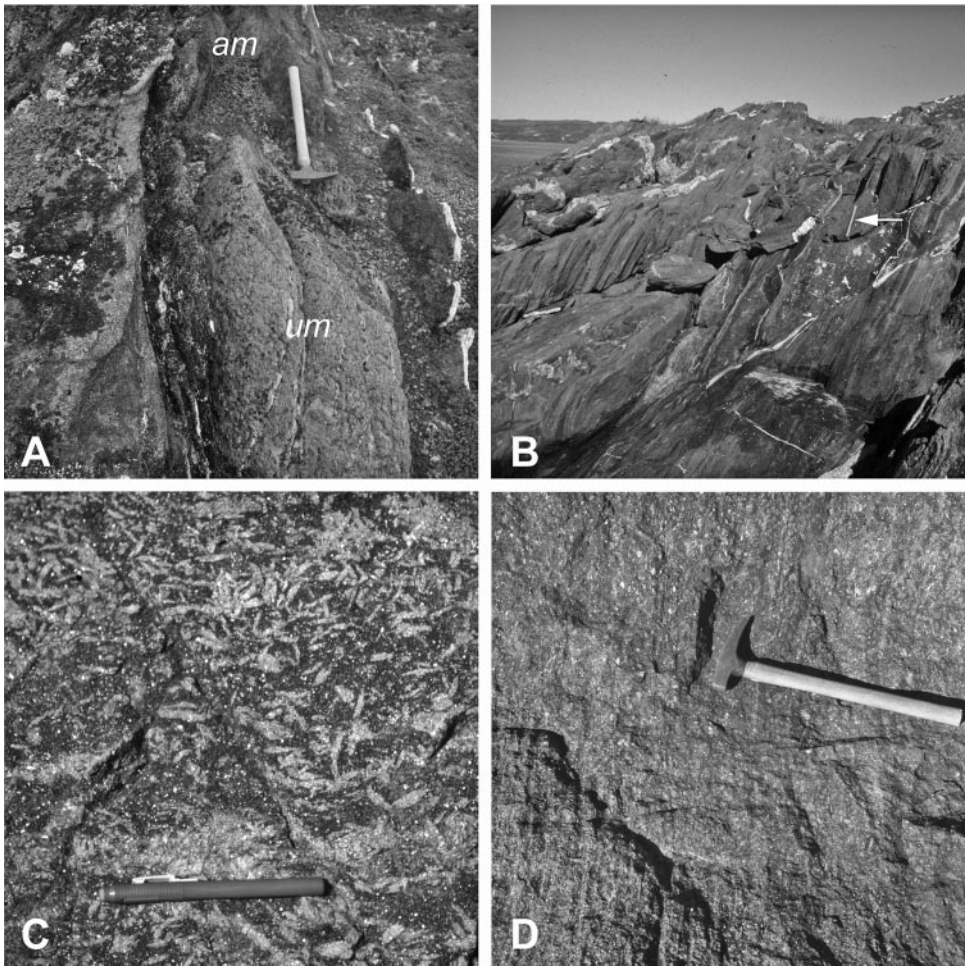


Fig. 4. Photographs of features in amphibolite and ultramafic units. (A) Meter-scale ultramafic lens (*Um*) in amphibolite (am) of the *Au* unit (hammer is 50 cm long). (B) Ultramafic-free amphibolite (*Am*) south of *Qp* at southern tip of peninsula, looking west. S1 folia dip steeply to southwest. Arrow shows hammer for scale. (C) Polycrystalline Fe-Mg amphibole pseudomorphs of jackstraw-textured olivine(?) in ultramafic block. Eraser is 13 cm long. (D) Weak S1 foliation in ultramafic block in *Au;* hammer for scale.

amphbibole (fig. 5B). The mineral assemblage is quartz, hedenbergitic clinopyroxene, Fe-Mg amphibole ± garnet, apatite, magnetite and sulfide. Boudin necks and crosscutting quartz- and pyroxene-rich veins are common (figs. 5C and D). Although common near contacts, the veins also occur throughout *Qp* units. They likely result from late brittle deformation and fluid migration.

We identified two discrete, sub-parallel *Qp* units with variable thickness. They reach their greatest width south of *Um,* consistent with minimal strain near this body (see below). Both *Qp* units thin significantly along strike and ultimately become discontinuous where strain is high. Lithologies in contact with *Qp* units are *Am* and amphibolite and ultramafic rocks of *Au.*

*Anthophyllite-garnet rock.*—A ~10 m long block of anthophyllite-garnet-biotite-plagioclase-quartz gneiss was noted in *Au* (sample GR00114; fig. 3). Its unique mineral assemblage and bulk composition (table 1) raised the possibility of a metasedimentary

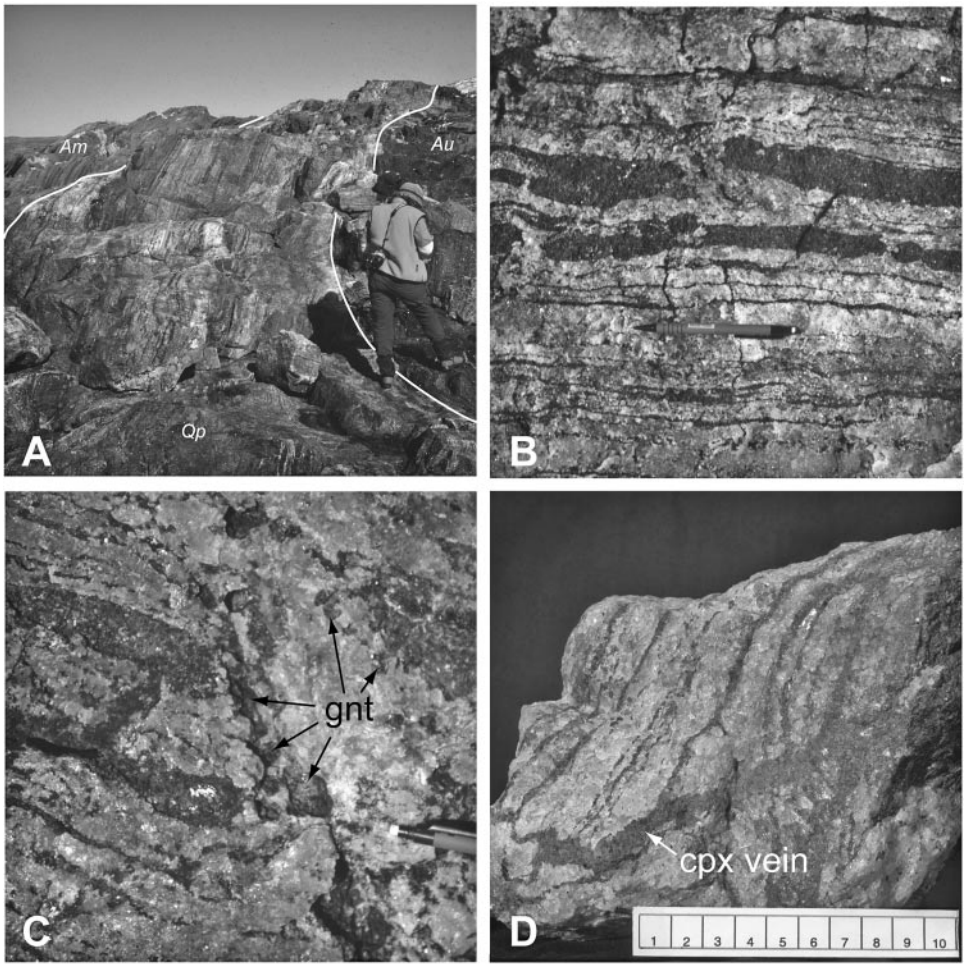


Fig. 5. Photographs of quartz-pyroxene gneisses. (A) Southernmost *Qp* layer, looking west (fig. 3). Bounding lithologies are *Am* and hornblende-rich ultramafic rock of *Au*. (B) Gneissic compositional banding (S1) in the *Qp* lithology. Quartz-rich layers alternate with layers rich in Ca-Fe clinopyroxene. Thickness ranges from <1 to several cm. Pencil is 12 cm long. (C) Granular quartz in vein crosscutting *Qp* gneissic layering. Garnet (gnt) occurs where veins cut pyroxene bands. End of pencil for scale. (D) Fe-Ca pyroxene (cpx) vein cutting *Qp* gneiss. Scale bar is in cm.

protolith, so this sample was included in our studies of geochemistry and zircon geochronology. A separate map unit was not defined because of its limited extent.

*Quartzofeldspathic gneisses.*—Heterogeneous quartzofeldspathic orthogneisses (*Ogn*) of the Amîtsoq Gneisses (McGregor, 1973) host, and occur within, the supracrustal package. The gneisses are foliated and display local color variations reflecting differing modes of plagioclase, quartz, K feldspar and biotite (figs. 6A and B). One large body (*Ogn-1*) and at least three smaller bodies (*Ogn-2, 3* and *4*) occur within the supracrustal rocks (fig. 3).

*Amphibolite dikes.*—Deformed, foliated mafic dikes with amphibolite-grade minerals (*Ad*) crosscut all supracrustal and *Ogn* units (fig. 6C). Minerals include hornblende, plagioclase, quartz, Fe oxide and sulfide ± clinopyroxene, biotite and titanite. Relict

TABLE 1

*Representative bulk-rock compositions from Akilia, West Greenland*

| | GR0019 | GR0020 | GR0030 | GR0031 | GR0033 | GR00114 | ANU92197 | GR9713 | GR9802 | GR0050 | GR0012 | GR0071 | GR9716 | GR9702 | GR0009 |
|---|---|---|---|---|---|---|---|---|---|---|---|---|---|---|---|
| | ultra-mafic | ultra-mafic | ultra-mafic | ultra-mafic | amphi-bolite | anth-gnt rock | Qp rock | Qp rock | Ogn-1 tonalite | Ogn-1 trond | Ogn-1 tonalite | Ogn-2 tonalite | Ogn-4 tonalite | Ogn tonalite | Lg trond |
| $SiO_2$ | 46.73 | 46.52 | 45.84 | 47.17 | 46.15 | 41.08 | 73.66 | 79.25 | 68.54 | 74.24 | 70.16 | 67.24 | 66.94 | 64.73 | 76.02 |
| $TiO_2$ | 0.38 | 0.28 | 0.46 | 0.34 | 1.64 | 0.97 | 0.02 | 0.05 | 0.33 | 0.09 | 0.24 | 0.42 | 0.41 | 0.60 | 0.07 |
| $Al_2O_3$ | 8.58 | 8.50 | 10.25 | 7.72 | 13.85 | 19.00 | 0.17 | 0.99 | 15.50 | 15.10 | 14.43 | 16.87 | 15.63 | 16.31 | 14.25 |
| FeO* | 11.20 | 9.82 | 11.59 | 10.49 | 14.38 | 20.65 | 17.87 | 6.65 | 3.35 | 0.97 | 2.84 | 2.07 | 3.55 | 4.43 | 0.59 |
| MnO | 0.18 | 0.16 | 0.18 | 0.16 | 0.20 | 0.36 | 0.28 | 0.14 | 0.05 | 0.02 | 0.03 | 0.01 | 0.07 | 0.08 | 0.02 |
| MgO | 21.03 | 25.3 | 13.8 | 23.28 | 8.53 | 7.94 | 4.27 | 4.69 | 1.13 | 0.29 | 2.62 | 2.14 | 2.43 | 2.06 | 0.17 |
| CaO | 6.39 | 4.79 | 12.44 | 5.2 | 9.23 | 3.17 | 2.33 | 7.92 | 3.16 | 3.35 | 3.35 | 4.40 | 4.62 | 5.48 | 2.35 |
| $Na_2O$ | 1.13 | 0.82 | 1.19 | 0.84 | 2.69 | 1.21 | 0.08 | 0.17 | 4.38 | 5.20 | 3.87 | 4.22 | 3.63 | 4.24 | 5.49 |
| $K_2O$ | 0.15 | 0.08 | 0.43 | 0.10 | 0.28 | 2.74 | 0.02 | 0.05 | 1.39 | 0.38 | 1.45 | 1.19 | 1.40 | 1.04 | 0.56 |
| $P_2O_5$ | 0.02 | 0.02 | 0.03 | 0.02 | 0.08 | 0.13 | 0.03 | 0.02 | 0.10 | 0.04 | 0.09 | 0.12 | 0.12 | 0.17 | 0.01 |
| L.O.I. | 2.44 | 2.35 | 1.45 | 3.17 | 0.49 | 0.09 | 0.02 | 0.10 | 0.64 | 0.09 | 0.81 | 0.49 | 0.98 | 0.52 | 0.23 |
| Total | 98.23 | 98.64 | 97.66 | 98.49 | 97.52 | 97.34 | 98.75 | 100.03 | 98.57 | 99.77 | 99.89 | 99.17 | 99.78 | 99.66 | 99.76 |
| Rb | 3 | 2 | 16 | | 3 | 188 | 0.22 | | 54 | | 98 | 51 | 76 | 46 | 22 |
| Sr | 13 | 19 | 33 | 11 | 100 | 38 | 2.3 | 15 | 234 | 220 | 267 | 448 | 117 | 282 | 133 |
| Y | 9 | 7 | 12 | 8 | 34 | 16 | 1.3 | | 17 | 3 | 2 | | 8 | 9 | 4 |
| Zr | 25 | 20 | 27 | 20 | 70 | 58 | 1.3 | 21 | 140 | 75 | 124 | 191 | 110 | 131 | 119 |
| Nb | | | | | 5 | 1 | 0.7 | | 2 | 2 | 2 | 2 | | | |
| La | 2.8 | 1.3 | 2.5 | 1.8 | 5.4 | 3.0 | 0.67 | 0.521 | 19.7 | 13.2 | 16.5 | 7.1 | 11.9 | 8.0 | 3.4 |
| Ce | 5.2 | 2.6 | 5.0 | 3.8 | 12.3 | 8.0 | 1.23 | 1.02 | 38.3 | 25 | 32 | 9.5 | 24 | 17 | 5 |
| Pr | | | | | | | 0.127 | | | | | | | | |
| Nd | 3.6 | 2.2 | 4.3 | 3.0 | 12.6 | 6 | 0.487 | 1.8 | 13.7 | 9.0 | 1.4 | 2.7 | 12 | 11 | 2 |
| Sm | 1.1 | 0.7 | 1.3 | 0.9 | 3.9 | 2.3 | 0.112 | 0.14 | 2.1 | 1.46 | 0.2 | 0.4 | 2.84 | 2.73 | 0.52 |
| Eu | 0.52 | 0.25 | 0.42 | 0.34 | 1.28 | 0.47 | 0.060 | 0.65 | 0.81 | 0.65 | 0.24 | 0.22 | 0.79 | 0.83 | 0.5 |
| Gd | 1.4 | 1.0 | 1.6 | 1.2 | 4.9 | 1.16 | 0.145 | | 1.5 | | 0.1 | 0.3 | | | |
| Tb | 0.3 | 0.2 | 0.3 | 0.2 | 0.9 | 0.4 | 0.025 | 0.03 | 0.2 | 0.2 | | | 0.5 | 0.4 | |
| Dy | 1.8 | 1.3 | 2.2 | 1.5 | 6.3 | 1.5 | 0.163 | | 1.3 | | | | | | |
| Ho | 0.4 | 0.3 | 0.5 | 0.3 | 1.4 | 0.29 | 0.038 | | 0.3 | | | | | | |
| Er | 1.2 | 1.0 | 1.4 | 1.0 | 4.3 | 0.96 | 0.106 | | 0.8 | | | | | | |

TABLE 1
*(Continued)*

| | GR0019 | GR0020 | GR0030 | GR0031 | GR0033 | GR00114 | ANU92197 | GR9713 | GR9802 | GR0050 | GR0012 | GR0071 | GR9716 | GR9702 | GR0009 |
|---|---|---|---|---|---|---|---|---|---|---|---|---|---|---|---|
| | ultra-mafic | ultra-mafic | ultra-mafic | ultra-mafic | amphi-bolite | anth-gnt rock | Qp rock | Qp rock | Ogn-1 tonalite | Ogn-1 trond | Ogn-1 tonalite | Ogn-2 tonalite | Ogn-4 tonalite | Ogn tonalite | Lg trond |
| Tm | 0.18 | 0.15 | 0.22 | 0.15 | 0.64 | 0.077 | | | 0.1 | | | | | | |
| Yb | 1.2 | 1.0 | 1.5 | 1.0 | 4.1 | 1.66 | 0.107 | 0.119 | 0.6 | 0.26 | 0.16 | | 0.89 | 0.78 | 0.73 |
| Lu | 0.18 | 0.17 | 0.22 | 0.16 | 0.63 | 0.25 | 0.017 | 0.018 | 0.09 | 0.04 | 0.02 | | 0.12 | 0.09 | 0.1 |
| Hf | 0.9 | 0.6 | 1.1 | 0.8 | 2.7 | 1.4 | 0.032 | | 4.0 | 1.3 | 3 | 5.6 | 4 | 3.2 | 6.7 |
| Pb | | | | | 13 | 13 | 0.42 | | 12 | 9 | 15 | 15 | 10 | 0.09 | 34 |
| Th | 0.3 | 0.1 | 0.2 | 0.2 | 0.3 | | 0.099 | 0.028 | 1.8 | 1.1 | 1.9 | 1 | 1.7 | 0.6 | 17.2 |
| U | 0.2 | | 0.2 | 0.3 | 0.6 | 0.5 | 0.062 | 0.054 | 0.2 | b.d. | 0.5 | 0.5 | 0.3 | 0.3 | 6.2 |
| Ni | 725 | 971 | 323 | 1150 | 53 | 124 | 104 | 64 | 10 | 6 | 114 | 42 | 56 | 43 | 2 |
| Co | 73 | 83 | 68 | 87 | 50 | 67.1 | 127 | 19 | 8 | 4.3 | 16.3 | 14 | 49.2 | 34.5 | 45.7 |
| Cr | 3180 | 2300 | 1570 | 2720 | 156 | 574 | 1.55 | 470 | 13.3 | 6.5 | 459 | 304 | 9.2 | 66.3 | |
| $T_{zircon}$ | -- | -- | -- | -- | -- | -- | -- | -- | 772 | 720 | 758 | 792 | 740 | 739 | 762 |
| Or | -- | -- | -- | -- | -- | -- | -- | -- | 13.1 | 3.4 | 14.4 | 10.7 | 13.1 | 9.2 | 5.2 |
| Ab | -- | -- | -- | -- | -- | -- | -- | -- | 62.9 | 71.5 | 58.5 | 57.4 | 51.7 | 57.1 | 76.8 |
| An | -- | -- | -- | -- | -- | -- | -- | -- | 24.0 | 25.1 | 27.0 | 31.9 | 35.1 | 33.6 | 18.1 |

*Notes:* Samples prepared by dividing freshly broken ~2 kg samples of unweathered rocks by diamond saws, crushing in steel mortars and reducing to powders in cleaned tungsten carbide mills. Analysis by XRF and ICP-MS at Activation Laboratories, except ANU92197 trace elements. Comparison of recommended and analyzed standard show deviations <1.5% relative for oxides, except MnO (6.3%), $Na_2O$ (6.5%) and $P_2O_5$ (23.1%), and for trace elements <20% relative, except Ni (21.4%). Pr had 47.6% relative error and is omitted. ANU92197 trace elements analyzed by solution ICP-MS at ANU PRISE laboratories (precisions not reported). FeO*, all Fe as FeO; L.O.I., loss on ignition; blank entries, below detection; $T_{zircon}$, zircon saturation temperature (°C) from Watson and Harrison (1983); *Ogn* rock names from Barker (1979) based on normative modes of albite (Ab), orthoclase (Or) and anorthite (An); (trond, trondhjemite); anth-gnt, anthophyllite-garnet. See figures 2 and 3 for sample locations.

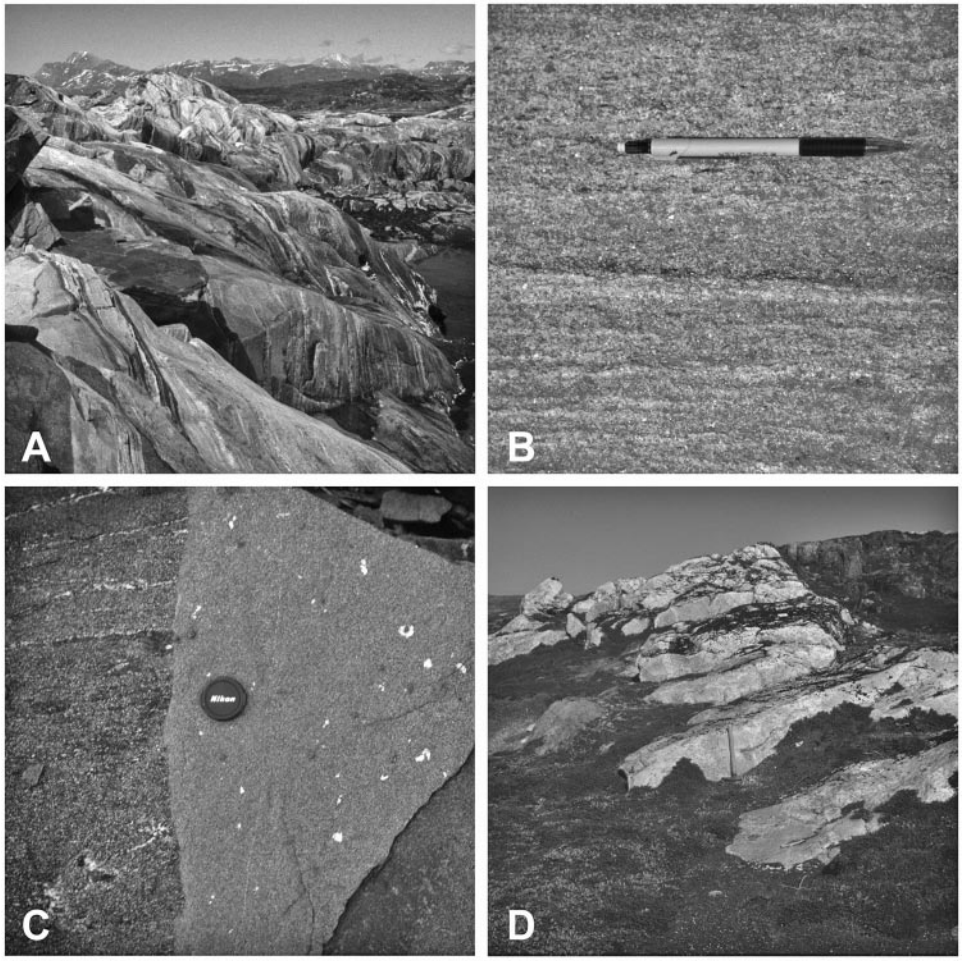


Fig. 6. (A) Heterogeneous orthogneiss at the east contact of the supracrustal enclave, looking north. (B) Gneissic layering (S1) in tonalitic phase of orthogneisses. Pencil for scale. (C) Metamorphosed amphibolite dike, locality F (fig. 3). Note that foliation (S1) in host amphibolite appears to terminate at contact. Lens cap is 7 cm across. (D) Leucogranite dike, looking west. Hammer for scale.

plagioclase glomeroporphyroblasts may occur. The dikes are discontinuous, and range up to several meters thick, with locally strong internal deformation and schlieren.

*Leucocratic granitoid dikes.*—Leucocratic quartz-feldspar ± biotite ± garnet veins, dikes and sills (*Lg*) crosscut all lithologies. They are up to several meters wide (fig. 6D), display variable grain size and range from K-feldspar rich to quartz rich. Figure 2 shows only bodies that are continuous for several meters or more; numerous irregular, discontinuous pods and lenses are ignored. The sills and dikes are locally foliated, with orientations subparallel to contacts.

### *Structural Evolution*

Three major ductile deformation events were identified: development of penetrative foliation (D1), isoclinal folding (D2) and tight refolding (D3). The geometric relations among the structures provide the framework for evaluation of the nature of contacts involving *Ogn* orthogneisses and amphibolite dikes.

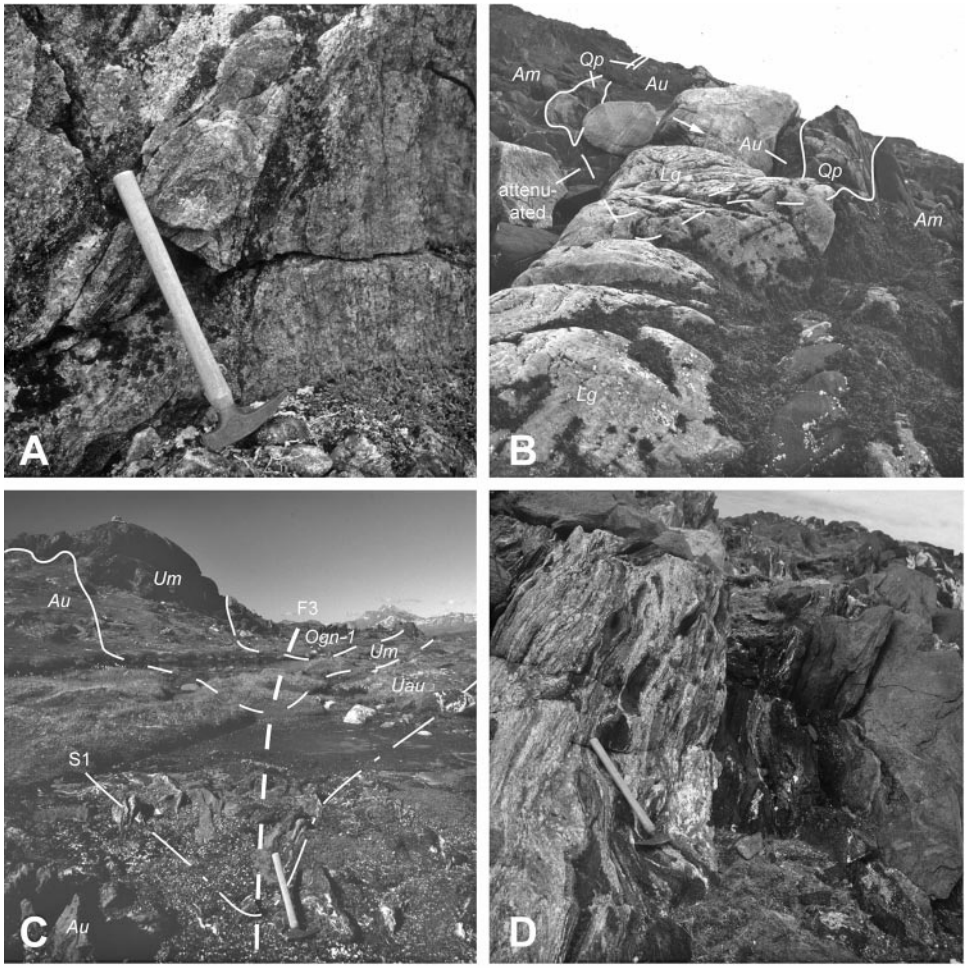


Fig. 7. Photographs of key structural features. (A) Upright, isoclinal, intrafolial folding of S1 in *Qp* rock. These folds are grouped with D1. Hammer for scale. (B) Inferred F2 closure of *Qp* rock on west side of peninsula (see fig. 3 for location). The *Qp* gneiss of the fold limbs is cut by an ~2 m wide *Lg* dike. Other features consistent with the interpreted hinge are: the consistent distribution of lithologies (*Am* and *Au*) and S1 hinges in *Am*. Arrow points to hammer for scale. (C) Hinge region of F3 fold, looking north. Hammer for scale. (D) S1-parallel quartz-plagioclase vein in the high-strain eastern limb of F3 fold. See figure 3 for location. Hammer for scale.

*D1.*—D1 produced a penetrative foliation now defined by amphibolite-facies minerals (S1; figs. 4-6). Compositional banding is locally developed in mafic rocks, but strongest in Fe-rich quartz-pyroxene rock. In ultramafic rocks, weak S1 is locally defined by Fe-Mg amphibole. S1 surfaces are subparallel to contacts between *Am, Au,* and *Qp* units (fig. 2). Rare asymmetric intrafolial folds of S1 in *Qp* gneiss may record transposition of earlier surfaces (fig. 7A); however, we include these with D1 for simplicity. Pre-S1 deformation and fabric development cannot be ruled out (Myers and Crowley, 2000), though supracrustal enclaves evidently behaved as competent bodies that experienced significantly lower strain than the host gneisses (Nutman and others, 1997).

*D2.*—D2 is represented by a large isoclinal fold with a hinge region in the southwest portion of the map area (figs. 2 and 3). Although complicated by an *Lg* dike

and discontinuous exposure of *Qp* marker units (fig. 7B), the hinge of the F2 fold can be identified from the map patterns of *Am, Au* and the *Qp* units, which indicate closure of these lithologies in a consistent pattern about the inferred F2 hinge surface (figs. 2 and 3). The location of the F2 hinge is also indicated by an observed closure in S1 surfaces in mafic amphibolite of *Au* ~15 m from the western coastline (locality B, fig. 3). In the westernmost portion of the map area the F2 hinge surface strikes NW–SE and dips ~70° SW; the F2 axis plunges steeply NNW. Leucogranite veins and sheets postdate D2.

*D3.*—The F2 structure was refolded in an asymmetric map-scale fold (F3; figs. 2 and 3). In the eastern F3 limb, S1 surfaces strike ~N20E and dip steeply W and E, but in the western limb they strike ~N45W and dip moderately to steeply SW. Thus, S1 surfaces define a subvertical to steeply west-dipping hinge-surface. S1 closures are evident in several outcrops (fig. 7C) and in the map pattern defined by *Am* and *Qp* units (figs. 2 and 3). In addition, numerous rootless intrafolial fold hinges occur in S1 layering in *Au* and *Ogn* units (fig. 3) within several meters of the F3 hinge-surface. Orientations of S1 surfaces in the F3 hinge region suggest that the plunge of the F3 axis is steep at the southernmost point of the island (~70° SSW), but shallows to ~40° S over a distance of ~50 m to the north.

Minor structures include layer-parallel flattening and boudinage where S1 compositional layering is well developed, especially in *Qp* (Whitehouse and Fedo, 2003). In addition, minor corrugations in *Qp* units and S1 folia in *Am* in the W limb of the map-scale F3 fold may be subparallel, parasitic F3 folds (fig. 3). This would explain the geometries of the southern *Qp* exposures and of contacts near the F2 axial surface.

Strain was partitioned heterogeneously during D3. Near the F3 hinge surface, the *Qp* and *Am* units are thinned significantly or boudinaged into discontinuous blocks and lenses. Strain increases in the eastern F3 limb, as indicated by poorly preserved lithologic contacts, attenuation of units and stronger fabric development. In particular, both *Qp* units are thinned and boudinaged in the eastern limb to the extent that they locally form discrete lenses, and ultimately cannot be traced to the northernmost part of the map area (fig. 2). Similarly, *Am* cannot be recognized more than ~10 m east of the hinge. Decimeter- to meter-scale swarms of quartz-plagioclase veins subparallel to the F3 axis are common in the hinge region and in the eastern limb (figs. 3 and 7D). In contrast, the western limb displays lower strain, as indicated by preservation of minor structures and lithologic contacts, and the absence of vein swarms. Comparison of unit thicknesses yields a strain difference of >100 percent. The heterogeneous distribution of strain could have resulted from interference between the F2 and F3 folds, as at locality C (fig. 3) where minor F2 folds are refolded by parasitic F3 folds to give the complex *Qp* map pattern. Or more likely—in view of the weak S1 foliation in *Um* (fig. 4D)—low strain in the eastern F3 limb resulted from a strain shadow near this large, relatively competent body.

*Emplacement of Ogn bodies.*—The nature of contacts involving *Ogn* orthogneisses is key to constraining the geology, age and origin of the Akilia supracrustals. If *Ogn* bodies are deformed, crosscutting igneous rocks, the date of their crystallization is the minimum age of their host rocks; if contacts are tectonic, *Ogn* bodies provide no constraint on supracrustal age.

*Ogn-1* is a 5 to 15 m wide body (fig. 3) of leucocratic to melanocratic, tonalitic gneiss. At its northernmost point, it is in contact with *Au* on the west and the large ultramafic body on the east. Its southern termination occurs in an F3 fold hinge defined by S1 folia (figs. 2 and 7C). West of the F3 fold hinge, *Ogn-1* can be traced into the large ultramafic body near the topographic high of the peninsula (fig. 2). Immediately north of the topographic high is an elevated, flat "shoulder" where exposure is poor, consisting of a few flat pavements (fig. 2). These exposures indicate

that *Ogn-1* is in contact with *Um* on either side. *Ogn-1* outcrops can be traced westward across the shoulder to a steep, grassy slope at the northwestern edge of the peninsula (fig. 2), where there is one in-place outcrop and several out-of-place blocks. Orientation of S1 folia in the outcrop interpreted to be in place are similar to those in nearby outcrops. An *Ogn* sheet W of ~5 m of cover (fig. 8A) consists of gray tonalitic orthogneiss in contact with foliated ultramafic and amphibolite of *Au*. S1 is coaxial in all lithologies at this locality. This sheet is interpreted to be the western continuation of *Ogn-1*.

Although *Ogn-1* is incompletely exposed, the best interpretation of the geometric relations associated with its E–W "arm" is that it crosscuts the *Um-Au* contact (figs. 2 and 3). The geometry does not support a fault or in-folding origin, but rather suggests that this portion of *Ogn-1* is an igneous dike or sill with preserved (though deformed) intrusive contact relations. S1 orientations in *Ogn-1* and *Um* (figs. 2 and 3) are discordant. Although used elsewhere as evidence of a crosscutting relationship (Nutman and others, 1997), the discordance may be a geometric artifact (Myers and Crowley, 2000). Even if real, it could simply reflect the large ductility contrast between the two lithologies. At the western coastline, *Ogn-1* is attenuated in *Au* and displays prominent meter-scale F3 folds with axes parallel to the main F3 axis. Evidently, the lower strain associated with the competent *Um* body led to better preservation of the original igneous contact.

*Ogn-2* is a small tonalitic orthogneiss body at the western coast ~15 m north of *Ogn-1* (fig. 3). It is ~15 cm wide, >2 m long and in contact with a massive, unfoliated hornblendite block within *Au* (fig. 8B). S1 foliation is coaxial with surrounding lithologies. Assignment to *Ogn* is based on lithologic similarity to *Ogn-1* and geochemistry (table 1), and is supported by zircon geochronology (see below). *Ogn-2* contains several inclusions of polycrystalline hornblendite (fig. 8B), which suggest an originally igneous crosscutting relationship.

Contacts involving the two other *Ogn* bodies are less certain than those of *Ogn-1* and *Ogn-2*. *Ogn-3* is represented by two discrete layers of banded gray gneiss that occur in *Au* amphibolite 2.5 meters west of *Ogn-1* at the northern coastline (fig. 3). Poor exposure and high strain render original geometry uncertain.

Contact relations of *Ogn-4* are controversial. *Ogn-4* is a heterogeneous body ~3 m W of the contact between the supracrustal enclave and the Amîtsoq Gneisses that has been the subject of extensive discussion (Nutman and others, 1997, 2000, 2002; Whitehouse and others, 1999; Myers and Crowley, 2000; Mojzsis and Harrison, 2002a; Whitehouse and Kamber, 2005). Nutman and others (1997, 2002) suggested that *Ogn-4* crosscuts the supracrustal rocks because: (1) there is ~10° of discordance in compositional layering with host *Uau,* (2) it contains *Uau* inclusions, and (3) it was claimed to be a homogenous quartz-diorite body, rather than composite gneiss such as would be expected for a random tectonic sliver of the heterogeneous host gneisses. Myers and Crowley (2000) countered that the layering discordance was only apparent, that *Ogn-4* is composed of two gneissic phases, and that evidence for a crosscutting relationship was not conclusive. We suggest that ambiguities about *Ogn-4* arise in part from its occurrence within the high-strain limb of the main F3 fold. We did not attempt further study of this body.

*Emplacement of mafic dikes.*—Two deformed mafic dikes (*Ad*) were traced across the map area (E and F, fig. 3). The northern dike possesses large plagioclase clots in a foliated amphibole-plagioclase matrix, suggesting affinity to regional Ameralik dikes. It crosscuts the contact between *Ogn-1* and supracrustal rocks (*Um* and *Au;* locality E, fig. 3). Within *Ogn-1* in the F3 hinge region it is complexly folded, thinned and disrupted (fig. 3). Thus, it postdates *Ogn-1* and formation of the supracrustal-*Ogn-1* contact, but predates D3.

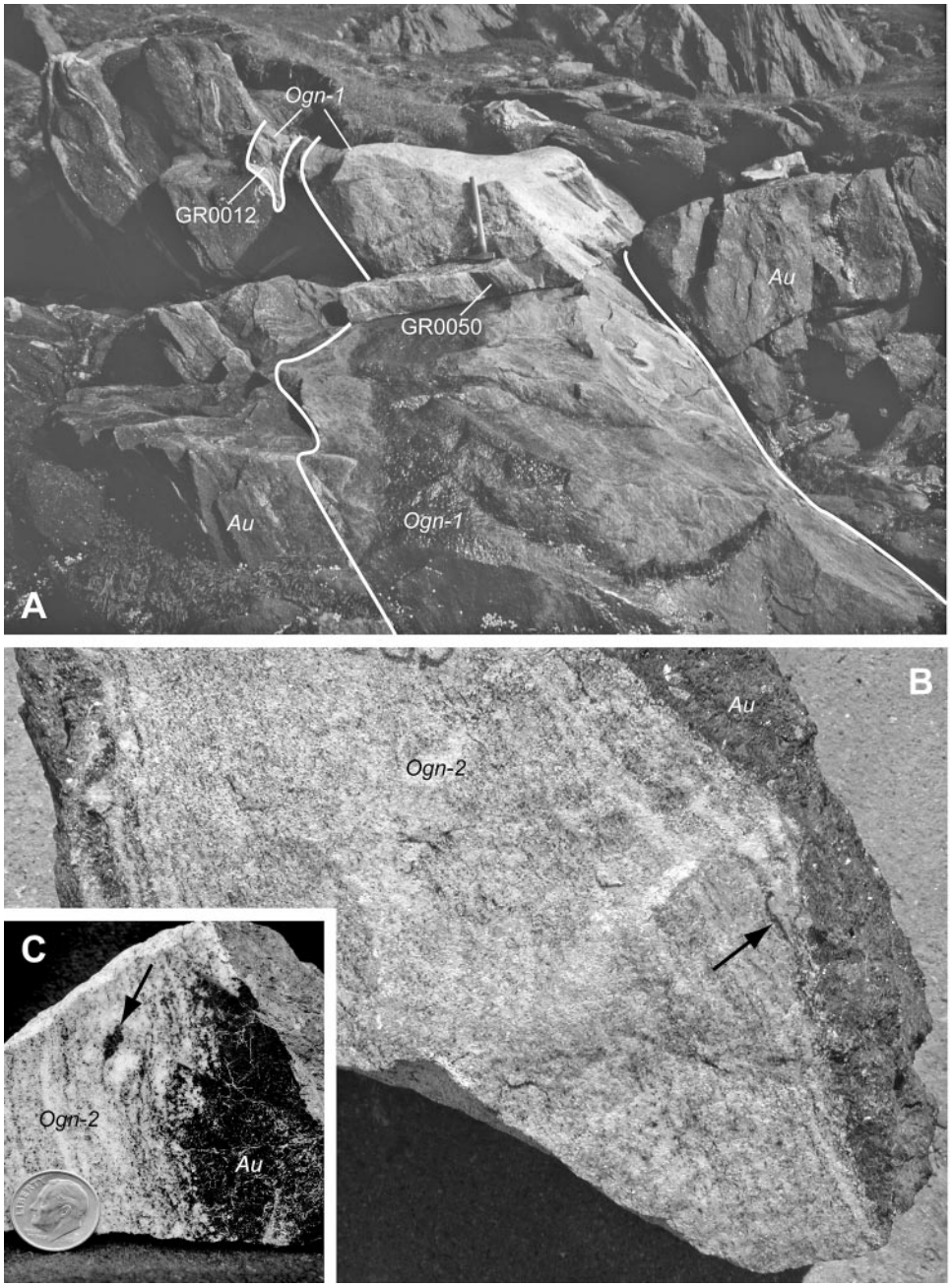


Fig. 8. (A) *Ogn-1* at western coastline, showing contacts with *Au* and locations of samples GR0050 and GR0012 (view to east; see fig. 3 for location). Note small decimeter-scale sheet to north of main body. Hammer for scale. (B) *Ogn-2* sample GR0071 collected in hornblendite within unit *Au* (see fig. 3 for location). *Ogn-2* is ~15 cm wide. Arrow shows hornblende clot from host ultramafic rock. (C) Split from *Ogn-2* sample GR0071, showing another hornblende inclusion (arrow) on cut, polished surface.

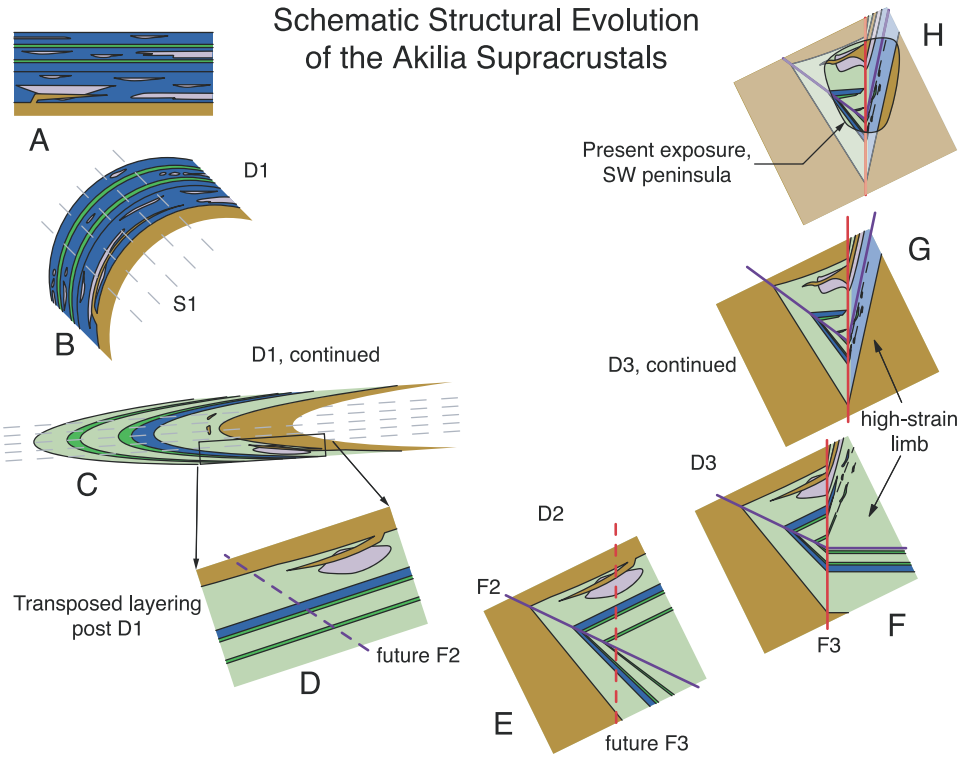


Fig. 9. Schematic structural evolution of the Akilia supracrustals. Colors keyed to figures 2 and 3. An originally layered mafic and ultramafic sequence (A) was deformed during D1 yielding prominent S1 layering (B, C). Multiple episodes are possible (D). The S1 fabric was then folded twice (D2 and D3; E-G). The present exposure limit is shown in H. Dikes omitted for clarity. Schematic evolution ignores transport in the third dimension, which may be significant.

A second mafic dike cuts the eastern F3 limb (fig. 3). Plagioclase porphyroblasts lack the glomeroporphyritic texture of Ameralik dikes, foliation in the host rock is strongly discordant to the dike margin, and the interior of the dike is unfoliated (fig. 6C). When coupled with minimal D3 strain, it appears that the dike is approximately late D3 (compare Chadwick, 1981) and younger than the other mafic dike.

*Summary and relative chronology.*—The lithologic contacts involving *Qp* and *Am* are significant because they are marker surfaces that tie the lithologies to a common syn- to post D1 history. The two *Qp* units and *Am* have a similar map pattern (fig. 2): they are folded around the F2 axis, are stretched and thinned away from the central *Um* exposure, and are ultimately lost in the high strain east limb of F3. S1 folia in these units are coaxial, and subparallel to those in bounding *Au*. Thus, these lithologic contacts predate the preserved supracrustal deformation and represent the oldest geometric features in the enclave.

This observation provides the starting point for the relative chronology schematically depicted in figure 9. Prior to deformation, the supracrustal package is interpreted as an interlayered sequence of mafic and ultramafic rocks. The absence of evidence for cumulate compositions suggests an extrusive volcanic sequence (Nutman and others, 2002, and see below). It has been proposed that *Qp* rocks originated by chemical sedimentation (Nutman and others, 1997) or by metasomatic alteration of ultramafic rocks (Fedo and Whitehouse, 2002a). Though we argue below for chemical sedimenta-

tion, the map relations discussed thus far require only that the *Qp* rocks were part of the supracrustal package before all preserved deformation.

Prior to or in the initial stages of deformation, the supracrustal sequence was intruded by tonalitic orthogneiss protolith. A schematic crosscutting body is shown in figure 9A. Early deformation generated S1 and caused stretching, thinning, rotation, and probably tansposition of most lithologic contacts (figs. 9B and C). This is designated D1 in figure 9, but there could have been multiple events. It is likely that strong gradients in competency led to the disruption, thinning and boudinage of ultramafic units within the enclave, leading to early formation of a tectonic mélange (*Au*) of amphibolite host with ultramafic blocks of varying size. Amphibolite in which these blocks are absent (*Am*) may thus simply be relicts of thicker zones in the original stratigraphy that had no interstratified ultramafic layers. It is likely that D1-style deformation at least partly preceded the emplacement of the Ameralik dike (E, fig. 3) because the dike crosscuts S1-parallel lithologic contacts. However, minerals in the dike and supracrustal rocks indicate similar metamorphic grade, and foliation in the dike is locally subparallel to S1 (fig. 2). This probably reflects later deformation and metamorphism, which rotated fabric into near parallelism and produced similar metamorphic assemblages.

After D1, D2 generated a tight, isoclinal F2 fold (figs. 9D and E). D3 subsequently formed a tight, asymmetric fold at a high angle to the crosscutting relation involving *Ogn-1*. Preferential strain accommodation in the east limb of F3 led to thinning, disaggregation, and layer-parallel transport that obscured lithologic contacts (fig. 9G). By contrast, lower strain in the western limb of F3 led to preservation of pre-D2 and -D3 history (fig. 9H).

D3 largely predated the emplacement of leucogranite veins and sheets. In the western limb of the F3 fold, these igneous rocks are unfoliated and crosscut all lithologic contacts and structures. Several of these bodies crosscut the inferred position of the F3 fold and they appear not to be deformed by the minor parasitic D3 folds (fig. 2). Their orientations are generally at high angles to the dominant fabric, though they exhibit minor folding. Thus, it appears that these bodies were emplaced primarily after D3 deformation, although minor D3 or later deformation may have postdated leucogranite emplacement in the east limb of F3. Late deformation (D4; Chadwick and Nutman, 1979; Myers and Crowley, 2000) warped F3 fold axes in regional, open folds with NE–SW axial surfaces; these structures are not evident at the scale of mapping in this study.

*Comparison to previous results.*—Our deformation history, mapped over a small area, is consistent with regional mapping by Chadwick and Nutman (1979). They recognized a regional D1 event that predated Ameralik dike emplacement, which would appear to correlate with our D1. Chadwick and Nutman's D2 and D3 correspond to post-Ameralik-dike thrusting, and major folding and nappe development, respectively. However, the Akilia supracrustals show no evidence of thrusting. Either Akilia D2 represents folding associated with the regional D2 thrust event and the Akilia and regional D3's are the same, or the Akilia D2 and D3 represent a continuum of deformation developed during Chadwick and Nutman's regional D3 event.

Our results yield new insight into the geometric relations and division of lithologic units, which help to give a clearer picture of the strain distribution and structural geometry preserved in the supracrustal enclave. This leads to interpretations that differ from previous results in several important respects. First, we recognize a strong strain gradient across the F3 fold hinge, which explains the better preservation of geometric relations—including the key outcrop of Mojzsis and others (1996; sample G91-26; archival number ANU92-197), Fedo and Whitehouse (2002), Whitehouse and Fedo (2003) and Dauphas and others (2004) (figs. 3 and 4A)—in the western part of the

map area where D3 strain is low. It also helps guide the search for useful geometric relations.

The new observations also depart from previous work (Nutman and others, 1997; Myers and Crowley, 2000; Friend and others, 2002a; Nutman and others, 2002) in that we noted a systematic variation in the distribution of ultramafic blocks within amphibolites that led to distinction of unit *Am*. This previously unrecognized layer provides a crucial additional marker for the structural evolution of the supracrustal lithologies.

The results clarify the distribution and history of the controversial *Qp* rocks. There are two discrete *Qp* bands that share the structural history experienced by the supracrustal amphibolites. Previous workers recognized but did not map other *Qp* outcrops in addition to the large body at the southern extreme of the peninsula (fig. 5A; Nutman and others, 1997; Myers and Crowley, 2000; Friend and others, 2002a; Nutman and others, 2002; Fedo and Whitehouse, 2002a; Whitehouse and Fedo, 2003). Our observations show that the exposures are not distributed randomly, but instead form two folded and attenuated layers that can be traced across the map area. The banding in the *Qp* rocks is metamorphic in origin as noted by Fedo and Whitehouse (2002a) and Whitehouse and Fedo (2003).

Perhaps the most important new insight into the geologic history is the location of the F2 hinge surface, which has important consequences for interpreting the geologic evolution of the Akilia supracrustals. Myers and Crowley (2000) placed the equivalent of the F2 hinge within *Ogn-1,* to the north of its location in figures 2 and 3 (see their fig. 3). In their interpretation, the *Ogn-1* sheet cores the F2 structure and terminates in a fold closure at locality D (fig. 3). If true, the *Ogn-1-Um* contact is likely younger than the *Ogn-1* crystallization age, precluding its use to constrain age of the adjacent rocks. However, three observations indicate that this cannot be the correct geometry. First, *Ogn-1* rocks can be traced beyond locality D to the western coast, such that they must crosscut the lithologic contact between *Um* and *Au* (figs. 2 and 3). The interpretation that *Ogn-1* extends to the coast is supported by geochemistry and zircon geochronology (see below). In addition, the Myers and Crowley (2000) interpretation is inconsistent with the distribution of lithologic contacts and other observations pointing to the location of the F2 hinge as shown in figures 2, 3, and 7B. Finally, the dike interpreted to be of Ameralik affinity (E, fig. 3) predates F2 and postdates the juxtaposition of *Ogn-1* and supracrustal rocks. If *Ogn-1* was in contact with supracrustal rocks before F2, this contact cannot be generated by F2 folding, as suggested by Myers and Crowley (2000). Instead, the juxtaposition of *Ogn-1* with supracrustal rocks evidently predates Ameralik dike emplacement, and appears to display geometric relations similar to those reported elsewhere in the Itsaq Gneiss Complex (Nutman and others, 1997, 2000, 2002).

## WHOLE-ROCK GEOCHEMISTRY

### *Major Oxides and Trace Elements*

Representative whole-rock analyses are given in table 1. The bulk composition of amphibolite sample GR0033 from *Au* (table 1; fig. 3) is basaltic (fig. 10A), with total REE slightly greater than mafic rocks from Isua (Polat and others, 2003) and the Akilia mafic rock of Nutman and others (1996). Sample GR0033 has a flat chondrite-normalized REE pattern ($La/Yb_N = 0.91$) and a minor negative Eu anomaly.

Ultramafic blocks in *Au* have Mg/Si and Al/Si of peridotitic to basaltic komatiites (fig. 10A). These compositions are similar to amphibolites and ultramafics of Akilia-type supracrustals (Nutman and others, 2002). No compositions suggesting mafic cumulates were noted (fig. 10A). Chondrite normalized REE patterns (fig. 10B) are similar to samples of Fedo and Whitehouse (2002a). As with mafic rocks, total REE in *Um* are higher than at Isua (Dymek and others, 1988). Samples within 0.4 m of the

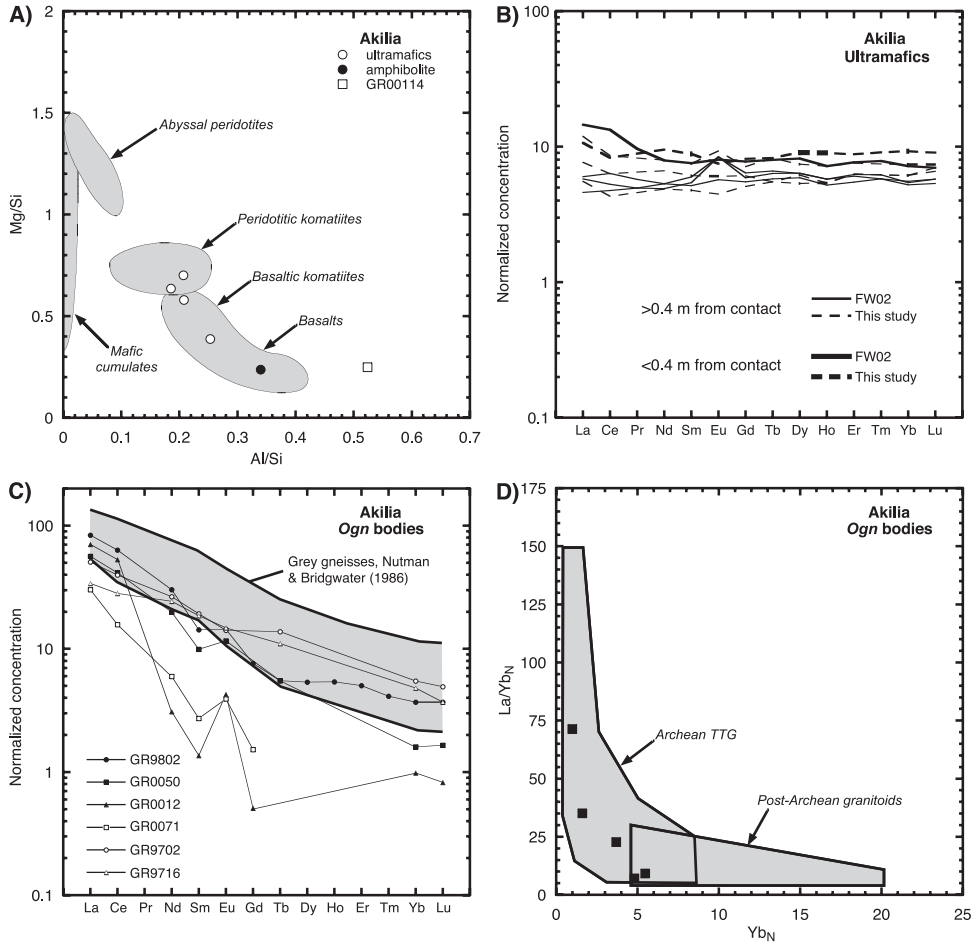


Fig. 10. Whole-rock geochemistry of amphibolites, ultramafic rocks, anthophyllite-garnet rock, and *Ogn* bodies. (A) Mg/Si vs. Al/Si for mafic, ultramafic and possible metasedimentary rocks from Akilia supracrustals. Data are from table 1 and sample locations in figure 3. Fields are taken from Nutman and others (2002). (B) Chondrite-normalized REE patterns of Akilia ultramafics (Fedo and Whitehouse, 2002a, and table 1). Samples <0.4 m from contact with *Qp* band show LREE enrichment. [Fedo and Whitehouse (2002a) samples other than AK05 assumed to be >1 m from contact]. (C) Chondrite-normalized rare-earth element patterns of *Ogn* bodies (table 1; fig. 3). (D) Chondrite-normalized La/Yb vs. Yb of Ogn bodies. Fields after Martin (1986). Normalizations to CI chondrite (Anders and Grevesse, 1989).

contact with *Qp* gneiss show elevated total REE and LREE enrichment, suggesting local REE mobility.

Bulk compositions of *Qp* rocks are strongly enriched in Fe (Fe# = 60-83, table 1 and Fedo and Whitehouse, 2002a). $SiO_2$ is high but variable due to different relative abundances of pyroxene and quartz. These observations led to early suggestions of a sedimentary iron-formation protolith (Bridgwater and others, 1976). However, major-element compositions differ in detail from typical quartz-oxide iron formations of Archean to Early Proterozoic age (fig. 11). For example, comparison with quartz-magnetite banded iron formation (BIF) from Isua and Kuruman, South Africa (figs. 11A and 11B), reveals higher MgO, CaO and $Na_2O$ in average *Qp* gneisses and average pyroxene-rich bands on a volatile-free basis. However, bulk compositions of various BIF

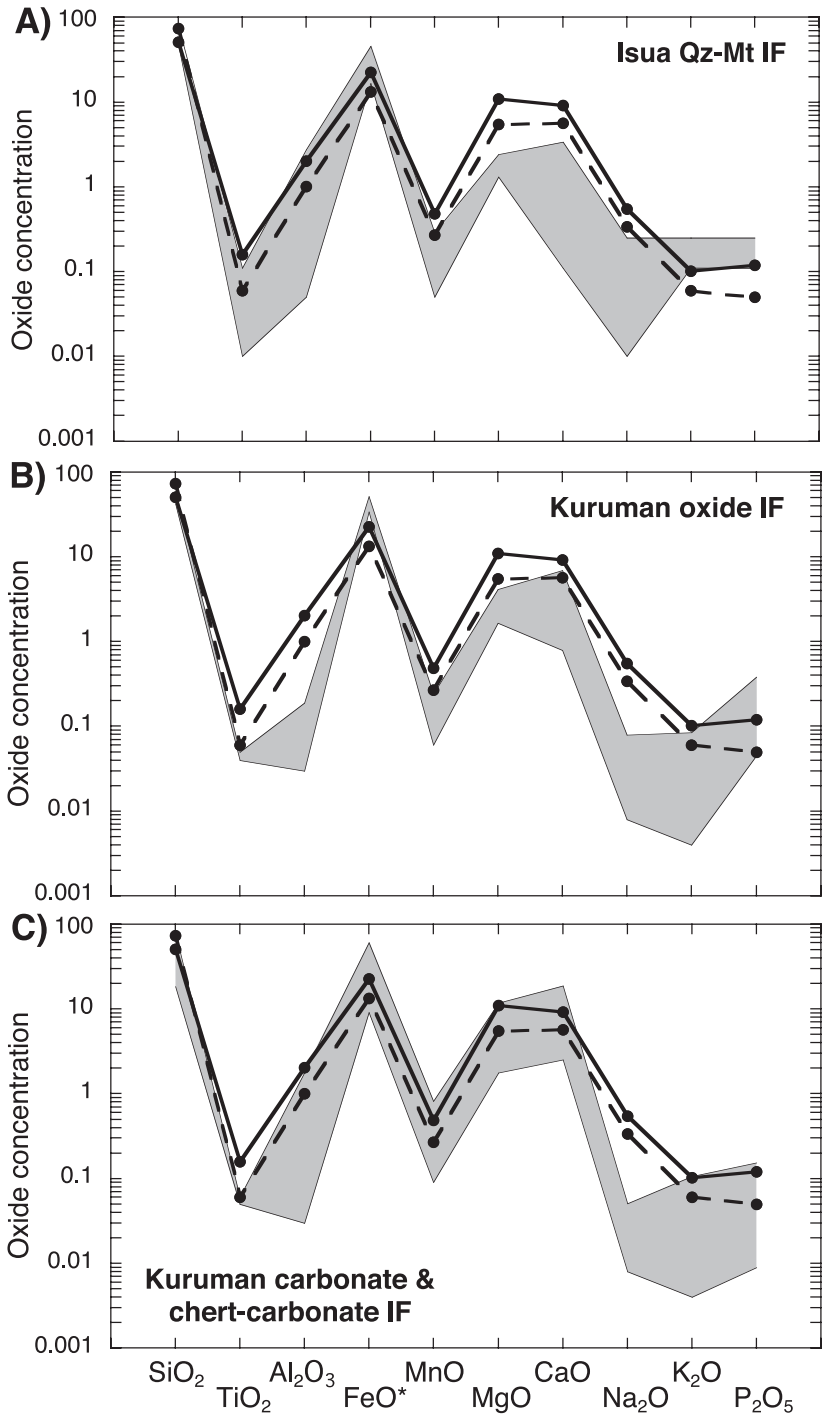


Fig. 11. Comparison of major and minor oxides in pyroxene bands (solid) and quartz-pyroxene rocks (dashed) from the Akilia *Qp* gneisses (table 1 and Fedo and Whitehouse, 2002a) with Isua quartz-magnetite iron formation (IF) (A) and Kuruman, South Africa, oxide iron formation (B) and carbonate and chert-carbonate iron formation (C) (Dymek and Klein, 1988; Klein and Beukes, 1989). Comparsions based on oxide wt % recalculated on a volatile-free basis.

types differ. Relatively high MgO and CaO are characteristic of carbonate and chert-carbonate iron formation (fig. 11C). Differences in $TiO_2$ and $Al_2O_3$ could reflect minor detrital input—as is widely noted in iron formations—and $Na_2O$ enrichment might have been the result of mobility during metamorphism. Thus, based on major elements alone, a plausible *Qp* protolith would be minor, local deposits of ferruginous, siliceous chemical sediment formed among extrusive mafic and ultramafic lithologies, with bulk compositions broadly similar to some iron formations. However, Whitehouse and Fedo (2002a) proposed a metasomatic origin for *Qp* rocks based on figure 11A and other trace elements and REE, which could suggest an altered ultramafic protolith. We will discuss *Qp* geochemistry in greater detail when the two models are compared below.

The major-element composition of the anthophyllite-garnet rock GR00114 (table 1; fig. 3) is distinctly different from the mafic and ultramafic rocks with which it is in contact, as well as from *Qp* rocks. It has high Al, Fe, and alkalis (including Rb), but low Si and Ca (table 1). Trace-element compositions other than Rb are intermediate between ultramafic and mafic compositions (table 1). Similarly, total REE are lower than amphibolite and *Qp* rocks, but higher than ultramafics, and chondrite-normalized pattern is flat ($La/Yb_N = 1.3$). When combined with superchondritic $Y/Ho = 55$, the composition suggests a sedimentary protolith composed of weathered or altered material locally derived from a mixed basaltic and ultramafic source, with possible incorporation of hydrothermal precipitates (Bau and Dulski, 1999).

Table 1 gives six analyses of orthogneiss samples from the map area. Sample GR9702 is a tonalite (Barker, 1979) from the host gneiesses at the eastern contact. The normalized REE pattern lies in the field for previously studied gray gneisses from the Itsaq Gneiss Complex (fig. 10C; Nutman and Bridgwater, 1986). Three samples interpreted to be part of *Ogn-1* were analyzed. GR0050 and GR9802 from the main portion of the sheet have similar bulk compositions (table 1) at the boundary between tonalite and trondhjemite (Barker, 1979). The samples are LREE enriched and similar in total REE and $La/Yb_N$ to Amîtsoq Gneisses and other Archean TTG (for example, O'Nions and Pankhurst, 1974; McGregor, 1979; Nutman and Bridgwater, 1986; Nutman and others, 1999; fig. 10D). Sample GR0012 is a small sheet within ~10 cm of the main *Ogn-1* body (fig. 8A); its lower REE abundance (fig. 10D) and strong enrichment of La and Ce relative to MREE suggests REE mobility. Nutman and Bridgwater's (1986) metasomatized sample 236961 is similar. A sample of *Ogn-2* (GR0071; figs. 3 and 8B) has lower total REE but does not show the same disturbed REE pattern as GR0012.

Leucogranitoid sample GR0009 from the large crosscutting *Lg* body in the southern part of the map area (fig. 2) is high in silica and $Na_2O$ but depleted in other oxides (table 1). Normative modes are trondhjemitic (Barker, 1979).

### *Oxygen-Isotope Geochemistry*

Table 2 gives whole-rock oxygen-isotope compositions of amphibolite, ultramafic rock, *Qp* gneiss along an ~10 m SW-NE transect across the quartzite at the southern tip of the peninsula (fig. 3). The transect is in the low-strain limb of the main F3 fold, near the section measured by Fedo and Whitehouse (2002a). Also included are data from *Ogn* samples. The amphibolites and ultramafics have $\delta^{18}O$ (SMOW) of 6.9 to 8.6 permil, with mean values of 7.6 ± 0.9 and 7.3 ± 0.3 permil (1σ). *Ogn* rocks have $\delta^{18}O$ similar to amphibolite and ultramafic rocks, with a mean of 8.0 permil (table 2).

Three aliquots of *Qp* sample ANU92-197 (fig. 3) have higher values of 11.9 to 13.2 permil, with an average of 12.6 ± 0.7 permil. The range in values is likely due to different proportions of quartz and pyroxene. The Akilia *Qp* sample is at the low end of the 12.9 to 20.4 permil range of Isua BIF (Perry and others, 1978) and within the range predicted for chert of this age (Knauth, 1992). If *Qp* rocks were originally Fe-Si-rich

TABLE 2

*Whole-rock oxygen isotope data for Akilia lithologies*

| Sample | Lithology | $\delta^{18}O_{SMOW}$ (‰) | Distance from *Qp* contact (m) |
|---|---|---|---|
| GR0014 | ultramafic | 7.4 | 3.5 |
| GR0019 | ultramafic | 7.1 | 1.6 |
| GR0020 | ultramafic | 7.1 | 2.1 |
| GR0028 | ultramafic | 7.1 | 5.1 |
| GR0029 | ultramafic | 7.9 | 5.0 |
| GR0030 | ultramafic | 7.4 | 0.3 |
| GR0031 | ultramafic | 7.3 | 1.0 |
| GR0024 | amphibolite | 8.6 | -1.5 |
| GR0026 | amphibolite | 7.2 | -5.0 |
| GR0033 | amphibolite | 6.9 | 6.0 |
| ANU92-197 | *Qp* gneiss | 11.9 | |
| ANU92-197A | *Qp* gneiss | 13.2 | |
| ANU92-197B | *Qp* gneiss | 12.8 | |
| GR9702 | *Ogn* tonalite | 8.2 | |
| GR9716 | *Ogn-4* tonalite | 8.3 | |
| GR9802 | *Ogn-1* tonalite | 7.2 | |
| GR0009 | *Lg* trondhjemite | 8.3 | |

*Notes:* Analytical error is ±0.2‰. Oxygen isotopes in silicates analyzed by the $BrF_6$ method, and reported in permil (‰) relative to standard mean ocean water (SMOW). Sample locations shown in figure 3. Amphibolite and ultramafic samples were projected onto SW-NE section (fig. 3); distances are relative to southern (negative) and northern (positive) contact. *Qp* lithology is ~3 m wide at this locality.

chemical sediments, it is sensible that they are similar to the least $^{18}O$-rich Isua BIF. The relatively small mass of *Qp* rocks compared to adjacent, low-$\delta^{18}O$ mafic and ultramafic lithologies could lead to $^{16}O$ enrichment via mechanical mixing (minor detrital input), or local fluid-rock interaction during diagenesis or metamorphism (Kalodny and Epstein, 1976; Jones and Knauth, 1979; Knauth, 1992).

## ZIRCON GEOCHRONOLOGY

We carried out ion-microprobe U-Pb isotopic analyses of zircons from two supracrustal lithologies (*Qp* and anthophyllite-garnet rock), and four samples of *Ogn* bodies from the low-strain region of the enclave. Analytical methods and data tables are given in the Appendix.

### *Quartz-Pyroxene Rock*

We collected ~10 kg of *Qp* rock (sample GR9713, fig. 3). Zircon yields were very low (~10 zircons/kg sample). Grains are equant/stubby, rounded and rarely >100 μm in the longest dimension (fig. A1). Interiors are dark or turbid, in contrast to generally lighter, featureless margins and terminations.

Seventy-six analyses of 46 zircon grains were collected in two analytical sessions (table A1, fig. 12A). Radiogenic $^{206}Pb$ is >99.5 percent. Pooled results from both sessions yield $^{207}Pb/^{206}Pb$ ages that range from 1878 to 3638 Ma, with clusters of largely concordant ages at ~3600 Ma and ~2700 Ma. Discordant ages are generally consistent with a mixing line between these two groups, with the exception of six analyses that are strongly discordant (≥10% difference between $^{207}Pb/^{206}Pb$ and $^{238}U/^{206}Pb$ ages; fig.

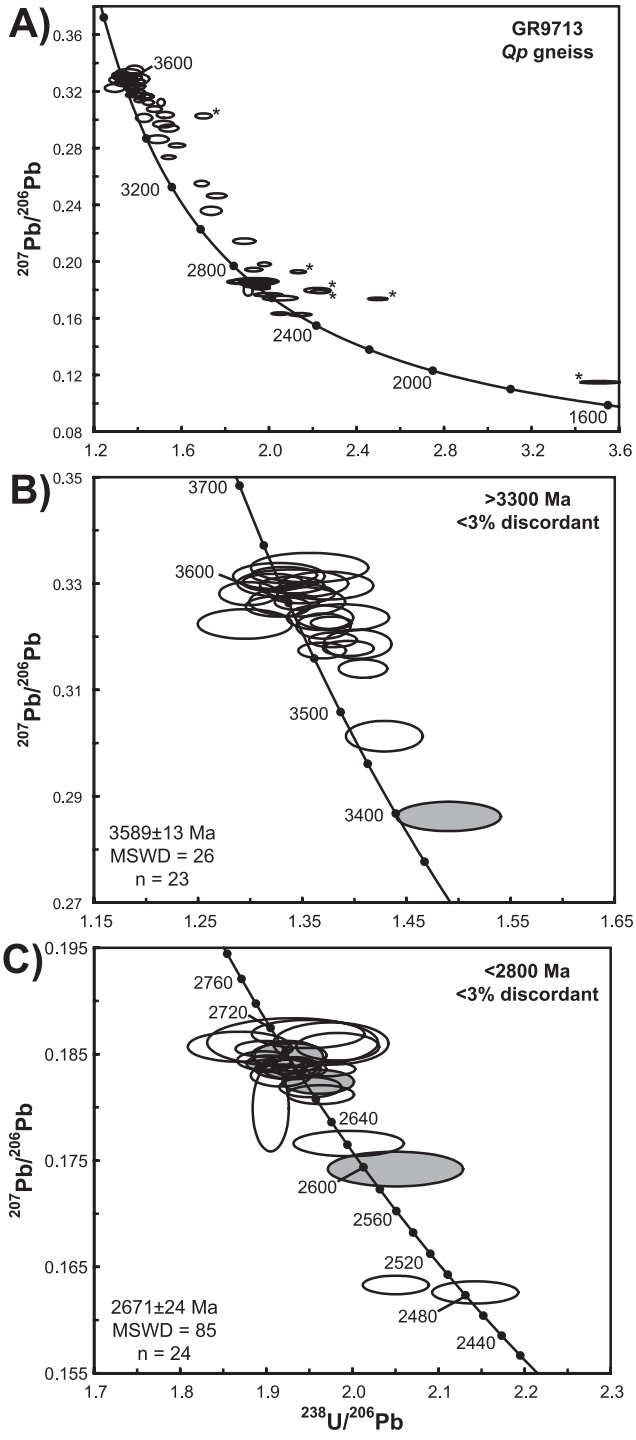


Fig. 12. Results of U-Pb analysis of zircons, *Qp* gneiss sample GR9713 (fig. 3). (A) Tera-Wasserburg diagram showing results from analysis sessions 1 and 2 (table A1). (B) Analyses with >3300 Ma $^{207}Pb/^{206}Pb$ ages and <3% discordance. (C) Analyses with <2800 Ma $^{207}Pb/^{206}Pb$ ages and <3% discordance. Error ellipses reflect 1σ absolute error. Shaded ellipses in (B) and (C) denote analyses from grain margins, open ellipses from grain interiors. Asterisks in (A) identify strongly discordant ages noted in text. Concordia shown by solid line, with selected ages (filled circles) identified in Ma.

12A). Ion-probe spots located near grain margins ("rims", table A1) yield ages no older than 3397 ± 10 Ma (all errors are 2σ), but otherwise yield a distribution of ages similar to analysis spots located in grain interiors.

The age of the older population of analyses was assessed by calculating weighted mean $^{207}Pb/^{206}Pb$ ages of spots from grain interiors as a function of discordance using an initial cutoff of 5 percent discordance. This initial cutoff was selected because all $^{207}Pb/^{206}Pb$ ages between 2800 and 3300 Ma are >5 percent discordant and define a mixing line between the ~3600 and ~2700 Ma age clusters (fig. 12A; table A1). The weighted mean $^{207}Pb/^{206}Pb$ age of the thirty three >3300 Ma spots having ≤5 percent discordance is 3570 ± 22 Ma (95% confidence interval). The mean square of weighted deviates (MSWD) is 112, indicating scatter well outside the analytical uncertainties. Reducing the maximum discordance to <3 percent gave 3589 ± 13 Ma (MSWD=26; fig. 12B). The large reduction of MSWD is due to exclusion of one outlier (311-1, table A1) and a weak correlation between age and discordance at 3 to 5 percent discordance. Further reduction of the maximum discordance yielded the same weighted-mean ages within uncertainty, and a minimum MSWD of 14. We take the 3589 ± 13 Ma of the <3 percent discordant spots as the best estimate of the older zircons of sample 9713, but we note that the high MSWD regardless of extent of discordance suggests inclusion of multiple age groups (see below).

The age of the younger population of zircons was evaluated using the same approach. The weighted mean $^{207}Pb/^{206}Pb$ age of the <2800 Ma spots (n=25) with <5 percent discordance is 2674 ± 24 Ma (95% confidence interval), with MSWD = 91. Reducing the discordance cutoff to <3 percent gave 2671 ± 24 Ma (MSWD = 85, n = 24; fig. 12C). Further decrease in maximum discordance did not change weighted mean ages within uncertainty and MSWD remained high. As with the older population, the high MSWD of the <2800 Ma zircon population in the quartz-pyroxene rock suggests inclusion of multiple age groups.

### *Anthophyllite-Garnet Rock*

As noted above, an anthophyllite-garnet-bearing rock within *Au* has a distinct bulk composition that suggests a sedimentary protolith. Sample GR00114 (fig. 3) had a low yield of zircon that was similar in texture to those from *Qp* sample GR9713: they are small and equant, with brownish turbid centers with clear translucent rims (fig. A2). Cores of ten grains yield two clusters of nearly concordant ages at ~3600 Ma (8 analyses) and ~2700 Ma (2 analyses) (table A1, fig. 13). The older group yields a weighted mean $^{207}Pb/^{206}Pb$ age of 3616 ± 28 Ma (MSWD = 16). As with the *Qp* rock, the high MSWD suggests inclusion of multiple age groups in the population. The two younger zircons have a midpoint $^{207}Pb/^{206}Pb$ age of 2715 Ma.

### *Ogn Bodies*

*Ogn-1.*—Zircons were separated from three samples (GR9802, GR0012 and GR0050) of the east-west trending "arm" of *Ogn-1* (fig. 3). Zircons from all three samples are dominantly prismatic to bipyramidal, have high aspect ratios, and range from 50 to 200 μm in length. A small fraction (<5%) is non-prismatic, and stubby to equant in habit. In transmitted light, they range from clear and structureless to brownish.

Sample GR9802 is a gray, tonalitic orthogneiss. We collected 61 analyses from 24 zircon grains in two analytical sessions (table A1, fig. A3). Analysis focused chiefly on grain interiors (46 of 61 analyses). Four analyses had <98 percent radiogenic $^{206}Pb$ and were not considered further. The pooled data set yields a cluster of near-concordant ages older than ~3600 Ma (fig. 14A). Approximately 70 percent of analyses with $^{207}Pb/^{206}Pb$ ages <3600 Ma are >5 percent discordant, and the extent of discordance increases weakly with decreasing age, suggesting Pb loss or partial analysis

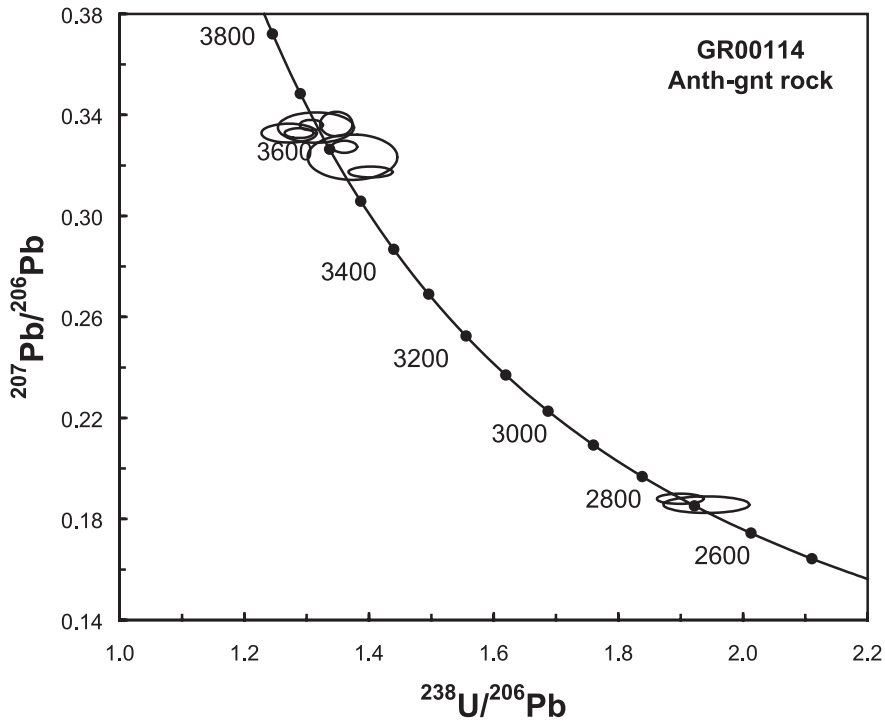


Fig. 13. Tera-Wasserburg diagram showing U-Pb ages of zircons from anthophyllite-garnet rock (sample GR00114; fig. 3; table A1). Symbols as in figure 12, caption.

of younger growth zones. The characteristics of the age distribution were therefore evaluated considering only those analyses showing <5 percent discordance (44 of 61, table A1).

Figures 14B and C show the age distribution and Th/U ratios of zircon analyses that are <5 percent discordant. The weighted mean $^{207}Pb/^{206}Pb$ age of all such analyses is 3674 ± 23 Ma (MSWD = 83). Consideration of grain interiors alone gives a similar age (3681 ± 29 Ma, MSWD = 95, n = 32). The irregular distribution of ages and high MSWD indicate multiple age populations. Calculation of the relative probability of ages reveals an older 3700 to 3760 Ma group or groups that is statistically distinct from <3700 Ma populations (fig. 14B). The older group has grain interiors with a weighted mean $^{207}Pb/^{206}Pb$ age of 3728 ± 8 Ma (MSWD = 4, n = 21), whereas <3700 Ma ages involve multiple populations with a weighted mean $^{207}Pb/^{206}Pb$ age of 3601 ± 54 Ma (MSWD = 105, n = 8). The mean Th/U ratios of the older and younger age groups differ. The mean Th/U of the >3700 Ma population is 0.25 ± 0.28 (1σ). In contrast, <3700 Ma ages yield bimodal Th/U, with two analyses showing very high mean Th/U of 1.8, whereas the rest are lower and significantly more scattered than the >3700 Ma population (mean Th/U = 0.12 ± 0.46).

Ion-microprobe analyses were also obtained from two additional samples of *Ogn-1*. Sample GR0050 is a massive, gray tonalitic orthogneiss from the westernmost exposure of *Ogn-1* (figs. 2 and 8). Analyses of interiors of two zircon grains (table A1, fig. A4) yield a concordant $^{207}Pb/^{206}Pb$ age of 3744 ± 7 Ma and a younger, discordant $^{207}Pb/^{206}Pb$ age of 3695 ± 19 Ma. Sample GR0012 is from an ~10 cm wide tonalitic gneiss sheet separated by 5 cm from the gray gneiss sheet from which GR0050 was

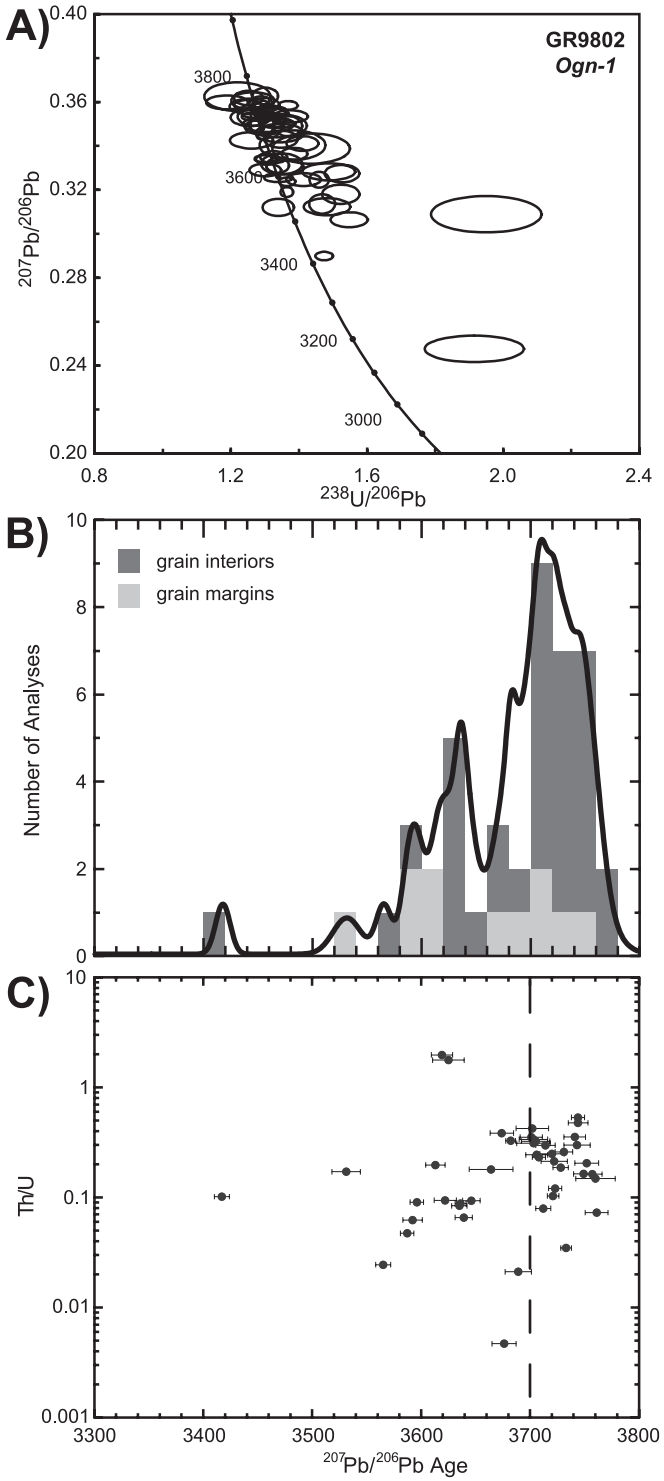


Fig. 14. Results of U-Pb analysis of zircons, *Ogn-1* sample GR9802 (fig. 3). (A) Tera-Wasserburg diagram showing results from analysis sessions 1 and 2 (table A1). Symbols as in figure 10, caption (analyses of grain interiors and margins not distinguished). (B) Histograms and relative probability (solid line) of $^{207}Pb/^{206}Pb$ ages. (C) $^{207}Pb/^{206}Pb$ age vs. Th/U ratio for zircons with <5% discordance (see text). Dashed line at 3700 Ma identifies break between older grains with high, more tightly clustered Th/U and younger grains with scattered Th/U (see text).

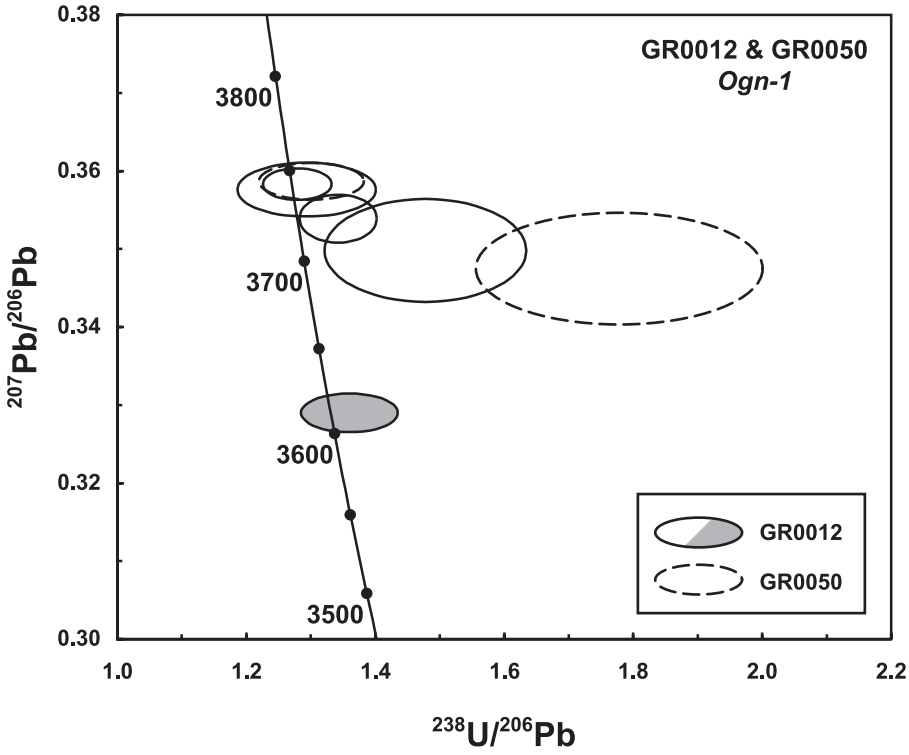


Fig. 15. Tera-Wasserburg diagram showing results of U-Pb analysis of zircons, *Ogn-1* samples GR0012 (solid elipses) and GR0050 (dashed ellipses). See figure 3 for sample locations and table A1 for data. Other symbols as in figure 12, caption.

taken (fig. 8). The intervening lithology is *Au*. Four analyses of zircon interiors (fig. A4) are concordant to slightly discordant (fig. 15), and give a weighted mean $^{207}Pb/^{206}Pb$ age of 3736 ± 8 Ma (MSWD = 2, n = 4). One rim has a younger $^{207}Pb/^{206}Pb$ age of 3613 ± 8 Ma.

*Ogn-2.*—Zircons were separated from *Ogn-2* sample GR0071 (figs. 3 and 8B). Twenty-nine measurements of 25 zircons (table A1, fig. A5) gave >98 percent radiogenic $^{206}Pb$ in all analyses. $^{207}Pb/^{206}Pb$ ages chiefly from grain interiors range from 3562 to 3845 Ma (fig. 16A). Because of somewhat high $^{238}U/^{206}Pb$ uncertainties (fig. 16A), some analyses showing 5 to 10 percent discordance are concordant at the 2σ level. The age distribution was therefore evaluated using those analyses showing <10 percent discordance (n = 22), rather than <5 percent as in previous samples. The distribution of $^{207}Pb/^{206}Pb$ ages shows a distinct group at >3768 Ma with the highest relative probability (fig. 16B). This population has a weighted mean $^{207}Pb/^{206}Pb$ age of 3810 ± 12 Ma (MSWD = 7; n = 13). In addition, two analyses give $^{207}Pb/^{206}Pb$ ages between 3700 to 3730 Ma, and seven yield ~3560 to 3660 Ma.

A depth-profiling study was undertaken on GR0071 grain #36 (table A2, fig. A5) to better constrain the ages recorded by this sample (see Appendix for methods). Continuous sputtering of ~30 μm from the outermost grain surface yielded age zones that increased with depth in the crystal (fig. 17A). The outer zone (<5 μm depth) gave a well-defined $^{207}Pb/^{206}Pb$ age of 2664 ± 26 Ma (MSWD = 2.2). An intermediate zone (5.0 – 10.1 μm depth), in which age varies continuously with depth, is interpreted to result from mixing of age populations as the ion beam sputtered across an inclined

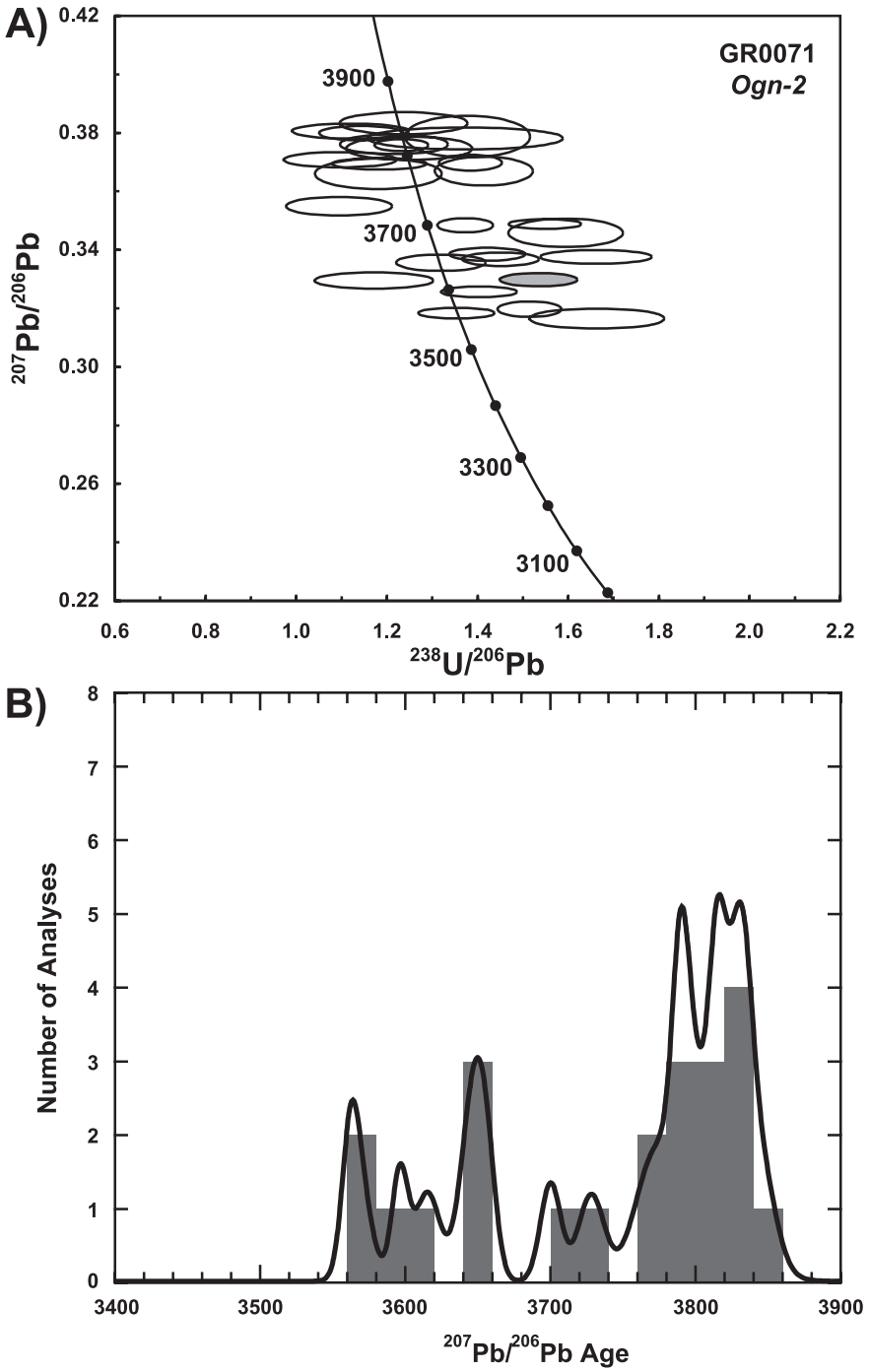


Fig. 16. Results of U-Pb analysis of zircons, *Ogn-2* sample GR0071 (fig. 3; table A1). (A) Tera-Wasserburg diagram showing ages. Symbols as in figure 12, caption. (B) Histogram and relative probability (solid line) of $^{207}Pb/^{206}Pb$ ages.

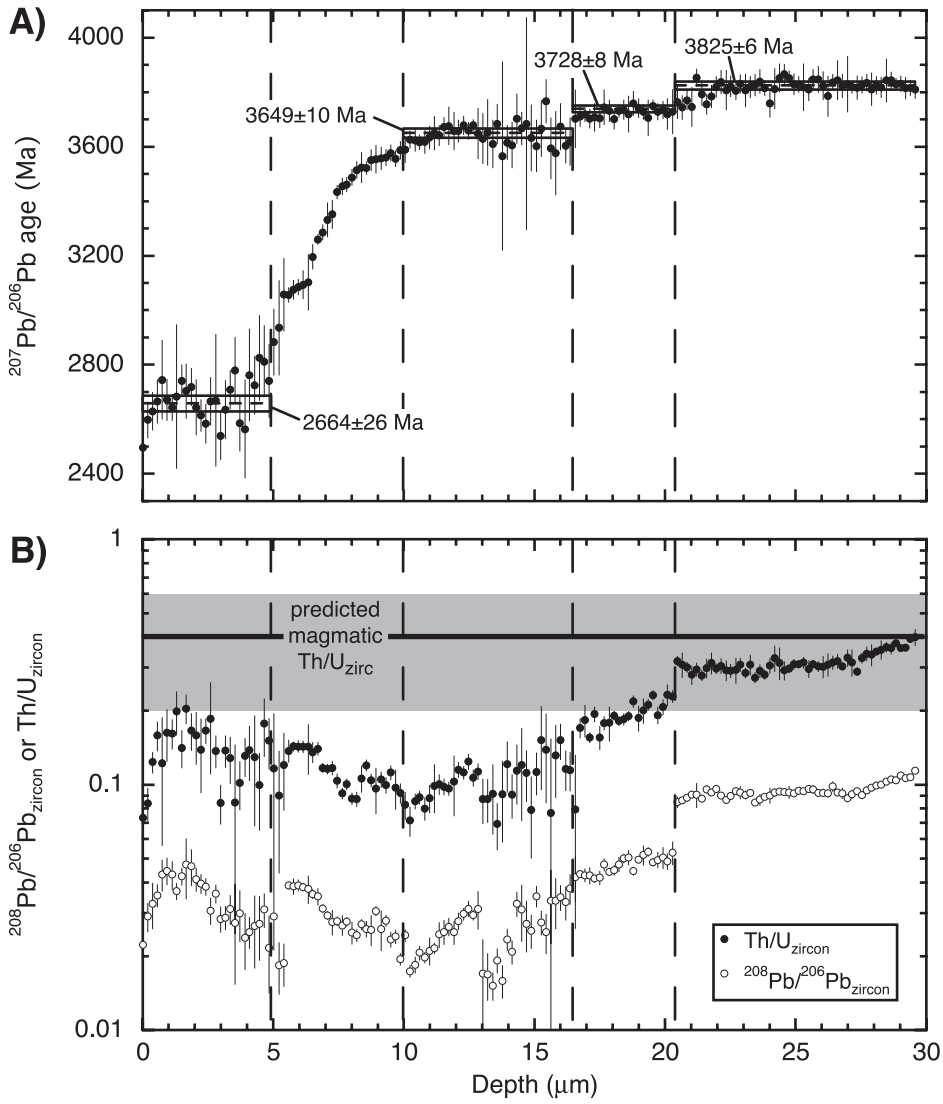


Fig. 17. Results of depth-profiling study of zircon grain #36, GR0071 (fig. A5; table A2). (A) $^{207}Pb/^{206}Pb$ age with depth, as estimated from number of cycles divided by total pit depth assuming constant sputtering rate. Dashed lines and boxes identify weighted mean $^{207}Pb/^{206}Pb$ age and 2σ uncertainty of distinct zones. (B) Variation in zircon Th/U (filled circles) and $^{208}Pb/^{206}Pb$ (open circles) with depth. The bold line and shaded region highlight the predicted Th/U in zircon based on whole-rock Th/U = 2 (table 1) and a partition coefficient of 0.2 ± 0.1. Only the oldest analyzed zone is consistent with Th/U exchange equilibrium with the host rock.

interface because of continuous, correlated variation in Th/U and related $^{208}Pb/^{206}Pb$ (fig. 17B). At 10.1 μm depth, this mixed zone gives way to a region of constant $^{207}Pb/^{206}Pb$ age of 3649 ± 10 Ma (MSWD = 1.2) that extends to 16.4 μm. Two additional discrete zones can be identified in the core of the zircon: a region yielding a constant age of 3728 ± 8 Ma (MSWD = 0.79, 16.4-20.5 μm), which overgrew a central zone of 3825 ± 8 Ma (MSWD = 1.1, >20.5 μm).

## DISCUSSION

### *Origin and Age of Supracrustal Mafic, Ultramafic and Anthophyllite-Garnet Rocks*

With the exception of *Qp* rocks (discussed separately below), the mapped lithologies of the Akilia supracrustal enclave consist of mafic, ultramafic and minor anthophyllite-garnet rocks. The geochemical data of this and previous studies (McGregor and Mason, 1977; Nutman and others, 2002; Fedo and Whitehouse, 2002a) suggest that amphibolites and ultramafic rocks had basaltic or peridotitic- to basaltic-komatiite protoliths, respectively. The anthophyllite-garnet rock has major element, trace element patterns and Y/Ho implying a sedimentary protolith derived from mafic and ultramafic material and hydrothermal precipitates.

Independent of the ages of crosscutting *Ogn* bodies, a provisional minimum age of the supracrustal enclave can be established based on the supracrustal lithologies alone. In the absence of magmatic or detrital zircons in any of the supracrustal litholigies of the enclave, the rocks must be older than ~3510 to 3260 Ma, the age of Ameralik dikes of the region (McGregor, 1968; White and others, 2000; Nutman and others, 2004b), although the dike in figure 2 has not been dated. Metamorphic ages of zircons suggest an even older provisional minimum age of the supracrustal sequence (fig. 18). Based on textures and statistical analysis, Friend and Nutman (2005a) concluded that zircons from Akilia amphibolite grew during subsolidus metamorphism. Of their two zircon age populations, the older group has a weighted mean $^{207}Pb/^{206}Pb$ age of 3604 ± 10 Ma (MSWD = 28). Zircon textures in our GR00114 sample of anthophyllite-garnet rock are similar to those reported by Friend and Nutman (2005a). The zircons likewise yield two concordant $^{207}Pb/^{206}Pb$ age clusters at ~3600 Ma and ~2700 (fig. 18). The weighted mean $^{207}Pb/^{206}Pb$ age of the older group is 3616 ± 28 Ma (MSWD = 16), which is statistically indistinguishable from the older group of Friend and Nutman (2005a). The ~3600 Ma age populations possess MSWD significantly greater than one, indicating scatter outside the analytical uncertainty, which Friend and Nutman (2005a) attributed to multiple high-grade metamorphic events between 3500 and 3700 Ma.

The similarity in the zircon textures and age populations among the Akilia supracrustal lithologies suggests juxtaposition and a shared history of zircon nucleation and growth. It is likely that zircon initially grew in these lithologies during the same metamorphic event or events, probably during breakdown of Zr-bearing silicates such as amphibole (for example, Fraser and others, 1997). The younger zircon population at 2600 to 2700 Ma (fig. 18) records Late Archean recrystallization, ripening, or new growth. Thus, zircon growth in supracrustal lithologies is best interpreted as metamorphic, and the age populations are consistent with regional granulite (~3600 Ma) and amphibolite (~2700 Ma) metamorphism (Friend and Nutman, 2005a). Regardless of the interpretation of *Ogn* crosscutting relations, it is clear that Akilia supracrustal rocks are at least ~3600 Ma.

### *Origin and Age of Orthogneiss Bodies*

Our geologic observations suggest that *Ogn-1* and *Ogn-2* represent two crosscutting igneous bodies preserved within the supracrustal enclave, consistent with results of Nutman and others (1996, 1997, 2000, 2002). In the case of *Ogn-1,* the geologic relations involve correlating individual outcrops through an area of incomplete exposure. The inferred correlation is supported by bulk chemical and U/Pb zircon data. Three samples of *Ogn-1* are tonalite/trondhjemite with broadly similar normative Ab-Or-An, and as a group have lower normative An than tonalites *Ogn-2* (GR0071), *Ogn-4* (GR9716) and GR9702 from the Amîtsoq Gneisses at the enclave's margin (table 1).

The zircon data also support the outcrop correlation used to define the geometry of *Ogn-1*. Sample GR9802 yielded a tightly clustered high Th/U population of

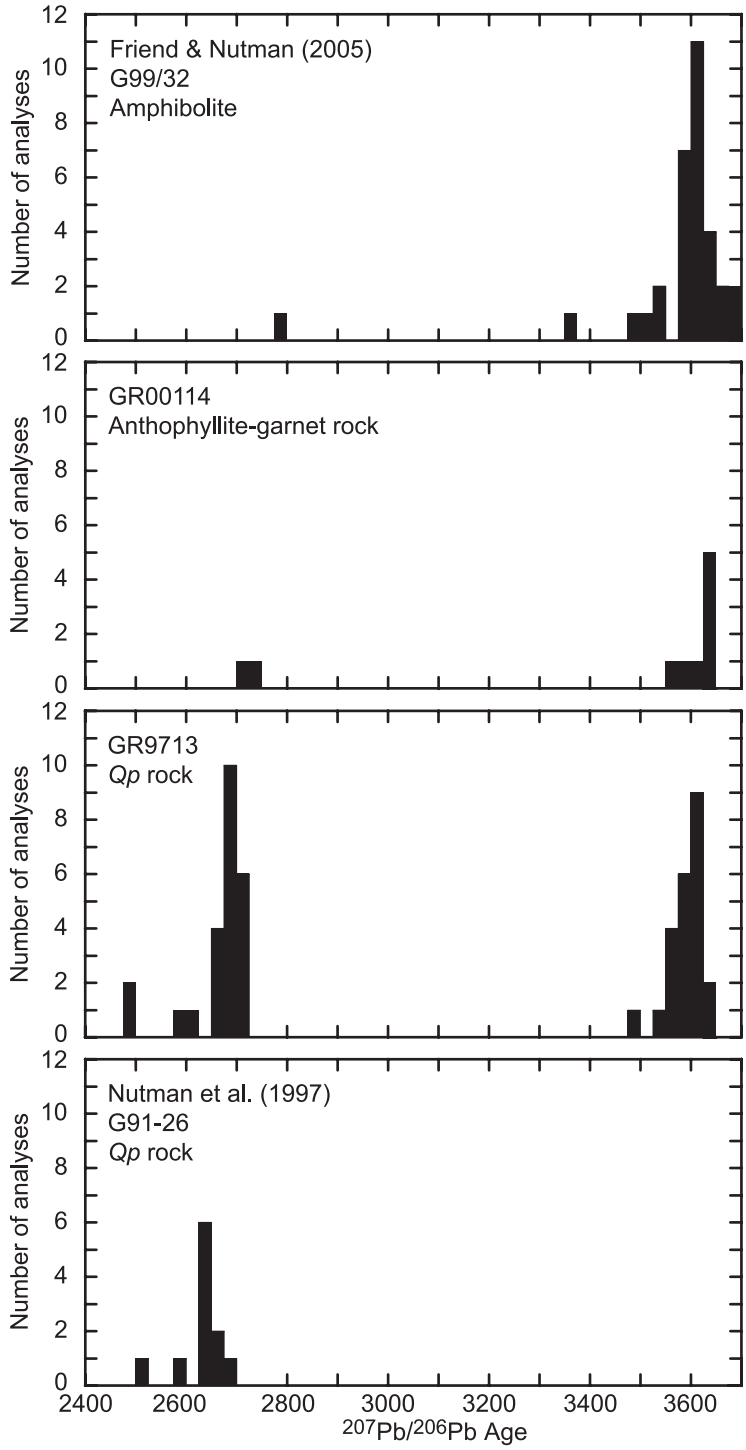


Fig. 18. Histograms of $^{207}Pb/^{206}Pb$ ages of zircons from supracrustal lithologies, including *Qp* gneiss (GR9713, this study, and G91-26, Nutman and others, 1997), anthophyllite-garnet rock (GR0014, this study), and amphibolite (G99/32, Friend and Nutman, 2005a).

$^{207}Pb/^{206}Pb$ ages for grain interiors of 3728 ± 8 Ma. This agrees reasonably well with analyses from *Ogn-1* samples GR0012 (3736 ± 8 Ma) and GR0050 (3744 ± 7 Ma), although the smaller number of analyzed grains in the latter samples precludes direct comparison of populations. Combination of all analyses of grain interiors with <5 percent discordance in the three samples gives a weighted mean $^{207}Pb/^{206}Pb$ age of 3730 ± 7 (MSWD = 4, n = 26), indicating that the mean age and population characteristics of the combined data are the same as for sample GR9802 alone. It is significant that none of the samples yields cores >3761 Ma (GR9802, analysis 212-2, table A1). The common occurrence of >3800 Ma zircon cores in the Amîtsoq Gneisses regionally, as well as in *Ogn* tens of meters away within the enclave (*Ogn-4:* Nutman and others, 1997, 2000; Mojzis and Harrison, 2002a; Whitehouse and Kamber, 2005; *Ogn-2:* this study), suggests that *Ogn-1* represents a discrete magmatic phase with a distinct population of ~3730 Ma zircon cores. Thus, the combination of bulk composition and zircon data support the inferred consanguinity of GR9802, GR0050 and GR0012, which requires that *Ogn-1* crosscut the lithologic contacts shown in figures 2 and 3.

*Ogn*-2 also shows evidence for magmatic crosscutting relations. Spot analyses of zircon grain interiors yielded multiple $^{207}Pb/^{206}Pb$ age groups of 3560 to 3660, 3700 to 3730, and 3810 ± 12 Ma. The same ages are recorded by an individual zircon, as revealed by depth profiling, in which three interior regions gave weighted mean $^{207}Pb/^{206}Pb$ ages of 3649 ± 10, 3728 ± 8, and 3825 ± 6 Ma (fig. 17). The oldest portion of the crystal is characterized by a high and roughly constant Th/U of ~0.3. In addition, the depth profile revealed a narrow margin of the zircon with a $^{207}Pb/^{206}Pb$ age of 2664 ± 26Ma.

Crosscutting igneous origins for *Ogn-1* and *Ogn-2* mean that their magmatic age gives a minimum estimate for the rocks they crosscut. However, the identification of which age population within these complexly zoned zircons corresponds to the crystallization age is controversial. Before discussing magmatic ages of *Ogn-1* and *Ogn-2* bodies, we review previous results on *Ogn-4* in the NW part of the enclave, which has been investigated in greater detail.

*Previous studies of Ogn-4.*—Irrespective of the debate about crosscuting relations involving *Ogn-4* (fig. 3; Nutman and others, 1997; Myers and Crowley, 2000), the use of zircon geochronology to establish its age has led to different interpretations. One model holds that zircon cores precipitated from a melt possessing the bulk composition of their host rock (Nutman and others, 1996, 1997, 2000; Mojzsis and Harrison, 2002a). In this *in-situ* growth model, the zircon cores would have crystallized either in the crustal magma chamber from which the crosscutting vein was sourced or in the vein itself, whereas younger portions grew during later metamorphic episodes which may have involved partial melting. The zircon cores show bright cathodoluminescence (CL), oscillatory zoning, and are typically euhedral (Whitehouse and Kamber, 2005). Recent, carefully constrained ages determined for zircon cores from samples of *Ogn-4* tonalitic gneiss all agree at 3841 ± 6 Ma (Nutman and others, 2000), 3828 ± 8 Ma (Mojzsis and Harrison, 2002a) and 3842 ± 5 Ma (Whitehouse and Kamber, 2005, group 1A). Rims and equant CL-dark grains yield younger ages of ~3700 to 3500 and ~2700 to 2500 Ma, which correlate with regional metamorphic events and are interpreted to reflect zircon growth during metamorphism perhaps with local anatexis. The primary support for this model is that zircon cores have high Th/U that yield distribution coefficients of 0.13 to 0.26 relative to bulk rock Th/U (Mojzsis and Harrison, 2002a; Whitehouse and Kamber, 2005), consistent with a zircon-melt distribution coefficient of 0.2 ± 0.1 in silicic rocks (Mahood and Hildreth, 1983; Mojzsis and Harrison, 2002a; Schmitt and others, 2003). In contrast, Th/U of zircon rims and CL-dark grains are lower, and calculated Th/U distribution coefficients are not consistent with magmatic zircon growth in equilibrium with the bulk rock. Supporting

the argument for *in situ* zircon growth at ~3840 Ma in *Ogn-4* are low whole-rock Zr contents, which yield low zircon saturation temperatures of ~750°C (Watson and Harrison, 1983; Mojzsis and Harrison, 2002a; Hanchar and Watson, 2003; table 1), significantly below the temperature expected for hornblende dehydration melting, the mechanism typically invoked for TTG generation (for example, Martin, 1986; Wyllie and others, 1997). Melt generation and emplacement at high temperature would minimize zircon inheritance (Harrison and Watson, 1983). Thus, in the *in-situ* growth model, the igneous age of *Ogn-4* is ~3840 Ma, consistent with results from similar bodies in other localities in the Itsaq Gneiss Complex (Nutman and others, 2000). Key assumptions are that magmas were produced by dehydration melting at temperature sufficiently high to preclude preservation of inherited zircon, that whole-rock Zr and Th/U have not been disturbed by later processes, and that calculated distribution coefficients between whole rock and zircon reflect exchange equilibrium at magmatic conditions.

In an alternative model for the age of *Ogn-4* (Whitehouse and others, 1999; Whitehouse and Kamber, 2003, 2005), the CL-bright euhdral cores were inherited during a voluminous ~3650 Ma magmatic event that precipitated zircon from tonalitic/granodioritic magma at this time. The xenocryst model was invoked in part to explain the inference based on Pb isotopes in feldspars that Amîtsoq Gneisses preserve no evidence for evolution in the crust prior to ~3650 Ma (Moorbath and others, 1997; Kamber and Moorbath, 1998). The xenocryst model is predicated on two assumptions. The first is that source melting did not occur by hornblende dehydration at high temperature. Trace-element data for Amîtsoq Gneisses have been interpreted to suggest water-saturated melting of the mantle wedge above an early Archean subduction zone (Kamber and others, 2002). Such melts could have entrained zircon xenocrysts while passing through the lower crust, and the probability of preservation would be high due to the assumed lower temperatures of $H_2O$-saturated melting. The second assumption is that Th/U ratios do not constrain zircon origin (Whitehouse and Fedo, 2005).

The xenocryst model is implausible for several reasons. In dismissing zircon Th/U constraints, Whitehouse and Fedo (2005) consider the ratio in zircon alone; however, the key constraint is in fact Th-U partitioning between zircon and melt (taken to be the bulk rock). Only the ~3840 Ma zircon cores have Th/U appropriate for magmatic exchange with their host rock, whereas the xenocryst model requires either that host-rock Th/U has shifted by a factor of ~100 relative to the value predicted for zircon-melt equilibrium (data from Mojzsis and Harrison, 2002a; Whitehouse and Kamber, 2005), or that zircons precipitated in extreme exchange disequilibrium with their host melt, while cores coincidently suggest apparent equilbrium with the whole rock. A second problem with the xenocryst model is that it invokes significant assimilation to explain the zircons, but assumes that trace elements nevertheless yield unmodified source characteristics (Kamber and others, 2002; Whitehouse and Kamber, 2005).

Rare-earth element data (Whitehouse and Kamber, 2005) lend additional support to the *in-situ* model for zircon growth in *Ogn-4* zircons. The ~3840 Ma cores have chondrite-normalized REE patterns with strong LREE/HREE fractionation, typical of igneous zircons. In contrast CL-dark, structureless zircons giving ~3600 Ma $^{207}Pb/^{206}Pb$ ages possess flat HREE patterns, consistent with exchange equilibrium with an HREE-fractionating mineral interpreted to be garnet. Whitehouse and Kamber (2005) argued that the latter zircons represent the age of *Ogn-4,* that the cores were inherited, and that garnet was present in the source region for the granodiorite hosting the zircons. However, for representative examples of these two populations (fig. 19), zircon-whole rock partition coefficients for cores are similar to magmatic values in

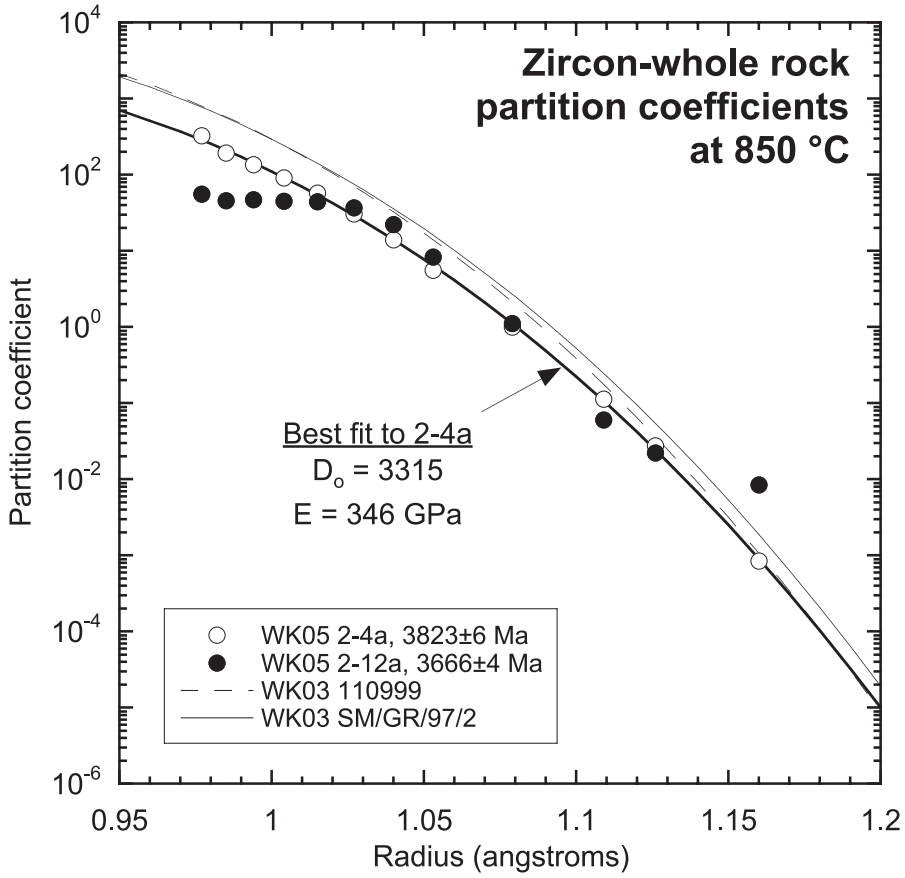


Fig. 19. Zircon-melt partition coefficients vs. radius of octahedrally coordinated trivalent REE, calculated from representative analyses of Whitehouse and Kamber (2005; WK05; Ce and Eu omitted) from *Ogn-4*. Open circles are for analysis 2-4a (3823 ± 6 Ma), from CL-bright, euhedral zircon core textural group, whereas filled circles are analysis 2-12a (3666 ± 4 Ma), from group of CL-dark featureless grains. The older analysis yields a parabolic functional form to the distribution coefficients calculated from bulk composition reported by Whitehouse and Kamber (2005). Assuming $r_o$ = 0.84 and 850 °C (Whitehouse and Kamber, 2003; WK03), a best fit to the lattice-strain equation of Blundy and Wood (1994) gives $D_o$ = 3315 and E = 346 GPa (see text). The best-fit parabola is in excellent agreement with other results from Amîtsoq Gneisses in the region (Whitehouse and Kamber, 2003). Analysis 2–12a could not have grown in exchange equilibrium with its host melt at equilibrium without either major REE mobility or violation of the assumptions of the lattice-strain equation, suggesting that the older zircon is the best estimate of crystallization age.

other Amîtsoq Gneisses (Whitehouse and Kamber, 2003) and yield typical lattice-strain parameters for mineral-melt exchange (Blundy and Wood, 1994; fig. 19). In contrast, the ~3600 Ma zircons interpreted to be magmatic do not yield the simple parabolic dependence of partition coefficient on ionic radius that should result from zircon growth from a melt with the composition of its host rock. If such zircons were in equilibrium with a TTG melt, that melt would have $La/Yb_N$ = 358 to 850 (parameters from fig. 19 and Whitehouse and Kamber, 2003), whereas maximum $La/Yb_N$ in Archean TTG rocks is roughly 150 (fig. 10D; Martin, 1986). Moreover, $La/Yb_N$ of the host rock must subsequently have shifted to its current value of 8.4; that is, by a factor of ~40 to 100. Given that flat HREE depletion is also characteristic of some ~2700 zircons, and that this depletion is more pronounced in zircons from *Ogn-4* than in

those from Amîtsoq Gneisses outside the enclave (Whitehouse and Kamber, 2002, 2003, 2005), it appears that, as with Th and U, REE in *Ogn-4* zircons show that only ~3840 zircon cores record exchange equilibrium with the host rock. The HREE depletion in younger zircon is simply explained by growth in the presence of garnet during ~3600 Ma granulite grade metamorphism and/or partial melting, and ~2700 Ma amphibolite facies recrystallization and deformation.

In summary, models for the magmatic age of the igneous rocks found within the Akilia enclave should satisfy to first order the geochemical constraints imposed both by zircon and its host rocks, unless evidence for disturbance exists. For *Ogn-4,* we find that only the CL-bright, oscillatory-zoned cores succeed, and that ~3840 Ma is therefore the best estimate of the magmatic age of the body.

*Ogn-1.*—The above approach can be used to assess the magmatic age of *Ogn-1.* Sample GR0012 has whole-rock Th/U = 3.8, and mean Th/U of zircon cores is 0.56, which gives a distribution coefficient of 0.14, consistent with magmatic values of 0.2 ± 0.1 (Mahood and Hildreth, 1983; Mojzsis and Harrison, 2002a; Schmitt and others, 2003). In contrast, GR0050 and GR9802 are characterized by lower U (table 1), and the latter sample has Th/U = 9. Zircon cores have Th/U of 0.62 and 0.21, respectively, giving much lower distribution coefficients of <0.02. The mean Th/U of the main group of <3700 Ma analyses in GR9802 is 0.08, which yields even lower bulk distribution coefficient. However, two <5 percent discordant rims yield Th/U = 1.8 ($^{207}Pb/^{206}Pb$ ages are 3619 ± 10 and 3625 ± 14 Ma), for a bulk distribution coefficient of 0.2. Given that selective leaching of U during high-grade metamorphism and partial melting (for example, Rollinson and Windley, 1980; Nozhkin and Turkina, 1995) raises whole-rock Th/U above expected values of 1 to 4 for mantle-derived tonalite, magmatic distribution coefficients for these two analyses and the elevated whole rock Th/U of GR9802 may suggest local anatexis during ~3600 Ma metamorphism. Therefore, the best estimate for the pre-metamorphic magmatic age of *Ogn-1* is the 3730 ± 7 age of the zircon cores, as suggested by Th/U data from GR0012. This is consistent with low calculated zircon-saturation temperatures of *Ogn-1* samples of 720 to 772 °C (table 1).

*Ogn-2.*—The magmatic age of *Ogn-2* is best established from the depth-profiling results because it gives Th/U as a function of age at high spatial resolution. The whole-rock Th/U of GR0071 is 2.0 (table 1), which would be in exchange equilibrium with magmatic zircon of Th/U = 0.4 ± 0.2. Figure 17 shows that only the inner 3825 ± 6 Ma portion of the grain yields the predicted magmatic Th/U. All younger zones give lower, non-magmatic distribution coefficients. As with *Ogn-1* and *Ogn-4,* this is consistent with low zircon-saturation temperature (table 1). Additional support for a 3825 Ma magmatic age is the statistically distinct zone of low Th/U zircon growth at 3728 ± 8 Ma (fig. 15). This age is identical within uncertainty to the age of *Ogn-1.* The close proximity *of Ogn-2* to *Ogn-1* (figs. 2 and 3) raises the possibility that *Ogn-2* experienced contact metamorphism at the time of emplacement of *Ogn-1.* Thus, the inferred magmatic age relations indicate that *Ogn-1* and *Ogn-2* record two temporally distinct intrusive events. Miminum age of the supracrustal enclave must be at least the age of the oldest crosscutting unit, that is, 3825 ± 6 Ma.

### *Origin and Age of Quartz-Pyroxene Rocks*

The origin of *Qp* rocks within the Akilia enclave is significant for two reasons. First, if they are sedimentary, they would be an original part of the Akilia supracrustal stratigraphy, and therefore >3825 ± 6 Ma—among the oldest preserved terrestrial sediments, along with those from the Isua Supracrustal Belt and islands south of Akilia (Cates and Mojzsis, 2006). In addition, C isotope evidence has been interpreted to indicate that biological fractionations are preserved in *Qp* rocks (Mojzsis and others, 1996), also in common with Isua metasediments (Rosing, 1999).

Nutman and others (1997) interpreted *Qp* rocks as banded iron-formation based in part on inferred similarities to Isua BIF. However, these comparisons are unsatisfactory in detail because of the high degree of metamorphism and poor correspondence of bulk composition data to quartz-magnetite BIF at Isua (fig. 11A; Fedo and Whitehouse, 2002a). Nevertheless, as noted above, major-elements are similar to some BIF, pointing to a possible origin as a minor Fe- and Si-rich chemical sediments with affinities to iron formation. The *Qp* rocks are polymetamorphic gneisses, and detailed observations indicate veining and at least internal remobilization of components (Friend and others, 2002). Still, it is possible that there has been relatively little mass transfer with host lithologies, and that many of the compositional characteristics of an original chemical sediment are preserved.

A second possibility is that *Qp* rocks originated as metasomatic rocks during metamorphism, after original formation of the other supracrustal lithologies. In their original description of the Fe-rich rocks of the Akilia association, McGregor and Mason (1977) noted widespread occurrence of Fe-rich lithologies in the region. They considered three possible origins for these rocks based on REE chemistry: (1) chemical sediment, (2) chemical sediment with detrital addition of REE, and (3) introduction of REE by metasomatism. They argued for option (1), but cautioned that many *Qp* rocks of the Akilia association have high contents of quartz and locally elevated Cr and Ni, which may suggest silica metasomatism of diverse protoliths (clinopyroxenites, other basic rocks, volcanic-detrital sediments, banded iron-formation). The *Qp* gneisses of Akilia are rich in quartz and, locally, Cr and Ni, and would appear to be examples of such rocks.

Fedo and Whitehouse (2002a) argued for a metasomatic origin of *Qp* rocks. They noted concave-downward REE patterns, in contrast to concave-up REE of Isua BIFs. A thick, unboudinaged band of Fe-rich pyroxene in the quartz-pyroxene lithology (their sample AK38) has Cr, Th/Sc, and Cr/Th, similar to adjacent ultramafic rocks. REE patterns of other pyroxene-rich boudins and quartz-rich samples are similar to AK38, though total REE in the latter are lower due to dilution by quartz. This suggests a shared protolith for all *Qp* rocks. In addition, Fedo and Whitehouse (2002a) suggest that $TiO_2$, $P_2O_5$, $TiO_2/P_2O_5$, Cr, and Y of *Qp* rocks are similar to ultramafics, but not comparable to BIF or mafic igneous rocks. They therefore proposed that *Qp* rocks originated as ultramafic rocks, which were "compositionally modified during repeated episodes of metasomatism [including carbonate replacement (Rosing and others, 1996; Rose and others, 1996), quartz veining and LREE addition], and metamorphism, whose intensity precludes constraining their timing and number."

Constraints on the two proposed models for the origin of *Qp* rocks are discussed below. The geologic and geochronologic results provide a minimum age of the lithology. Within this framework, specific field and petrologic tests reveal that key observations are not only consistent with a sedimentary origin, but contravene predictions of the metasomatic hypothesis. In addition, independent geochemical tests can be explained by the sedimentary model but not by the metasomatic model. In light of these constraints, we conclude that *Qp* rocks originated as local deposits of chemical sediment with minor input of mafic and ultramafic detritus.

*Age of Qp rocks.*—Zircons from *Qp* sample GR9713 have textures similar to those of supracrustal amphibolites (Friend and Nutman, 2005a) and anthophyllite-garnet rock (A1, A2), consistent with a metamorphic origin. In addition, they yield ~3600 Ma and ~2700 $^{207}Pb/^{206}Pb$ age clusters (fig. 16). A weighted mean $^{207}Pb/^{206}Pb$ age of concordant analyses from the older group is 3589 ± 13 Ma (MSWD = 26), identical within uncertainty to mean zircon ages of the supracrustal lithologies. All three of the ~3600 Ma age populations possess MSWD significantly greater than one, indicating scatter outside the analytical uncertainty. Nutman and others (1997) reported concor-

dant zircons from a *Qp* rock giving $^{207}Pb/^{206}Pb$ ages ranging from 2516 ± 11 to 2682 ± 6 Ma (fig. 16), with a weighted mean $^{207}Pb/^{206}Pb$ age of 2636 ± 20 (MSWD = 28) similar to that of the younger population in our samples. It is not clear why their zircon separate failed to yield the older zircon components found in the present study.

The older metamorphic zircon age-group indicates that *Qp* rocks are ≥3589 ± 13 Ma. Our mapping results reveal that *Qp* rocks shared the entire deformation history recorded in the enclave, including the formation of the currently exposed lithologic contacts. If *Qp* rocks are metasomatic in origin, their age predates all preserved deformation and is bracketed between the age of the supracrustal rocks and the age of the oldest zircon age group; that is, from at least 3825 ± 6 to 3589 ± 6 Ma. Alternatively, if *Qp* are metasediments, then as a primary component of the supracrustal enclave they must be >3825 ± 6 Ma.

*Field and petrologic considerations.*—Contacts between *Qp* gneiss bands and their host rocks are subparallel to the *Am-Amu* contact, and internal S1 fabric is coaxial with that in bounding lithologies. Thus, in addition to sharing with supracrustal rocks the same history of metamorphic zircon growth, *Qp* rocks also experienced the same history of preserved deformation. Part of this deformation involved veining and mass transfer on a local scale. Amphibolites of *Am* locally contain garnet within ~1 m of *Qp,* and *Um* bodies show somewhat elevated $SiO_2$ contents. These features are consistent with local component exchange during metamorphism of lithologies with strongly contrasting protolith composition, and do not require major fluid flow. Post-S1 quartz and Fe-rich clinopyroxene veins within are widespread in *Qp* rocks (figs. 5C and D). Orientations at high angles to lithologic contacts and S1 are common, but many also show complex geometry (fig. 5D).

The foregoing field relations are consistent with either a sedimentary or metasomatic origin. If *Qp* rocks were originally chemical sediments, all features are the expected chemical and rheological responses to multiple metamorphic and deformational episodes. Several scenarios for metasomatism can also be envisioned, subject to the same constraints. For example, as at Isua (Rosing and others, 1996; Rose and others, 1996; Frei and others, 2002), metasomatic alteration could have accompanied metamorphic devolatilization during prograde heating, although the sources and processes would have to differ fundamentally at Akilia. Alternatively, *Ogn* emplacement or oceanic hydrothermal alteration could have caused metasomatism. However, three additional field and petrologic considerations pose challenges that make a metasomatic origin implausible.

First, the quartz-pyroxene exposure that has received the most attention is a locality where ultramafics form one contact (amphibolite is the other); however, this contact relationship is not consistently observed along the *Qp* exposures (fig. 2 and Friend and others, 2002). In general, contact rocks are dominated by amphibolite rather than ultramafic rocks. If the metasomatic model is valid, it must provide a mechanism for generating the ultramafic protolith at contacts where only amphibolite is now observed. Primary formation processes and/or subsequent deformation generated discontinuous ultramafic blocks and boudins, but *Qp* rocks form two distinct bands within the low-strain limb of F3. The requirement of an ultramafic protolith dictates that continuous bands of this lithology exist as precursors to the *Qp* lithology, which conflicts with its disruption into blocks and boudins in the low-strain F3 limb.

A second challenge to the metasomatic model is that the posited quartz veining is inconsistent with the preserved chemical-potential gradients. If metasomatic fluids were derived from bounding lithologies, those rocks must have been capable of generating sufficient dissolved $SiO_2$ to yield the voluminous quartz of *Qp* rocks. However, the host rocks are low-silica ultramafic and mafic rocks. Although $SiO_2$ is soluble in an $H_2O$-rich fluid equilibrated with either lithology at amphibolite to

granulite grades (Manning, 1994a; Newton and Manning, 2002), the chemical-potential gradient between ultramafic and mafic compositions does not favor major $SiO_2$ mass transfer and quartz deposition by locally derived fluid (Newton and Manning, 2000a). Increasing concentrations of $CO_2$ or NaCl only reduce capacity to transfer $SiO_2$ (Newton and Manning, 2000b). Even if the fluid were externally derived, the metasomatic model requires significant $SiO_2$ infiltration without the corresponding production of an alteration halo recording a chemical-potential gradient in $SiO_2$ between quartz-rich *Qp* rocks and ultramafic lithologies.

A third problem is that the quartz veining postulated in the metasomatic hypothesis must have been highly localized, as the veins are not found elsewhere in *Am* and *Amu*. Such concentration of veining contravenes the typical self-similar clustering of fractures and veins (Manning, 1994b).

Thus, field and petrologic relations suggest that an origin of *Qp* rocks by metasomatic fluid sourced in bounding lithologies is problematic. An origin by an exotic fluid focused into veins requires the special geometric scenario in which contiguous ultramafic bands not seen elsewhere are preferentially altered by veins that do not display the self-similar scaling properties of typical vein systems. Finally, the outcrop-scale chemical effects of metasomatism were limited, so that there was no significant silica mass transfer into host lithologies.

*Geochemical considerations: O isotopes.*—A metasomatic event of even modest scale will modify oxygen-isotopic ratios in the rocks surrounding the fluid flow channels (for example, Valley, 1986; Kerrich, 1987; Nabelek, 1991; Ferry and Gerdes, 1998). To assess the extent of metasomatic exchange, we measured whole rock $\delta^{18}O$ on a traverse across the southernmost *Qp* band (fig. 3, table 2). Figure 20A shows that there is no systematic variation in $\delta^{18}O$ with distance from either *Qp* contact. The lack of correlation of $\delta^{18}O$ with distance from the northern *Qp* contact suggests that the slightly more variable values to the south are due to normal scatter.

The sharp contrast in $\delta^{18}O$ between *Qp* rocks and amphibolite and ultramafic rocks rules out large-scale metasomatic exchange of oxygen between *Qp* rocks and any other lithology. Because the *Qp* rocks are dominantly quartz, $\delta^{18}O_{rock} \sim \delta^{18}O_{qtz} \sim 13$ permil, which allows $\delta^{18}O_{fluid}$ to be estimated (Matsuhisa and others, 1979). O-isotope exchange between this fluid and an initial ultramafic rock with the minimum observed value of 7 permil will increase $\delta^{18}O_{rock}$ to varying extents depending on temperature and water-rock ratio (Taylor, 1977). Using amphibole-water fractionation ($\Delta_{amp\text{-}H2O}$) calculated from $\Delta_{qtz\text{-}H2O}$ and $\Delta_{qtz\text{-}amp}$ (Bottinga and Javoy, 1975) and assuming $\delta^{18}O_{rock} = \delta^{18}O_{amp}$ for ultramafic rocks (which are >80% amphibole), it is possible to calculate the water-rock ratio required to produce the maximum $\delta^{18}O_{rock}$ observed in the lithologies bounding the *Qp* band.

Figure 20B shows that, at >400 °C, the water-rock ratio can be no more than 0.5 in the most conservative case (1.5‰ shift, closed system, lowest temperature). At lower temperature, amphibole is unstable with respect to serpentine in ultramafic bulk compositions. The same calculation using serpentine-$H_2O$ fractionation (Wenner and Taylor, 1971) requires negative (impossible) water-rock ratios to produce a positive shift in $\delta^{18}O_{rock}$. Thus, O-isotope data preclude large-scale metasomatic mass transfer by a water-rich fluid—the only type of fluid that would have the solvent power sufficient to transport major elements at the scale proposed. Although more rigorous modeling of O-isotope exchange is possible (for example, Baumgartner and Rumble, 1988), this simple test showing that the fluid volume cannot have been significant indicates that such treatment is not warranted.

*Geochemical considerations: nontraditional stable isotopes.*—Terrestrial igneous rocks show tightly clustered Fe stable-isotope ratios, whereas iron formations show strong deviations (Johnson and others, 2003; Beard and Johnson, 2004). Dauphas and

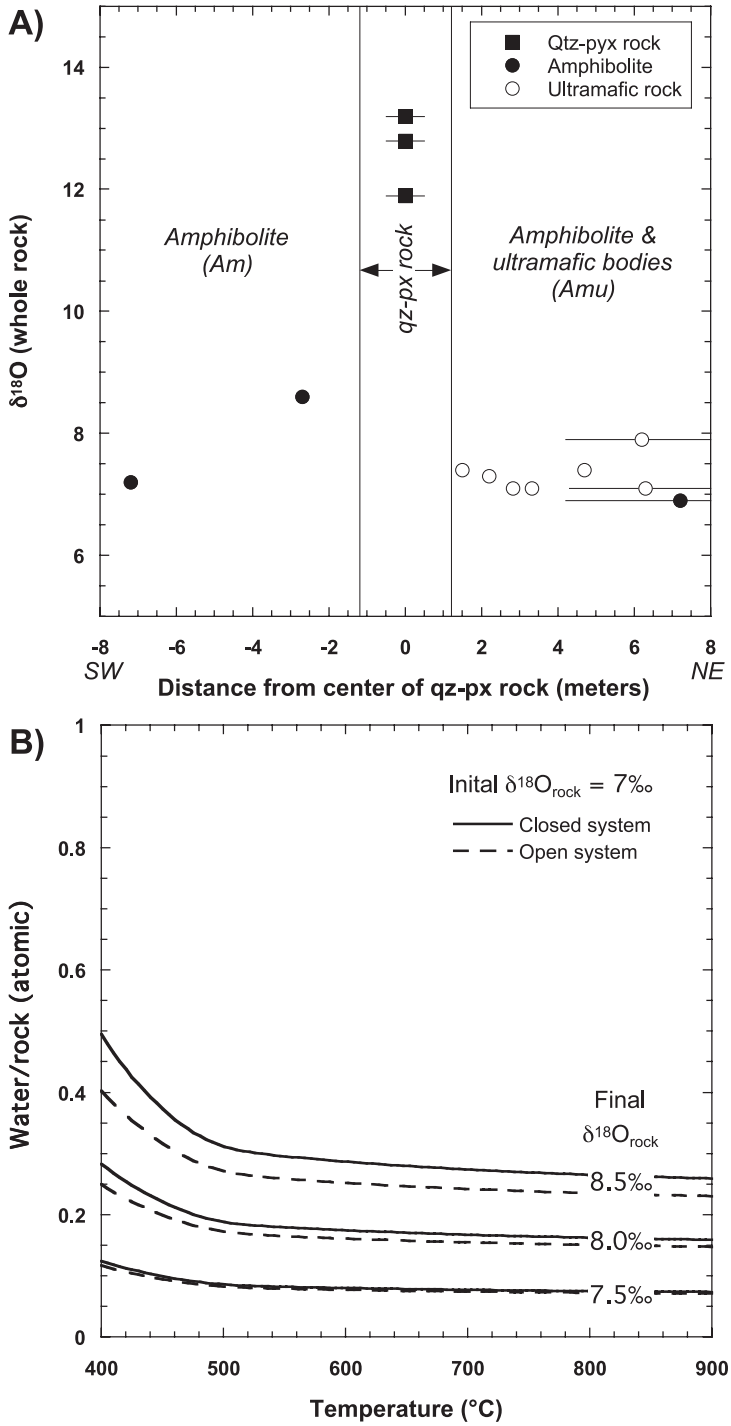


Fig. 20. (A) Whole-rock oxygen-isotope data for *Qp*, ultramafic, and amphibolitic rocks along a transect through the southernmost *Qp* band (fig. 3). Samples are projected onto the transect; negative values indicate samples southwest of band and positive values are samples to the northeast. (B) Variation in water-rock ratio (Taylor, 1977) with temperature for the postulated metasomatic event. Curves show atomic ratio of fluid to rock required for a fluid in O-isotope equilibrium with *Qp* quartz to shift host ultramafic rock or amphibolite above background values. O-isotope exchange was modeled using fluid-amphibole equilibrium (see text).

others (2004) found that Akilia supracrustal mafic and ultramafic rocks had average enrichments in $^{56}Fe$ and $^{57}Fe$ relative to $^{54}Fe$ ($F_{Fe}$) of 0.024 ± 0.013 ‰/amu with respect to IRMM-014 standard, identical to average terrestrial igneous rocks (0.040 ± 0.009 ‰/amu). In contrast, Akilia *Qp* rocks are enriched in the heavy Fe isotopes and more variable than mantle-derived rocks ($F_{Fe}$ = 0.062 to 0.522 ‰/amu), similar to silicate-oxide iron formation of Isua and the Kaapvaal Craton. Metasomatic production of such large shifts would require very high fluid-rock ratios because high-temperature mineral-fluid fractionation must be low for such small differences in isotopic mass. However, high fluid-rock ratios are precluded by the O-isotope results. Dauphas and others (2004) also rule out an origin by a process analogous to mid-ocean ridge hydrothermal alteration because it is not consistent with bulk Fe/Ti. In contrast, enrichment in heavy Fe isotopes is readily explained by oxidation of hydrothermally derived ferrous iron and precipitation as insoluble oxyhydroxides during chemical sedimentation. Thus, Fe isotopes support a sedimentary but not a metasomatic model for the *Qp* protolith.

Si isotope data are also consistent with a *Qp* origin by chemical sedimentation. André and others (2006) report $\delta^{30}Si = -0.36$ permil (NBS28) for Akilia *Qp* rocks. Although this is heavier than values determined for quartz from Isua BIF, it is within the range measured for metachert and sea-floor siliceous sediment derived from hydrothermal fluids—the origin proposed here for the *Qp* bands. However, $\delta^{30}Si$ of many such deposits, along with *Qp* rocks, also lies within the range of fresh mafic igneous rocks (−1.0 to −0.2 ‰). Evidently, Si isotopes do not alone provide the discrimination needed to resolve the problem.

*Geochemical considerations: S isotopes.*—Mass-independent fractionation sulfur stable isotopes in Archean sedimentary sulfide and sulfate (Farquhar and others, 2000) have also been used to evaluate protolith origins. Mass-dependent fraction of $^{32}S$, $^{33}S$ and $^{34}S$ yields no departure from the predicted dependence of $\delta^{33}S$ on $\delta^{34}S$ ($\Delta^{33}S = 0$). Mass-independent, nonzero $\Delta^{33}S$ were produced by photolytic reactions on $H_2S$ and $SO_2$ molecules in the ozone-poor Archean atmosphere, and deposition of S aerosols into surface waters transferred this signal to Archean sedimentary rocks. Thus, nonzero $\Delta^{33}S$ signifies incorporation of Archean atmospheric S.

Mojzsis and others (2003a) determined S isotope values in *Qp* sulfides and found that composite chalcopyrite-pyrrhotite grains show statistically significant mass-independent fractionation ($\Delta^{33}S = +0.57$). The grains are likely exsolution products from a single sulfide that recrystallized at high metamorphic grade, but the $\Delta^{33}S$ signal is conservative and indicates incorporation of atmosphere-derived S. Non-zero $\Delta^{33}S$ is similar to Archean BIF (Farquhar and others, 2000; Mojzsis and others, 2003a). However, Whitehouse and others (2005) found $\Delta^{33}S = 0$ in sulfides from a different sample from the *Qp* unit and used this with Pb-isotope data to argue that S isotope results are ambiguous tracers of sedimentary origin. Both sedimentary and metasomatic processes could produce heterogeneous $\Delta^{33}S$, either through variable sampling of atmospheric and mantle S reservoirs during deposition, or through remobilization of the signal. Further study is needed to explore the implications of the S isotopic results, but the presence of nonzero $\Delta^{33}S$ is consistent with the Archean origin of *Qp* rocks inferred by independent methods.

*Geochemical considerations: immobile elements.*—In the metasomatic model, pyroxene bands and boudins in *Qp* rocks are metasomatized ultramafic protoliths invaded by quartz veins. A pyroxene layer inferred to be the least altered has ultramafic concentrations of some nominally immobile elements (Fedo and Whitehouse, 2002a). If *Qp* rocks formed by metasomatism, then all quartz-free pyroxene bands and boudins should have ultramafic immobile-element signatures. In addition, when samples with variable quartz abundance are considered, analyzed *Qp* rocks should reflect a mechani-

TABLE 3

*Number of the four Qp pyroxene bands with ultramafic element ratios*

| | Ti | Al | Y | Zr | Cr |
|---|---|---|---|---|---|
| Al | 2 | | | | |
| Y | 0 | 0 | | | |
| Zr | 2 | 1 | 2 | | |
| Cr | 1 | 1 | 0 | 1 | |
| Sc | 2 | 2 | 2 | 2 | 1 |

Entries indicate number of *Qp* bands possessing ratios of nominally immobile elements that are similar to ultramafic rocks when column element is divided by row element. Data from Fedo and Whitehouse (2002a).

cal mixture of quartz veins and altered ultramafics, and element ratios should obey simple two-component mixing rules. In contrast, a sedimentary model requires instead that immobile-element ratios are similar to known values for the postulated protolith. We use the data of Fedo and Whitehouse (2002a) to show that only a sedimentary origin is favored.

Ti, Al, REE, Y, Zr, Cr, Sc, Th and platinum-group elements (PGE) were either implicitly assumed to be immobile in the metasomatic model (Fedo and Whitehouse, 2002a), or are known to be immobile during secondary processes affecting mafic and ultramafic lithologies (Floyd and Winchester, 1975; Pearce, 1975; Sun and Nesbitt, 1979; Ludden and Gelinas, 1982; Ludden and others, 1982; Jochum and others, 1991; Arndt, 1994; Büno and Meisel, 1994). Inspection of the data of Fedo and Whitehouse (2002a) shows that relative to average ultramafic rock, LREE are more enriched than HREE in pyroxene bands, so all REE cannot be immobile during hypothesized metasomatism. A comparison of ratios of the remaining elements in pyroxene bands and boudins to those in average ultramafic rock (table 3) reveals that no ratio has an ultramafic value in all four analyzed bands. Of the fifteen independent ratios, there are seven for which two of four bands have ultramafic ratios, but not the same pair of bands in each case. There are five ratios for which only one of the four bands has an ultramafic ratio and, in three cases, none. Comparison of PGE gives similar results (Anbar and others, 2001).

A further test of a metasomatic origin involves analysis of two-component mixing based on ratios of nominally immobile elements. In the metasomatic model, the *Qp* lithology is a metamorphosed mechanical mixture of altered ultramafic protolith and quartz-rich vein material (Fedo and Whitehouse, 2002a, 2002b, 2002c). Accordingly, immobile-element ratios in pyroxene bands and *Qp* gneisses should define mixing curves between these end members and indicate the geochemical affinity of the hypothesized protolith. Figure 21A compares $TiO_2/P_2O_5$ and Cr/Y in *Qp* and ultramafic rocks. The sample hypothesized to be least altered and to most faithfully preserve an ultramafic protolith is AK38 (Fedo and Whitehouse, 2002a), which plots near ultramafic rocks (fig. 21A). Sample AK31, with $TiO_2/P_2O_5$ and Cr/Y of ~1 and ~20, has the highest $SiO_2$ of the *Qp* rocks, and should therefore reflect a composition closest to the hypothesized quartz vein end member. The metasomatic hypothesis predicts that the other samples lie on a mixing line between these end members; however, all other *Qp* rocks and pyroxene bands lie at lower $TiO_2/P_2O_5$ and Cr/Y than AK31. No choice of end members can explain the observed pattern. Two-component mixing also fails to explain variation

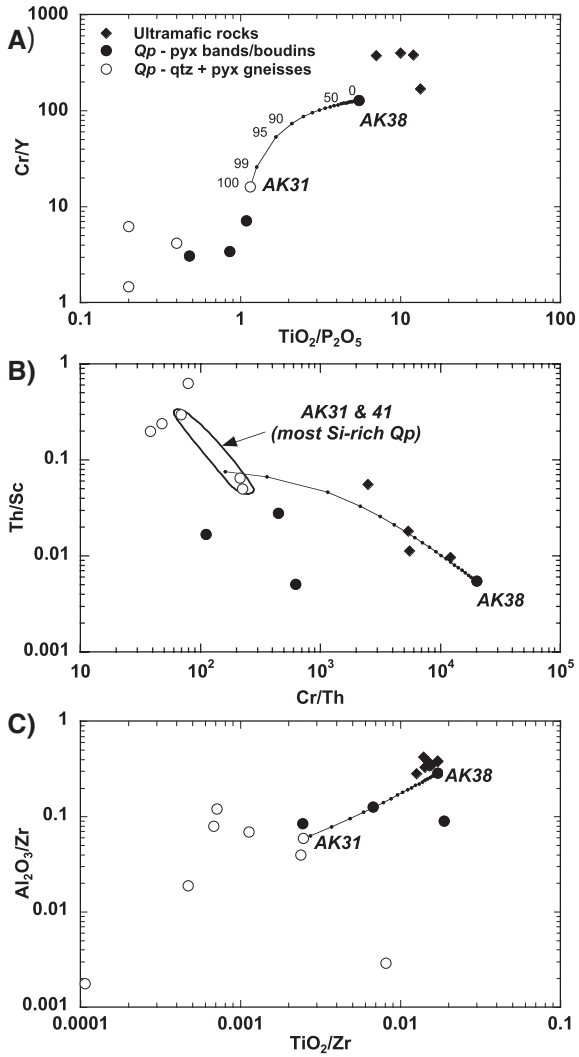


Fig. 21. Selected concentration ratios from ultramafic rocks and *Qp* lithologies (~quartz-free pyroxene bands/boudins and gneisses containing quartz and pyroxene), using data from Fedo and Whitehouse (2002a). The concentration ratios represent elements either assumed to be immobile in the formulation of the metasomatic model, or commonly observed to have low mobility during metasomatism in other environments. In the metasomatic model, *Qp* rocks are pyroxene-rich bands that represent metasomatized ultramafic protolith, crosscut by quartz veins. The *Qp* compositional data should therefore lie on two-component mixing curves (solid lines) between the hypothesized least-altered protolith (AK38) and the most $SiO_2$-rich samples (AK31 or the mean of AK31 and AK41, depending on data availability). Points show increasing $SiO_2$-rich component added to AK38, in percent, at 5% increments (the 99% composition is also shown); selected percentages are labelled. The data do not lie on the mixing lines, indicating that the metasomatic model does not explain the data.

in Cr/Th with respect to Th/Sc (fig. 21B) and $TiO_2$/Zr with respect to $Al_2O_3$/Zr (fig. 21C). The only scenario in which metasomatism could explain the data of Fedo and Whitehouse (2002a) would be that all of the plotted elements were mobilized by a metasomatic fluid, and that the effects varied from sample to sample in a random manner.

Ratios of elements that have low mobility in metamorphic environments can also be used to investigate a sedimentary origin. Figure 22A shows that average Archean lithologies (Condie, 1993), as well as rock types from the Akilia region, are readily discriminated in a plot of $TiO_2/P_2O_5$ vs. Cr/Y. In particular, Isua BIFs, like Archean BIFs globally, have $TiO_2/P_2O_5 < 3$ and $Cr/Y < 20$. This probably results from the fact that Y and P, along with REE, are enriched in hydrothermal fluids and precipitates that lead to BIF deposition (Graf, 1978; Dymek and Klein, 1988; Bau and Dulski, 1996, 1999), whereas Cr and $TiO_2$ are low. With the exception of AK38, Akilia *Qp* rocks have $TiO_2/P_2O_5$ and Cr/Y similar to Isua BIF (fig. 22B). In discounting a similar observation by Palin (2002), Fedo and Whitehouse (2002c) appealed to quartz dilution; however, this would not change the ratios significantly because of the low concentrations of the elements in quartz. The ratios therefore reflect protolith compositions, and the protolith that matches best is Isua BIF in all cases except AK38, which lies within the ultramafic field.

The $TiO_2/P_2O_5$ and Cr/Y signatures of Akilia *Qp* rocks (and Isua BIF) are readily explained by detrital input of mafic and ultramafic components (fig. 22B). The Isua BIF field trends toward higher $TiO_2/P_2O_5$ and Cr/Y along mixing curves between model endmembers that are consistent with addition of a mafic component (amphibolite protolith). Most of the *Qp* rocks have ratios that extend along the BIF-amphibolite mixing line, and require no more than ~25 percent mixing of the elements comprising the ratios. AK38 is the only *Qp* sample lying off the trend, and would imply a more ultramafic source component. Certain mineral grains can be expected to have high leverage for changing these and related ratios, but will yield little shift in other element patterns such as REE. For example, addition of $<<1$ percent by mass detrital chromite to the *Qp* protolith would shift Cr/Y to the observed value in AK38 by virtue of its low REE content (Melcher and others, 1999). Similar arguments can be made for $TiO_2$-bearing oxide phases.

The same conclusion is reached based on ratios of other immobile trace elements (fig. 22). Variation in Cr/Th and Th/Sc in Isua BIFs is negatively correlated and overlaps with other lithologies at their extremes; however, most BIFs cluster in a compositionally distinct region near ~20 and ~0.2. Quartz-bearing *Qp* rocks from Akilia are best fit by the Isua BIF field. The pyroxene bands and boudins extend to higher Cr/Th and lower Th/Sc. Mixing lines from basaltic and ultramafic compositions suggest that these values may result from detrital input. The high fraction of non-BIF component required by this model implies that these ratios are controlled entirely by the sedimentary source, which is consistent with the very low Th and Cr concentrations in BIF. $Al_2O_3/Zr$ and $TiO_2/Zr$ do not discriminate lithologies as well, but BIFs are unique in their much wider range in these ratios, and in their being the only rock type with very low ratios (that is, $TiO_2/Zr<10^{-3}$ and $Al_2O_3/Zr<4 \times 10^{-2}$; many BIF values are maxima because $TiO_2$ is below detection). Akilia *Qp* rocks show large variations in these ratios, like Isua BIF, and pyroxene bands are most consistent with admixtures of minor basaltic or ultramafic material.

*Geochemical considerations: REE.*—Akilia *Qp* REE patterns differ from those of Isua BIF in their concave-downward LREE and more fractionated middle to heavy REE on normalized plots (figs. 23A and B; Fedo and Whitehouse, 2002a; Bolhar and others, 2004). Use of REE as tracers of chemical sedimentary origin is complicated by REE modification during diagenesis (Johannesson and others, 2006). Some aspects of the contrasting REE and Y chemistry are clearly not diagnostic of origin. Fedo and Whitehouse (2002a) noted that different Eu anomalies may be caused by diagenesis and metamorphism (Bau, 1991, 1993). Similarly, Y/Ho is superchondritic in Isua BIF (up to 48) but 30 to 33 in Akila *Qp* rocks only slightly above

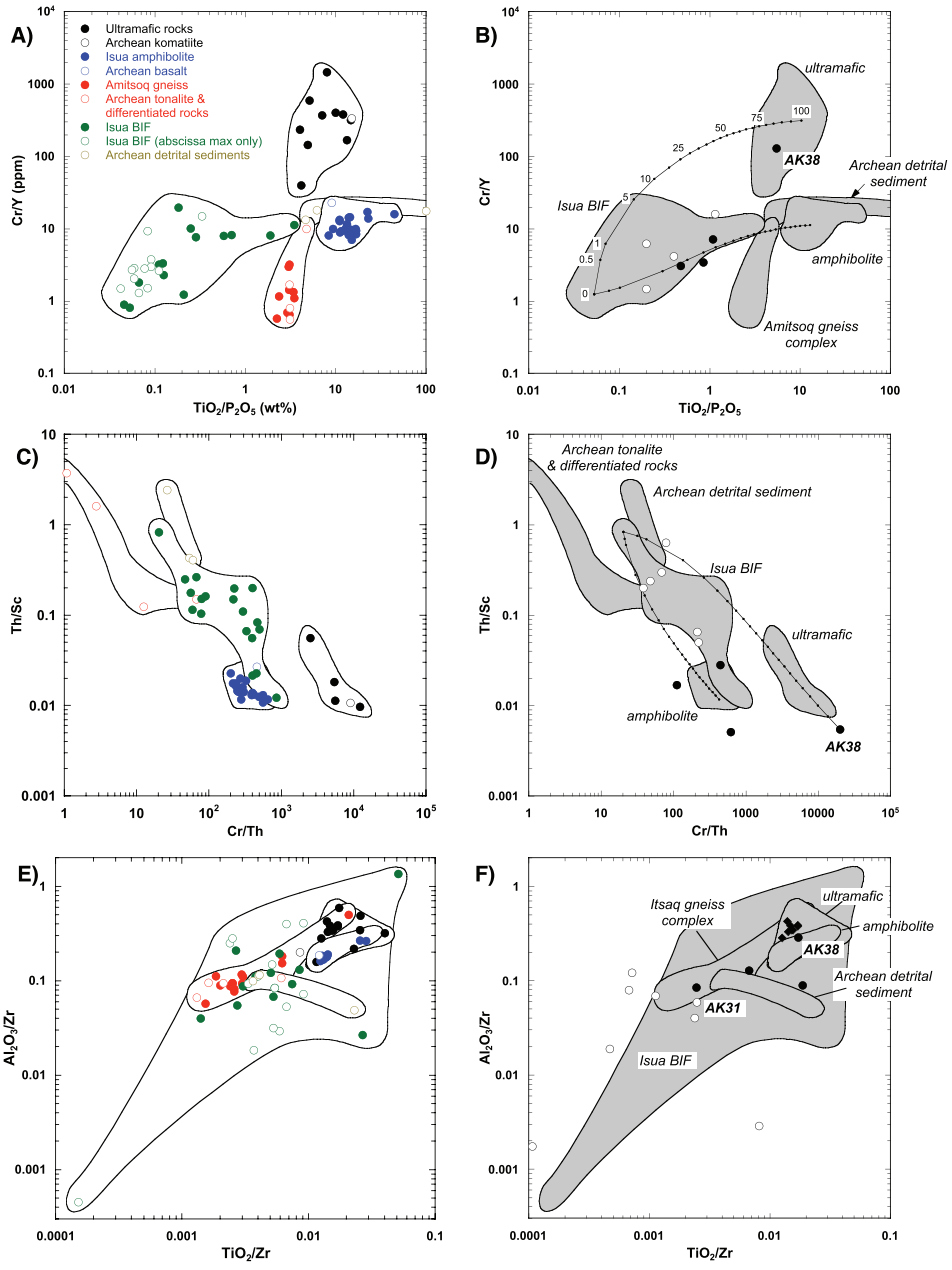


Fig. 22. Selected element and oxide ratios in Archean lithologies (Panels A, C, and E), and Akilia *Qp* and ultramafic rocks (Panels B, D, and F). In A, C and E, filled symbols represent ratios for local and regional lithologies of the Itsaq Gneiss Complex (McGregor and Mason, 1977; Nutman and Bridgwater, 1986; Dymek and Klein, 1988; Fedo and Whitehouse, 2002a; Polat and others, 2003), and open symbols denote averages for Archean rocks worldwide (Condie, 1993). In B, D and F, open and filled symbols are as in fig. 21, and the shaded fields are taken from the corresponding figure to the left. B and D show mixing lines between postulated detritus-free BIF composition with ultramafic and mafic detritus (see text), at increments of 5% detrital addition (0.5 and 1% increments also shown).

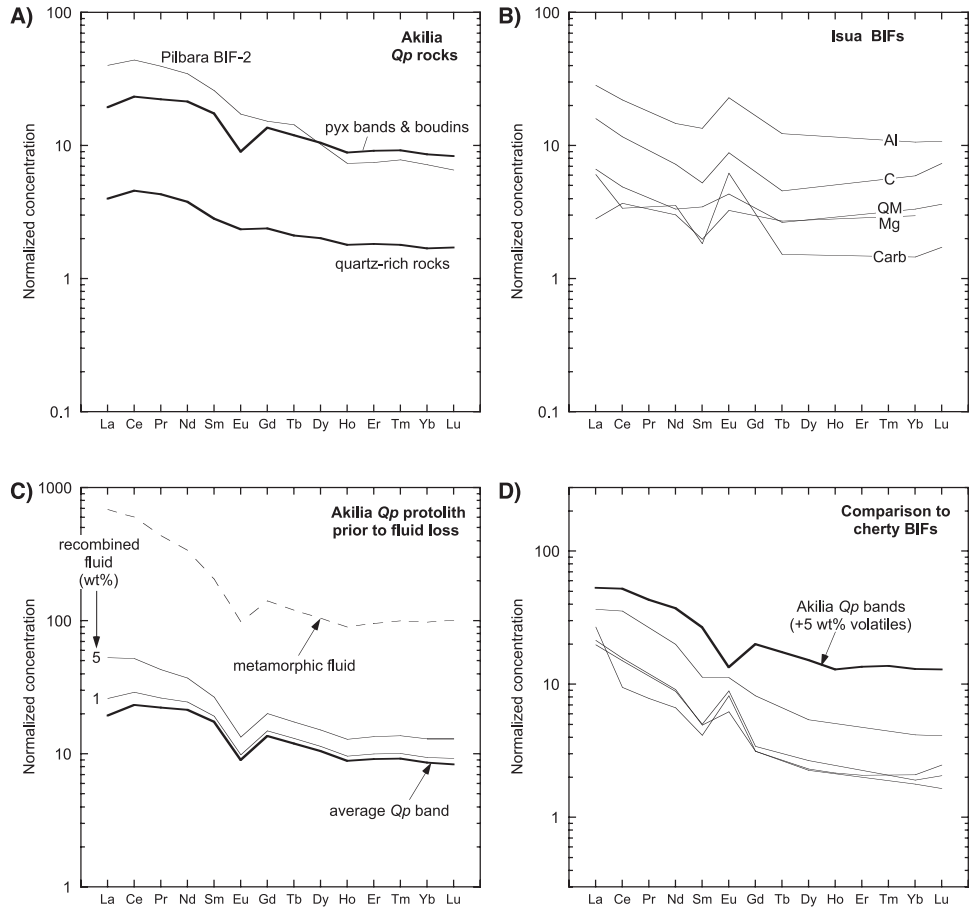


Fig. 23. Chondrite-normalized REE patterns of *Qp* and other lithologies. (A) Average pyroxene bands/boudins and quartz-pyroxene rocks (Fedo and Whitehouse, 2002a) compared with Pilbara BIF-2 (Kato and others, 1998). (B) Average Isua BIFs (Dymek and Klein, 1988); Al, aluminous; C, carbonaceous; Carb, carbonate; Mg, magnesian; QM, quartz-magnetite. (C) Calculated consequences of clinopyroxene formation during metamorphic devolatilization at 700 °C, 10 kbar (Griffin and others, 1980). Clinopyroxene-fluid equilibrium partition coefficients were calculated from lattice-strain model (Blundy and Wood, 1994) by fitting 700 °C data of Cullers and others (1973) to give Young's modulus (E) and optimum radius ($r_o$), assuming octahedral coordination of REE on M2. The unstrained partition coefficient ($D_o^{px\text{-}fluid}$) at 10 kbar was derived by scaling $D_{Sm}^{px\text{-}fluid}$ from 1kbar, 700°C, by the amount found between 5 and 10 kbar at 1100°C (Mysen, 1979). Resulting parameters are: $D_o^{px\text{-}fluid} = 0.1$, $r_o = 1.03$ Å, E = 144 GPa. Metamorphic fluid in equilibrium with clinopyroxene was calculated from the average pyroxene band composition and recombined in the amounts shown to simulate lower grade equivalents of *Qp* rocks. (D) Comparison of chondrite-normalized REE of low-grade equivalent of pyroxene band (5 wt% recombined volatiles) with Archean cherty BIFs (Barrett and others, 1988).

chondritic values of ~28 (Bolhar and others, 2004). However, nonchondritic Y/Ho ratios are not diagnostic because they occur both in modern hydrothermal particles (Edmonds and German, 2004) and hydrothermal vein minerals (Bau, 1996). But it can be shown further that even if REE patterns survive burial unchanged, the concave-down pattern and middle REE enrichment used to reject a BIF origin are in fact consistent with a chemical-sediment protolith for Akilia *Qp* rocks.

If primary, the difference between Isua and Akilia REE patterns may simply be due to local REE variations in hydrothermal fluid and detrital input. Hydrothermal-fluid REE in a given vent field may vary in time and space, giving rise simultaneously to concave-up and concave-down normalized LREE patterns (James and others, 1995). Basin evolution and tectonic transport also play a role. In Pilbara BIFs, western Australia, minor detrital input yields the pattern shown in figure 23A, in a sequence with REE otherwise similar to Isua (Kato and others, 1998). The pattern is similar to *Qp* pyroxene bands in its concave-down LREE and $Gd/Yb_N > 1$, though $La/Yb_N$ is greater. In short, differences between REE in Fe-rich rocks of Isua and Akilia could simply reflect the strong local influences on depositional environment typical of Archean sedimentation (McLennan and others, 1984; Taylor and others, 1986).

Accounting for expected contrasts in metamorphic effects on REE at Akilia and Isua lends further support to a sedimentary origin for *Qp* rocks. Metamorphism at ~3600 Ma may have reached granulite facies at Akilia but only amphibolite facies at Isua (Griffin and others, 1980). The dominant reservoir for REE in *Qp* rocks is clinopyroxene, which was probably produced at high grade. Concave-downward normalized LREE is typical of granulite-grade clinopyroxene (Reitan and others, 1980; Pride and Muecke, 1981; Friend and others, 2002a), so *Qp* patterns may simply reflect preferential LREE exclusion during clinopyroxene growth. This is illustrated in figure 23C, which shows that LREE are predicted to be strongly enriched in a fluid in equilibrium with clinopyroxene during devolatilization. Recombination of this fluid with the average *Qp* band of Fedo and Whitehouse (2002a) shows that low-grade equivalents of *Qp* rocks were likely richer in LREE (fig. 23C). A model low-grade *Qp* band to which REE from 5 weight percent volatiles are added would have had a normalized pattern similar to Archean cherty BIF (fig. 23D). The required LREE mobility during metamorphism is supported by elevated LREE in ultramafics from <0.4 m of the *Qp* contact (fig. 10B). A similar pattern in a more distal ultramafic sample is consistent with heterogeneous exchange during metamorphism.

*Summary of age and origin Qp rocks.*—Two models have been proposed for the origin of *Qp* gneisses on Akilia. All field, petrologic and geochemical tests are consistent with a sedimentary origin, but the metasomatic model either fails the same tests or yields ambiguous results. We conclude that *Qp* rocks had a chemical-sedimentary protolith, and most likely originated as volumetrically minor accumulations of ferruginous and siliceous hydrothermal precipitates, with minor admixture of locally derived mafic and ultramafic detritus. As a primary component of the supracrustal enclave, they have the same minimum age of 3825 ± 6 Ma derived from crosscutting relations involving *Ogn-2* and *Au*.

## CONCLUDING REMARKS

This study shows that the supracrustal enclave on Akilia experienced a complex deformational and metamorphic history, but that key aspects of its origin and age can nevertheless be identified. Field relations indicate that the lithologic package is dominated by amphibolite and meta-ultramafic rocks which display two map-scale folds. Comparatively low strain is preserved in a fold limb in the western half of the map area, probably caused by involvement of a large, competant ultramafic body. In and near this body, two orthogneiss sheets are found in primary magmatic (but deformed) crosscutting relation to host supracrustal rocks. Zircon ages and Th/U indicate that they represent discrete magmatic phases emplaced at 3730 ± 7 and 3825 ± 6 Ma. It has been proposed that quartz-pyroxene rocks found within the supracrustal enclave have either a sedimentary or a metasomatic origin, but only an origin as chemical sediment with minor detrital input satisfies all field, petrologic and

geochemical tests. Because the *Qp* rocks represent an original, primary lithology that must have been deposited as part of the original stratigraphy, the *Qp* rocks have the same age as the enclave as a whole, which is ≥3825 Ma. Metamorphism and deformation of Akilia supracrustal rocks occurred at ~3600 Ma and ~2700, as recorded by zircon U-Pb data.

Our results confirm that the Akilia enclave shares key features with supracrustal bodies regionally. The sequences preserve Early Archean metamorphosed and deformed mafic-ultramafic volcanic successions. Fe-rich chemical sediments are common. Crosscutting relations involving the oldest components of *Ogn* tonalites are rare but consistently observed in zones of lowest strain. Thus, the model derived here for the Akilia supracustals is consonant with results in the region (Bridgwater and others, 1976; McGregor and Mason, 1977; Nutman and others, 1997, 2000, 2002, 2004). These observations give confidence that, with appropriate control for metamorphism and deformation, supracrustal sequences on Akilia and elsewhere can provide important information on terrestrial surficial processes in the Early Archean.

ACKNOWLEDGMENTS

This work was supported by NSF EAR9978241 and EAR0228999 and the NASA Astrobiobiology Institute. We thank Anders and Halfdan Nilssen for logistical support in Greenland. N. Caciagli assisted with the field work. Our ideas about Akilia have been clarified by discussion and debate with C. Friend, M. Grove, M. Holness, A. Lepland, A. Nutman, M. Rosing, M. van Zuilen. The manuscript benefited from comments by A. Yin and M. Rosing, as well as reviews by H. Day and two anonymous referees.

## APPENDIX

### *Zircon Geochronology Methods and Data*

*Sample preparation.*—Zircons were separated using standard heavy-mineral techniques. Separated zircon grains were hand picked under a binocular microscope, cast in epoxy and polished in stages to 0.25 μm alumina. All mounted zircons were subsequently characterized by optical and back-scattered electron microscopy, cleaned in an ultrasonic bath of 1N HCl to reduce common Pb contamination from the sample preparation process, rinsed in ultrapure water and coated with ~100 Å of Au prior to ion microprobe analysis.

*Conventional ion-microprobe methods.*—U-Pb zircon geochronology in this study was determined using the UCLA CAMECA ims 1270 high-resolution ion microprobe following previously reported methods (Schuhmacher and others, 1994; Quidelleur and others, 1997; Mojzsis and Harrison; 2002a; Mojzsis and others, 2003b) using standard zircon AS-3 with an age of 1099.1 ± 0.5 Ma (Paces and Miller, 1993; Schmitt and others, 2003).

A ~15 min measurement cycle yields $^{206}Pb/^{238}U$ ages with typically better than ±2 percent precision. The uncertainties in these measurements primarily reflect the variability in the $^{254}UO^{+}/^{238}U^{+}$ vs. $^{206}Pb/^{238}U^{+}$ calibration; the Pb in the grains analyzed for this study is typically >99 percent radiogenic. Minor reverse discordance in a small subset of the data is not significant at the 2σ level. Age calculations employed ISOPLOT/Ex (Ludwig, 2000). $^{207}Pb/^{206}Pb$ ages given as weighted means are reported with uncertainties at the 95 percent confidence level.

Several spots were analyzed twice in succession (replicate analyses labeled with "+" in table A1). Replicate analyses served only to confirm reproducibility and were not used in plots or age calculations.

For two samples (GR9713 and GR0071), the same grains were analyzed in two separate sessions, between which the sample mount was repolished and recoated with Au. This enabled analysis of different parts of the same zircon crystals following repolishing, and served as a further check on reproducibility. For each sample, the ion-microprobe spots from the two sessions were pooled during plotting and data analysis.

*Depth-profiling ion-microprobe methods.*—To better characterize the nature of zircon growth events, we also conducted ion-microprobe depth profiling study of zircon grain #36, sample GR0071. In spot analysis mode, the two-dimensional spatial selectivity of the ion microprobe is limited by the size of the primary beam, typically 10 to 30 μm. In the case where a crystal contains symmetrical overgrowths, it is possible to use the ion microprobe in depth profiling mode on an initially unpolished surface to

increase spatial resolution by up to two orders of magnitude (Carson and others, 2002; Mojzsis and Harrison, 2002a).

After initial characterization in conventional spot mode, grain #36 was plucked from its epoxy mount, placed on adhesive tape together with grains of standard zircon AS-3, recast with epoxy, ultrasonically cleaned in 1N HCl, Au coated, and analyzed without further polishing. The internal distributions of Pb/U and Th/U were then obtained by depth profiling using the methods of Mojzsis and Harrison (2002a). Pre-sputtering times for the initial cycles were 120 s and analyses comprised a minimum of 15 cycles of 10 s measurements. Analytical sessions in depth-profiling mode involve a continuous collection time (~60-180 min) from the same spot as the ion beam slowly sputters into the unpolished zircon sample. Because the U/Pb calibration begins to deteriorate with increasing pit depth, the mount was removed after sputtering to ~6 μm depth. The pit depth was measured with a surface profilometer, allowing estimation of depth of penetration per analysis cycle by assuming constant rate of sputtering. After the sample was re-polished until the crater was ≤1 μm deep, cleaned and recoated with Au, the depth profile was continued.

*Results.*—U/Pb isotopic ratios and 1σ errors for ion-microprobe spot and depth-profiling analyses obtained as described above are presented in tables A1 and A2, respectively, along with calculated $^{207}Pb/^{206}Pb$ age, % radiogenic $^{206}Pb^*$ and Th/U ratios. Analysis spots on individual grains are shown in figures A1–A5.

TABLE A1

*Ion microprobe U-Pb analyses of zircons from Akilia, West Greenland*

| Grain-Spot | $^{206}Pb^*/^{238}U$ ratio | 1σ | $^{207}Pb^*/^{235}U$ ratio | 1σ | $^{207}Pb^*/^{206}Pb^*$ ratio | 1σ | $^{207}Pb/^{206}Pb$ age (Ma) | 1σ | $^{206}Pb^*$ (%) | Th/U | 1σ | $^{208}Pb/^{206}Pb$ ratio |
|---|---|---|---|---|---|---|---|---|---|---|---|---|
| *GR9713, Fe-rich quartz-pyroxene rock, session 1* | | | | | | | | | | | | |
| 11-1 | 0.6892 | 0.0069 | 30.08 | 0.26 | 0.3165 | 0.0010 | 3553 | 5 | 99.96 | 0.0092 | 0.0006 | 0.0034 |
| 11-2 | 0.6961 | 0.0087 | 30.40 | 0.38 | 0.3167 | 0.0010 | 3554 | 5 | 99.96 | 0.0098 | 0.0005 | 0.0038 |
| 12-1 | 0.5043 | 0.0081 | 12.91 | 0.20 | 0.1857 | 0.0009 | 2704 | 8 | 99.97 | 0.0331 | 0.0013 | 0.0110 |
| 13-1 | 0.5063 | 0.0113 | 12.99 | 0.28 | 0.1860 | 0.0013 | 2707 | 12 | 99.94 | 0.0184 | 0.0011 | 0.0077 |
| 14-1 | 0.4503 | 0.0079 | 11.16 | 0.18 | 0.1797 | 0.0011 | 2650 | 11 | 99.80 | 0.0141 | 0.0016 | 0.0080 |
| 15-1 | 0.5125 | 0.0062 | 12.86 | 0.15 | 0.1819 | 0.0006 | 2671 | 6 | 99.98 | 0.0332 | 0.0009 | 0.0112 |
| 16-1 | 0.4667 | 0.0072 | 10.46 | 0.17 | 0.1626 | 0.0007 | 2483 | 7 | 99.64 | 0.0018 | 0.0003 | 0.0101 |
| 17-1 | 0.5270 | 0.0061 | 13.48 | 0.15 | 0.1855 | 0.0005 | 2703 | 4 | 99.99 | 0.0403 | 0.0006 | 0.0133 |
| 18-1 | 0.6777 | 0.0103 | 28.73 | 0.41 | 0.3075 | 0.0013 | 3508 | 7 | 99.91 | 0.0694 | 0.0015 | 0.0236 |
| 19-1 | 0.7722 | 0.0178 | 34.32 | 0.76 | 0.3224 | 0.0018 | 3581 | 9 | 99.96 | 0.1616 | 0.0036 | 0.0516 |
| 31-1 | 0.6591 | 0.0134 | 26.99 | 0.56 | 0.2969 | 0.0016 | 3454 | 8 | 99.85 | 0.0550 | 0.0019 | 0.0198 |
| 32-1 | 0.7185 | 0.0146 | 32.30 | 0.65 | 0.3260 | 0.0018 | 3598 | 9 | 99.83 | 0.2677 | 0.0075 | 0.0816 |
| 110-1 | 0.7031 | 0.0120 | 30.69 | 0.56 | 0.3166 | 0.0017 | 3553 | 8 | 99.78 | 0.0517 | 0.0018 | 0.0218 |
| 111-1 | 0.5094 | 0.0066 | 12.73 | 0.17 | 0.1812 | 0.0006 | 2664 | 5 | 99.93 | 0.0066 | 0.0007 | 0.0035 |
| 113-1 | 0.6488 | 0.0123 | 26.31 | 0.50 | 0.2941 | 0.0016 | 3439 | 9 | 99.93 | 0.2226 | 0.0049 | 0.0701 |
| 114-1r | 0.5192 | 0.0071 | 13.22 | 0.19 | 0.1847 | 0.0010 | 2696 | 9 | 99.53 | 0.0274 | 0.0013 | 0.0185 |
| 115-1 | 0.7369 | 0.0202 | 33.84 | 0.94 | 0.3330 | 0.0018 | 3631 | 8 | 99.93 | 0.2603 | 0.0080 | 0.0824 |
| 115-2 | 0.7702 | 0.0110 | 34.85 | 0.47 | 0.3281 | 0.0014 | 3608 | 7 | 99.97 | 0.3509 | 0.0055 | 0.1084 |
| 116-1 | 0.7458 | 0.0196 | 33.93 | 0.93 | 0.3300 | 0.0018 | 3617 | 8 | 99.98 | 0.2469 | 0.0060 | 0.0781 |
| 118-1 | 0.5217 | 0.0063 | 13.17 | 0.15 | 0.1830 | 0.0007 | 2681 | 6 | 99.95 | 0.0265 | 0.0010 | 0.0090 |
| 119-1r | 0.5101 | 0.0071 | 12.82 | 0.18 | 0.1824 | 0.0007 | 2674 | 7 | 99.98 | 0.0319 | 0.0007 | 0.0103 |
| 119-2 | 0.7533 | 0.0164 | 34.42 | 0.77 | 0.3314 | 0.0016 | 3624 | 8 | 99.93 | 0.2721 | 0.0053 | 0.0850 |
| 119-3r | 0.5186 | 0.0074 | 13.13 | 0.19 | 0.1836 | 0.0006 | 2686 | 6 | 99.98 | 0.0330 | 0.0009 | 0.0114 |
| 35-1 | 0.7220 | 0.0141 | 33.30 | 0.63 | 0.3345 | 0.0025 | 3638 | 11 | 99.90 | 0.3315 | 0.0079 | 0.0990 |
| 36-1 | 0.7202 | 0.0153 | 32.13 | 0.65 | 0.3236 | 0.0017 | 3587 | 8 | 99.96 | 0.1023 | 0.0029 | 0.0309 |
| 37-1 | 0.7127 | 0.0109 | 31.31 | 0.47 | 0.3186 | 0.0018 | 3563 | 9 | 99.88 | 0.0296 | 0.0013 | 0.0103 |
| 38-1 | 0.5082 | 0.0061 | 12.87 | 0.16 | 0.1836 | 0.0005 | 2686 | 4 | 99.98 | 0.0361 | 0.0009 | 0.0122 |
| 39-1 | 0.7298 | 0.0092 | 32.40 | 0.40 | 0.3220 | 0.0016 | 3579 | 7 | 99.97 | 0.0007 | 0.0002 | 0.0008 |
| 42-1 | 0.7173 | 0.0140 | 32.30 | 0.66 | 0.3266 | 0.0015 | 3601 | 7 | 99.92 | 0.3882 | 0.0058 | 0.1176 |
| 43-1 | 0.7434 | 0.0167 | 33.48 | 0.76 | 0.3266 | 0.0018 | 3601 | 9 | 99.89 | 0.2585 | 0.0063 | 0.0857 |
| 47-1 | 0.5011 | 0.0106 | 12.20 | 0.27 | 0.1766 | 0.0008 | 2621 | 7 | 99.94 | 0.0188 | 0.0010 | 0.0075 |
| 48-1 | 0.5191 | 0.0077 | 13.23 | 0.19 | 0.1849 | 0.0008 | 2697 | 7 | 99.97 | 0.0337 | 0.0016 | 0.0111 |
| 48-1+ | 0.5086 | 0.0079 | 13.04 | 0.19 | 0.1859 | 0.0009 | 2706 | 8 | 99.99 | 0.0340 | 0.0010 | 0.0109 |
| 49-1 | 0.4005 | 0.0046 | 9.59 | 0.12 | 0.1737 | 0.0006 | 2593 | 6 | 99.90 | 0.0042 | 0.0003 | 0.0029 |
| 51-1 | 0.5132 | 0.0114 | 13.22 | 0.31 | 0.1869 | 0.0009 | 2715 | 8 | 99.94 | 0.0307 | 0.0015 | 0.0106 |
| 52-1 | 0.6999 | 0.0119 | 29.08 | 0.57 | 0.3013 | 0.0019 | 3477 | 10 | 99.90 | 0.1365 | 0.0048 | 0.0485 |
| 53-1 | 0.4474 | 0.0056 | 11.03 | 0.14 | 0.1789 | 0.0008 | 2642 | 7 | 99.89 | 0.0288 | 0.0010 | 0.0117 |
| 55-1 | 0.5681 | 0.0094 | 19.30 | 0.34 | 0.2464 | 0.0012 | 3162 | 7 | 99.93 | 0.1166 | 0.0034 | 0.0398 |
| 112-1 | 0.2848 | 0.0049 | 4.51 | 0.08 | 0.1149 | 0.0006 | 1878 | 9 | 99.70 | 0.0002 | 0.0001 | 0.0066 |
| 117-1 | 0.5270 | 0.0058 | 13.40 | 0.15 | 0.1844 | 0.0006 | 2693 | 5 | 99.96 | 0.0343 | 0.0012 | 0.0119 |
| 310-1 | 0.5180 | 0.0176 | 13.29 | 0.45 | 0.1861 | 0.0015 | 2708 | 13 | 99.84 | 0.0180 | 0.0017 | 0.0072 |
| 311-1 | 0.5881 | 0.0085 | 24.55 | 0.37 | 0.3027 | 0.0012 | 3484 | 6 | 99.65 | 0.0819 | 0.0016 | 0.0337 |
| 312-1 | 0.5912 | 0.0073 | 20.79 | 0.29 | 0.2550 | 0.0013 | 3216 | 8 | 99.94 | 0.0295 | 0.0010 | 0.0091 |
| 312-2r | 0.5182 | 0.0068 | 13.88 | 0.20 | 0.1943 | 0.0008 | 2779 | 7 | 99.95 | 0.0332 | 0.0012 | 0.0116 |
| 313-1r | 0.5762 | 0.0104 | 18.73 | 0.34 | 0.2358 | 0.0020 | 3092 | 13 | 98.32 | 0.0132 | 0.0008 | 0.0431 |
| 314-1 | 0.7198 | 0.0217 | 32.63 | 0.95 | 0.3288 | 0.0026 | 3611 | 12 | 99.78 | 0.3223 | 0.0131 | 0.0984 |
| 315-1 | 0.7315 | 0.0113 | 32.63 | 0.51 | 0.3236 | 0.0015 | 3587 | 7 | 99.92 | 0.0814 | 0.0035 | 0.0113 |
| 316-1 | 0.6905 | 0.0079 | 29.72 | 0.33 | 0.3122 | 0.0012 | 3532 | 6 | 99.77 | 0.1710 | 0.0028 | 0.0589 |
| 317-1 | 0.5182 | 0.0060 | 13.12 | 0.15 | 0.1836 | 0.0006 | 2685 | 5 | 99.96 | 0.0441 | 0.0007 | 0.0149 |
| 318-1 | 0.6555 | 0.0110 | 27.42 | 0.45 | 0.3034 | 0.0014 | 3488 | 7 | 99.91 | 0.0040 | 0.0003 | 0.0033 |
| 318-2r | 0.4878 | 0.0124 | 11.72 | 0.30 | 0.1742 | 0.0011 | 2598 | 10 | 99.65 | 0.0012 | 0.0002 | 0.0072 |
| 319-1 | 0.7282 | 0.0157 | 33.10 | 0.78 | 0.3296 | 0.0017 | 3615 | 8 | 99.82 | 0.2651 | 0.0077 | 0.0864 |
| 319-2r | 0.5300 | 0.0094 | 15.67 | 0.29 | 0.2144 | 0.0013 | 2939 | 10 | 99.91 | 0.0813 | 0.0033 | 0.0326 |
| 320-1r | 0.6709 | 0.0149 | 26.47 | 0.60 | 0.2862 | 0.0018 | 3397 | 10 | 99.93 | 0.2032 | 0.0052 | 0.0685 |
| *GR9713, Fe-rich quartz-pyroxene rock, session 2* | | | | | | | | | | | | |
| 11-1 | 0.6637 | 0.0049 | 28.56 | 0.21 | 0.3121 | 0.0017 | 3531 | 8 | 99.87 | 0.0081 | 0.0004 | 0.0050 |
| 11-2r | 0.5054 | 0.0049 | 13.80 | 0.14 | 0.1981 | 0.0009 | 2810 | 7 | 99.84 | 0.0116 | 0.0005 | 0.0069 |
| 12-1 | 0.4688 | 0.0050 | 12.47 | 0.14 | 0.1928 | 0.0007 | 2767 | 6 | 99.90 | 0.0181 | 0.0006 | 0.0087 |

TABLE A1
*(continued)*

| Grain-spot | $^{206}Pb^*/^{238}U$ ratio | 1σ | $^{207}Pb^*/^{235}U$ ratio | 1σ | $^{207}Pb^*/^{206}Pb^*$ ratio | 1σ | $^{207}Pb/^{206}Pb$ age (Ma) | 1σ | $^{206}Pb^*$ (%) | Th/U | 1σ | $^{208}Pb/^{206}Pb$ ratio |
|---|---|---|---|---|---|---|---|---|---|---|---|---|
| *GR9713-2, Fe-rich quartz-pyroxene rock, session 2 (continued)* | | | | | | | | | | | | |
| 13-1 | 0.7249 | 0.0080 | 31.92 | 0.36 | 0.3194 | 0.0009 | 3567 | 4 | 99.76 | 0.0536 | 0.0013 | 0.0218 |
| 14-1 | 0.6334 | 0.0098 | 24.62 | 0.39 | 0.2819 | 0.0009 | 3374 | 5 | 99.77 | 0.1515 | 0.0019 | 0.0520 |
| 15-1 | 0.5249 | 0.0038 | 13.02 | 0.20 | 0.1799 | 0.0027 | 2652 | 25 | 99.98 | 0.0359 | 0.0009 | 0.0120 |
| 16-1 | 0.4877 | 0.0060 | 10.98 | 0.12 | 0.1633 | 0.0006 | 2490 | 6 | 99.93 | 0.0027 | 0.0003 | 0.0018 |
| 17-1 | 0.5183 | 0.0034 | 13.15 | 0.09 | 0.1840 | 0.0004 | 2689 | 4 | 99.98 | 0.0409 | 0.0006 | 0.0129 |
| 18-1 | 0.7101 | 0.0078 | 30.75 | 0.33 | 0.3140 | 0.0011 | 3541 | 6 | 99.95 | 0.0763 | 0.0021 | 0.0237 |
| 19-1 | 0.7172 | 0.0082 | 31.43 | 0.38 | 0.3178 | 0.0009 | 3559 | 5 | 99.96 | 0.2328 | 0.0031 | 0.0720 |
| 31-1 | 0.7304 | 0.0081 | 31.97 | 0.36 | 0.3174 | 0.0010 | 3557 | 5 | 99.90 | 0.1084 | 0.0023 | 0.0330 |
| 32-1 | 0.7538 | 0.0116 | 33.85 | 0.54 | 0.3257 | 0.0013 | 3597 | 6 | 99.94 | 0.2703 | 0.0058 | 0.0818 |
| 110-1 | 0.7258 | 0.0068 | 32.28 | 0.31 | 0.3226 | 0.0008 | 3582 | 4 | 99.98 | 0.0960 | 0.0012 | 0.0293 |
| 110-2r | 0.5254 | 0.0048 | 13.33 | 0.12 | 0.1841 | 0.0005 | 2690 | 5 | 99.93 | 0.0107 | 0.0004 | 0.0046 |
| 111-1 | 0.7437 | 0.0077 | 33.48 | 0.32 | 0.3265 | 0.0009 | 3601 | 4 | 99.47 | 0.2383 | 0.0028 | 0.0828 |
| 113-1 | 0.6490 | 0.0086 | 24.49 | 0.33 | 0.2736 | 0.0008 | 3327 | 5 | 99.92 | 0.1731 | 0.0036 | 0.0569 |
| 114-1 | 0.5352 | 0.0113 | 13.70 | 0.28 | 0.1857 | 0.0009 | 2705 | 8 | 98.83 | 0.0243 | 0.0012 | 0.0318 |
| 115-1 | 0.7462 | 0.0113 | 33.93 | 0.51 | 0.3297 | 0.0010 | 3616 | 5 | 99.92 | 0.3506 | 0.0057 | 0.1057 |
| 115-2 | 0.7566 | 0.0110 | 34.45 | 0.50 | 0.3302 | 0.0011 | 3618 | 5 | 99.94 | 0.3541 | 0.0066 | 0.1067 |
| 116-1 | 0.7411 | 0.0115 | 33.52 | 0.57 | 0.3281 | 0.0012 | 3608 | 6 | 99.90 | 0.2454 | 0.0059 | 0.0738 |
| 118-1 | 0.5172 | 0.0047 | 13.11 | 0.11 | 0.1838 | 0.0006 | 2687 | 5 | 99.84 | 0.0301 | 0.0010 | 0.0116 |
| 119-1 | 0.7504 | 0.0117 | 34.31 | 0.53 | 0.3316 | 0.0010 | 3625 | 5 | 99.95 | 0.2889 | 0.0054 | 0.0883 |
| *GR00114, anthophyllite-garnet schist* | | | | | | | | | | | | |
| 2-1 | 0.7350 | 0.0072 | 33.18 | 0.32 | 0.3274 | 0.0016 | 3605 | 7 | 99.78 | 0.0693 | 0.0023 | 0.0236 |
| 5-1 | 0.7421 | 0.0094 | 34.42 | 0.47 | 0.3364 | 0.0032 | 3646 | 15 | 99.66 | 0.2186 | 0.0092 | 0.0745 |
| 6-1 | 0.7130 | 0.0119 | 31.20 | 0.53 | 0.3174 | 0.0014 | 3557 | 7 | 99.84 | 0.2067 | 0.0077 | 0.0643 |
| 10-1 | 0.5265 | 0.0068 | 13.65 | 0.16 | 0.1880 | 0.0013 | 2725 | 12 | 99.78 | 0.0229 | 0.0016 | 0.0081 |
| 26-1 | 0.7862 | 0.0181 | 36.07 | 0.87 | 0.3328 | 0.0025 | 3630 | 11 | 99.60 | 0.2502 | 0.0132 | 0.0694 |
| 29-1 | 0.5151 | 0.0121 | 13.19 | 0.34 | 0.1857 | 0.0022 | 2705 | 19 | 99.37 | 0.0198 | 0.0035 | 0.0103 |
| 210-1 | 0.7765 | 0.0092 | 35.64 | 0.45 | 0.3328 | 0.0013 | 3630 | 6 | 99.81 | 0.3489 | 0.0060 | 0.1118 |
| 211-1 | 0.7281 | 0.0252 | 32.45 | 1.30 | 0.3233 | 0.0059 | 3586 | 28 | 98.64 | 0.1997 | 0.0165 | 0.0766 |
| 212-1 | 0.7649 | 0.0072 | 35.43 | 0.28 | 0.3360 | 0.0014 | 3645 | 6 | 99.82 | 0.2173 | 0.0044 | 0.0685 |
| 311-1 | 0.7606 | 0.0233 | 35.13 | 1.20 | 0.3350 | 0.0040 | 3640 | 18 | 99.48 | 0.2060 | 0.0183 | 0.0621 |
| *GR9802, tonalitic orthogneiss, session 1* | | | | | | | | | | | | |
| 11-1 | 0.7595 | 0.0121 | 36.54 | 0.64 | 0.3489 | 0.0033 | 3702 | 15 | 99.40 | 0.4259 | 0.0189 | 0.1578 |
| 11-2 | 0.7310 | 0.0146 | 35.18 | 0.72 | 0.3490 | 0.0030 | 3703 | 13 | 99.31 | 0.3379 | 0.0166 | 0.1150 |
| 11-3 | 0.8412 | 0.0287 | 41.74 | 1.39 | 0.3598 | 0.0021 | 3749 | 9 | 99.56 | 0.1643 | 0.0047 | 0.1087 |
| 12-1 | 0.6812 | 0.0116 | 29.46 | 0.48 | 0.3136 | 0.0029 | 3539 | 14 | 99.51 | 0.1163 | 0.0063 | 0.0490 |
| 15-1 | 0.7311 | 0.0100 | 36.12 | 0.53 | 0.3584 | 0.0013 | 3743 | 5 | 99.90 | 0.0414 | 0.0012 | 0.0274 |
| 16-1 | 0.8200 | 0.0432 | 40.98 | 2.29 | 0.3625 | 0.0043 | 3760 | 18 | 99.12 | 0.1491 | 0.0048 | 0.1222 |
| 17-1 | 0.7525 | 0.0130 | 36.94 | 0.64 | 0.3560 | 0.0013 | 3733 | 5 | 99.75 | 0.0348 | 0.0005 | 0.0263 |
| 18-1 | 0.7630 | 0.0288 | 36.81 | 1.39 | 0.3499 | 0.0023 | 3706 | 10 | 99.27 | 0.2443 | 0.0052 | 0.1603 |
| 19-1 | 0.5875 | 0.0383 | 22.99 | 1.76 | 0.2839 | 0.0077 | 3384 | 42 | 97.26 | 0.3976 | 0.0179 | 0.3143 |
| 19-2r | 0.6667 | 0.0911 | 29.26 | 4.47 | 0.3184 | 0.0117 | 3562 | 57 | 92.60 | 0.9328 | 0.0498 | 0.7804 |
| 21-1 | 0.6852 | 0.0088 | 30.66 | 0.38 | 0.3246 | 0.0024 | 3592 | 11 | 99.68 | 0.0293 | 0.0019 | 0.0133 |
| 24-1 | 0.7762 | 0.0139 | 38.34 | 0.71 | 0.3583 | 0.0028 | 3743 | 12 | 99.62 | 0.2997 | 0.0089 | 0.1022 |
| 24-2 | 0.7988 | 0.0181 | 39.84 | 0.90 | 0.3618 | 0.0022 | 3757 | 9 | 99.76 | 0.1635 | 0.0028 | 0.1073 |
| 25-1 | 0.7329 | 0.0066 | 32.23 | 0.30 | 0.3190 | 0.0015 | 3565 | 7 | 99.75 | 0.0246 | 0.0012 | 0.0119 |
| 27-1 | 0.7691 | 0.0268 | 37.62 | 1.31 | 0.3548 | 0.0017 | 3728 | 7 | 99.53 | 0.1873 | 0.0027 | 0.1219 |
| 28-1 | 0.5222 | 0.0262 | 17.83 | 0.89 | 0.2476 | 0.0040 | 3170 | 25 | 99.13 | 0.0746 | 0.0049 | 0.0700 |
| 111-1 | 0.7460 | 0.0178 | 36.02 | 0.88 | 0.3501 | 0.0013 | 3708 | 6 | 99.57 | 0.2322 | 0.0051 | 0.1429 |
| 111-2r | 0.6746 | 0.0205 | 29.05 | 0.89 | 0.3123 | 0.0026 | 3532 | 13 | 99.05 | 0.0506 | 0.0015 | 0.0489 |
| 210-1r | 0.7074 | 0.0169 | 31.68 | 0.79 | 0.3247 | 0.0019 | 3592 | 9 | 99.52 | 0.0626 | 0.0016 | 0.0486 |
| 211-1 | 0.7545 | 0.0148 | 34.84 | 0.67 | 0.3349 | 0.0018 | 3639 | 8 | 99.87 | 0.0659 | 0.0020 | 0.0444 |
| 211-2 | 0.7661 | 0.0122 | 35.27 | 0.53 | 0.3339 | 0.0016 | 3635 | 7 | 99.80 | 0.0843 | 0.0013 | 0.0559 |
| 212-1r | 0.7424 | 0.0180 | 35.12 | 0.90 | 0.3431 | 0.0026 | 3676 | 11 | 99.90 | 0.0047 | 0.0004 | 0.0058 |
| 26-1 | 0.7274 | 0.0179 | 35.44 | 0.86 | 0.3534 | 0.0018 | 3722 | 8 | 99.94 | 0.1503 | 0.0015 | 0.0914 |
| 31-1 | 0.6723 | 0.0231 | 30.42 | 1.04 | 0.3282 | 0.0025 | 3609 | 12 | 99.54 | 0.0504 | 0.0025 | 0.0436 |
| 34-1 | 0.7442 | 0.0258 | 35.48 | 1.20 | 0.3458 | 0.0027 | 3689 | 12 | 99.48 | 0.0212 | 0.0016 | 0.0157 |

TABLE A1
*(continued)*

| Grain-spot | $^{206}Pb^*/^{238}U$ ratio | 1σ | $^{207}Pb^*/^{235}U$ ratio | 1σ | $^{207}Pb^*/^{206}Pb^*$ ratio | 1σ | $^{207}Pb/^{206}Pb$ age (Ma) | 1σ | $^{206}Pb^*$ (%) | Th/U | 1σ | $^{208}Pb/^{206}Pb$ ratio |
|---|---|---|---|---|---|---|---|---|---|---|---|---|
| *GR9802, tonalitic orthogneiss, session 2* | | | | | | | | | | | | |
| 11-1r | 0.7749 | 0.0126 | 37.80 | 0.60 | 0.3538 | 0.0015 | 3560 | 14 | 99.04 | 0.3710 | 0.0104 | 0.1411 |
| 11-2 | 0.7686 | 0.0146 | 38.44 | 0.86 | 0.3627 | 0.0025 | 3744 | 9 | 99.53 | 0.4782 | 0.0091 | 0.1608 |
| 12-1 | 0.7959 | 0.0251 | 39.29 | 1.26 | 0.3580 | 0.0023 | 3664 | 20 | 98.30 | 0.1805 | 0.0080 | 0.0924 |
| 12-2r | 0.7477 | 0.0124 | 34.13 | 0.61 | 0.3311 | 0.0022 | 3622 | 10 | 99.28 | 0.0945 | 0.0028 | 0.0418 |
| 15-1r | 0.7726 | 0.0070 | 36.68 | 0.34 | 0.3443 | 0.0010 | 3605 | 12 | 98.58 | 0.4254 | 0.0087 | 0.1749 |
| 15-2r | 0.7679 | 0.0127 | 35.37 | 0.57 | 0.3341 | 0.0011 | 3636 | 5 | 99.75 | 0.0881 | 0.0021 | 0.0326 |
| 15-3 | 0.8006 | 0.0170 | 39.58 | 0.88 | 0.3586 | 0.0015 | 3744 | 6 | 99.62 | 0.5337 | 0.0076 | 0.1737 |
| 16-1r | 0.6462 | 0.0151 | 27.30 | 0.69 | 0.3064 | 0.0023 | 3721 | 5 | 99.62 | 0.1036 | 0.0021 | 0.0386 |
| 16-2 | 0.7951 | 0.0245 | 38.70 | 1.22 | 0.3530 | 0.0026 | 3720 | 11 | 99.22 | 0.2498 | 0.0071 | 0.0930 |
| 16-3 | 0.7699 | 0.0226 | 37.01 | 1.13 | 0.3486 | 0.0023 | 3701 | 10 | 99.49 | 0.3543 | 0.0090 | 0.1227 |
| 16-4r | 0.7894 | 0.0191 | 38.47 | 0.87 | 0.3534 | 0.0028 | 3722 | 12 | 98.96 | 0.2134 | 0.0071 | 0.0871 |
| 17-1r | 0.7357 | 0.0195 | 33.51 | 0.92 | 0.3304 | 0.0021 | 3619 | 10 | 99.18 | 1.9749 | 0.0191 | 0.6553 |
| 17-2 | 0.7327 | 0.0086 | 32.70 | 0.42 | 0.3237 | 0.0013 | 3587 | 6 | 99.62 | 0.0475 | 0.0014 | 0.0216 |
| 18-1 | 0.7211 | 0.0129 | 33.44 | 0.63 | 0.3364 | 0.0018 | 3674 | 11 | 99.42 | 0.3848 | 0.0098 | 0.1296 |
| 18-2r | 0.7466 | 0.0155 | 33.51 | 0.72 | 0.3255 | 0.0013 | 3596 | 6 | 99.57 | 0.0908 | 0.0027 | 0.0382 |
| 19-1r | 0.7907 | 0.0262 | 39.30 | 1.31 | 0.3605 | 0.0026 | 2751 | 71 | 96.44 | 0.1642 | 0.0097 | 0.1450 |
| 19-2 | 0.7473 | 0.0314 | 35.98 | 1.49 | 0.3492 | 0.0035 | 3703 | 15 | 98.84 | 0.3121 | 0.0148 | 0.1083 |
| 21-1 | 0.6784 | 0.0079 | 27.11 | 0.36 | 0.2899 | 0.0013 | 3417 | 7 | 99.96 | 0.1020 | 0.0019 | 0.0386 |
| 21-2 | 0.5128 | 0.0282 | 21.84 | 1.25 | 0.3089 | 0.0054 | 3515 | 27 | 98.12 | 1.0109 | 0.0551 | 0.3548 |
| 24-1 | 0.5311 | 0.0378 | 13.99 | 1.26 | 0.1910 | 0.0083 | 3752 | 11 | 99.57 | 0.2056 | 0.0111 | 0.0717 |
| 25-1 | 0.7933 | 0.0263 | 37.47 | 1.28 | 0.3425 | 0.0024 | 3646 | 8 | 99.30 | 0.0940 | 0.0030 | 0.0398 |
| 27-1 | 0.7882 | 0.0151 | 38.40 | 0.75 | 0.3533 | 0.0012 | 3503 | 11 | 98.89 | 0.3194 | 0.0081 | 0.1302 |
| 28-1 | 0.6551 | 0.0145 | 29.58 | 0.74 | 0.3274 | 0.0026 | 3682 | 4 | 99.91 | 0.3277 | 0.0031 | 0.1040 |
| 111-1 | 0.7687 | 0.0182 | 34.88 | 0.89 | 0.3290 | 0.0019 | 3668 | 10 | 99.60 | 0.3584 | 0.0088 | 0.1181 |
| 111-2r | 0.7411 | 0.0220 | 33.90 | 1.09 | 0.3318 | 0.0031 | 3625 | 14 | 98.64 | 1.7718 | 0.0227 | 0.5387 |
| 210-1 | 0.7605 | 0.0236 | 36.17 | 1.18 | 0.3449 | 0.0037 | 3731 | 8 | 98.80 | 0.2611 | 0.0048 | 0.1029 |
| 211-1 | 0.7239 | 0.0335 | 33.97 | 1.66 | 0.3403 | 0.0045 | 3741 | 10 | 99.15 | 0.3551 | 0.0099 | 0.1317 |
| 212-1 | 0.6568 | 0.0156 | 28.80 | 0.80 | 0.3180 | 0.0029 | 3723 | 6 | 99.61 | 0.1212 | 0.0035 | 0.0448 |
| 212-2 | 0.7679 | 0.0156 | 37.97 | 0.84 | 0.3586 | 0.0021 | 3761 | 10 | 99.59 | 0.0732 | 0.0050 | 0.0306 |
| 13-1 | 0.7613 | 0.0192 | 37.31 | 0.99 | 0.3555 | 0.0019 | 3685 | 16 | 97.90 | 0.2479 | 0.0074 | 0.1139 |
| 13-2r | 0.7741 | 0.0136 | 37.30 | 0.71 | 0.3495 | 0.0030 | 3705 | 13 | 99.22 | 0.3251 | 0.0075 | 0.1187 |
| 14-1 | 0.7573 | 0.0154 | 36.72 | 0.81 | 0.3516 | 0.0022 | 3714 | 9 | 99.01 | 0.2989 | 0.0077 | 0.1185 |
| 14-2r | 0.7466 | 0.0169 | 32.12 | 0.73 | 0.3120 | 0.0026 | 3531 | 13 | 99.35 | 0.1716 | 0.0052 | 0.0651 |
| 22-1r | 0.7091 | 0.0155 | 33.35 | 0.73 | 0.3411 | 0.0022 | 3613 | 9 | 99.80 | 0.1980 | 0.0051 | 0.0609 |
| 23-1 | 0.6965 | 0.0364 | 32.53 | 1.85 | 0.3388 | 0.0045 | 3712 | 7 | 99.87 | 0.0799 | 0.0015 | 0.0269 |
| 110-1 | 0.7633 | 0.0099 | 36.97 | 0.56 | 0.3512 | 0.0015 | 3657 | 20 | 98.01 | 0.3977 | 0.0157 | 0.1602 |
| *GR0012, tonalitic orthogneiss* | | | | | | | | | | | | |
| 1-1 | 0.7731 | 0.0424 | 38.11 | 2.10 | 0.3576 | 0.0023 | 3740 | 10 | 99.49 | 0.4112 | 0.0112 | 0.1173 |
| 1-2r | 0.7353 | 0.0268 | 33.36 | 1.24 | 0.3290 | 0.0016 | 3613 | 8 | 99.52 | 0.4581 | 0.0072 | 0.1339 |
| 2-1 | 0.6767 | 0.0473 | 32.64 | 2.25 | 0.3498 | 0.0043 | 3706 | 19 | 98.49 | 0.7661 | 0.0341 | 0.2383 |
| 3-1 | 0.7819 | 0.0215 | 38.62 | 1.12 | 0.3583 | 0.0013 | 3743 | 6 | 99.44 | 0.6420 | 0.0077 | 0.1704 |
| 4-1 | 0.7449 | 0.0220 | 36.40 | 1.09 | 0.3539 | 0.0020 | 3724 | 9 | 99.65 | 0.4380 | 0.0085 | 0.1207 |
| *GR0050, tonalitic orthogneiss* | | | | | | | | | | | | |
| 1-1 | 0.5621 | 0.0465 | 26.90 | 2.28 | 0.3474 | 0.0047 | 3695 | 19 | 98.29 | 0.6413 | 0.0152 | 0.1412 |
| 2-1 | 0.7686 | 0.0317 | 38.00 | 1.57 | 0.3587 | 0.0016 | 3744 | 7 | 99.66 | 0.5889 | 0.0097 | 0.1615 |
| *GR0071, tonalitic orthogneiss* | | | | | | | | | | | | |
| 19-1 | 0.9134 | 0.0648 | 44.69 | 3.19 | 0.3549 | 0.0021 | 3728 | 9 | 99.78 | 0.3000 | 0.0074 | 0.3905 |
| 21-1 | 0.9116 | 0.0685 | 46.60 | 3.52 | 0.3708 | 0.0017 | 3795 | 7 | 99.76 | 0.3421 | 0.0094 | 0.2537 |
| 21-2r | 0.6516 | 0.0241 | 29.63 | 1.15 | 0.3298 | 0.0015 | 3616 | 7 | 99.85 | 0.1681 | 0.0042 | 0.2123 |
| 21-2r+ | 0.6563 | 0.0778 | 30.24 | 3.64 | 0.3342 | 0.0044 | 3636 | 20 | 98.48 | 0.7341 | 0.0391 | 1.5540 |
| 22-1 | 0.7283 | 0.0757 | 37.97 | 3.99 | 0.3781 | 0.0025 | 3824 | 10 | 99.81 | 0.4118 | 0.0129 | 0.4596 |
| 22-1+ | 0.7265 | 0.0462 | 37.41 | 2.37 | 0.3734 | 0.0021 | 3805 | 8 | 100.00 | 0.4052 | 0.0126 | 0.4743 |
| 24-1 | 0.6019 | 0.0294 | 28.01 | 1.41 | 0.3376 | 0.0015 | 3652 | 7 | 99.71 | 0.7071 | 0.0092 | 0.2034 |
| 25-1 | 0.7580 | 0.0376 | 35.07 | 1.75 | 0.3356 | 0.0018 | 3643 | 8 | 99.71 | 0.3092 | 0.0082 | 0.2834 |

TABLE A1
*(continued)*

| Grain-spot | $^{206}Pb^*/^{238}U$ ratio | 1σ | $^{207}Pb^*/^{235}U$ ratio | 1σ | $^{207}Pb^*/^{206}Pb^*$ ratio | 1σ | $^{207}Pb/^{206}Pb$ age (Ma) | 1σ | $^{206}Pb^*$ (%) | Th/U | 1σ | $^{208}Pb/^{206}Pb$ ratio |
|---|---|---|---|---|---|---|---|---|---|---|---|---|
| | | | | | *GR0071, tonalitic orthogneiss* | | | | | | | |
| 26-1 | 0.8931 | 0.0679 | 46.86 | 3.57 | 0.3806 | 0.0017 | 3834 | 7 | 99.89 | 0.7087 | 0.0124 | 0.1945 |
| 27-1 | 0.7073 | 0.0357 | 35.78 | 1.79 | 0.3669 | 0.0033 | 3779 | 13 | 99.80 | 0.4668 | 0.0115 | 0.3128 |
| 28-1 | 0.7126 | 0.0282 | 31.99 | 1.25 | 0.3256 | 0.0012 | 3596 | 6 | 99.77 | 0.6931 | 0.0076 | 0.0475 |
| 29-1 | 0.8534 | 0.0631 | 38.77 | 2.84 | 0.3295 | 0.0018 | 3615 | 9 | 99.78 | 0.3362 | 0.0114 | 0.3345 |
| 210-1 | 0.8084 | 0.0610 | 42.72 | 3.19 | 0.3833 | 0.0025 | 3845 | 10 | 99.46 | 0.4950 | 0.0154 | 0.4323 |
| 31-1 | 0.8002 | 0.0589 | 41.33 | 3.13 | 0.3747 | 0.0026 | 3810 | 11 | 99.57 | 0.4247 | 0.0111 | 0.4057 |
| 32-1 | 0.6456 | 0.0221 | 31.05 | 1.08 | 0.3488 | 0.0011 | 3702 | 5 | 99.85 | 0.1357 | 0.0021 | 0.0696 |
| 33-1 | 0.6012 | 0.0356 | 26.24 | 1.57 | 0.3165 | 0.0023 | 3553 | 11 | 99.69 | 0.2799 | 0.0075 | 0.3041 |
| 34a-1 | 0.8225 | 0.0533 | 42.66 | 2.76 | 0.3761 | 0.0022 | 3816 | 9 | 99.79 | 0.3273 | 0.0086 | 0.3199 |
| 34b-1 | 0.8115 | 0.0258 | 42.05 | 1.33 | 0.3758 | 0.0013 | 3815 | 5 | 99.71 | 0.7015 | 0.0096 | 0.1277 |
| 36-1 | 0.7259 | 0.0480 | 37.91 | 2.46 | 0.3787 | 0.0047 | 3827 | 19 | 99.84 | 0.5073 | 0.0104 | 0.1917 |
| 37b-1 | 0.7387 | 0.0305 | 32.43 | 1.33 | 0.3184 | 0.0012 | 3562 | 6 | 99.86 | 0.0479 | 0.0020 | 0.1789 |
| 38-1 | 0.7036 | 0.0274 | 32.84 | 1.27 | 0.3385 | 0.0015 | 3656 | 7 | 99.86 | 0.4105 | 0.0067 | 0.1228 |
| 39-1 | 0.8447 | 0.0494 | 43.03 | 2.48 | 0.3694 | 0.0013 | 3789 | 5 | 99.90 | 0.4191 | 0.0067 | 0.1768 |
| 310-1 | 0.8742 | 0.0469 | 45.79 | 2.45 | 0.3799 | 0.0016 | 3831 | 6 | 99.85 | 0.5641 | 0.0099 | 0.2042 |
| 41-1 | 0.8465 | 0.0663 | 42.54 | 3.44 | 0.3660 | 0.0035 | 3768 | 13 | 98.80 | 0.2799 | 0.0125 | 0.066 |
| 43-1 | 0.7224 | 0.0241 | 36.83 | 1.25 | 0.3698 | 0.0018 | 3791 | 7 | 99.27 | 0.6420 | 0.0127 | 0.024 |
| 43-2 | 0.6890 | 0.0266 | 31.99 | 1.24 | 0.3368 | 0.0015 | 3648 | 7 | 99.38 | 0.4176 | 0.0052 | 0.027 |
| 44-1 | 0.7285 | 0.0216 | 35.00 | 1.03 | 0.3484 | 0.0016 | 3700 | 7 | 99.24 | 0.5535 | 0.0097 | 0.022 |
| 47-1 | 0.6602 | 0.0203 | 29.10 | 0.90 | 0.3197 | 0.0018 | 3568 | 8 | 98.94 | 0.0590 | 0.0024 | 0.020 |
| 49-1 | 0.6271 | 0.0328 | 29.90 | 1.49 | 0.3458 | 0.0032 | 3689 | 14 | 98.72 | 0.6489 | 0.0267 | 0.033 |

Notes: Sample locations given in figure 3. Grain and analysis numbers in left column are keyed to figures A1–A5; 'r' denotes analysis near grain rim, '+' denotes repeat analysis of same spot during the same analytical session. Samples GR9713 and GR9802 were analyzed over two sessions. The samples were re-polished between sessions. Isotopic ratios have been corrected for common Pb. Ages were determined by comparison with a working curve defined by measurement of standard zircon AS-3, which yields concordant $^{206}Pb/^{238}U$ and $^{207}Pb/^{235}U$ ages of 1099.1 ± 0.5 Ma by conventional methods. Th/U ratios were calibrated against independently determined values for AS-3. All uncertainties are reported at the 1σ levels.

TABLE A2

*Results of depth-profiling study of zircon grain #36, GR0071*

| Depth (μm) | $^{206}Pb^*/^{238}U$ ratio | 1se | $^{207}Pb^*/^{235}U$ ratio | 1se | $^{207}Pb^*/^{206}Pb^*$ ratio | 1se | $^{207}Pb/^{206}Pb$ age (Ma) | 1se | $^{206}Pb^*$ (%) | Th/U | 1se | $^{208}Pb/^{206}Pb$ ratio |
|---|---|---|---|---|---|---|---|---|---|---|---|---|
| 0.00 | 0.5534 | 0.1430 | 12.51 | 3.27 | 0.1640 | 0.00545 | 2497 | 56 | 99.58 | 0.07345 | 0.01554 | 0.02226 |
| 0.19 | 0.6396 | 0.2670 | 15.37 | 6.57 | 0.1742 | 0.00694 | 2599 | 66 | 99.78 | 0.08433 | 0.01277 | 0.02914 |
| 0.37 | 0.5951 | 0.1400 | 14.57 | 3.56 | 0.1775 | 0.00745 | 2630 | 70 | 99.66 | 0.1239 | 0.01223 | 0.03282 |
| 0.56 | 0.5428 | 0.0885 | 13.58 | 2.18 | 0.1815 | 0.00873 | 2666 | 80 | 100.00 | 0.1593 | 0.02175 | 0.03546 |
| 0.74 | 0.5553 | 0.1840 | 14.57 | 4.81 | 0.1903 | 0.0168 | 2745 | 145 | 100.00 | 0.1225 | 0.06597 | 0.0431 |
| 0.93 | 0.6033 | 0.2410 | 15.14 | 6.07 | 0.1821 | 0.0084 | 2672 | 76 | 100.00 | 0.1636 | 0.03917 | 0.04474 |
| 1.12 | 0.5412 | 0.0793 | 13.37 | 1.94 | 0.1791 | 0.00533 | 2645 | 49 | 100.00 | 0.1620 | 0.02237 | 0.04308 |
| 1.30 | 0.5208 | 0.1160 | 13.17 | 2.93 | 0.1834 | 0.0293 | 2684 | 264 | 100.00 | 0.1996 | 0.04045 | 0.03688 |
| 1.49 | 0.5471 | 0.0907 | 14.33 | 2.43 | 0.1900 | 0.00672 | 2742 | 58 | 99.76 | 0.1418 | 0.02483 | 0.04236 |
| 1.67 | 0.4223 | 0.0908 | 10.81 | 2.25 | 0.1857 | 0.0113 | 2704 | 100 | 100.00 | 0.2048 | 0.02788 | 0.0473 |
| 1.86 | 0.5160 | 0.0941 | 13.33 | 2.37 | 0.1873 | 0.0078 | 2719 | 69 | 100.00 | 0.1670 | 0.02882 | 0.04663 |
| 2.05 | 0.4891 | 0.1050 | 12.08 | 2.52 | 0.1791 | 0.0110 | 2645 | 102 | 100.00 | 0.1595 | 0.03826 | 0.0413 |
| 2.23 | 0.5513 | 0.1190 | 13.37 | 2.91 | 0.1759 | 0.00615 | 2615 | 58 | 100.00 | 0.1393 | 0.04651 | 0.03959 |
| 2.42 | 0.4995 | 0.0843 | 11.89 | 1.95 | 0.1727 | 0.00745 | 2584 | 72 | 100.00 | 0.1667 | 0.01942 | 0.03845 |
| 2.60 | 0.5863 | 0.1840 | 14.66 | 4.55 | 0.1814 | 0.00963 | 2666 | 88 | 100.00 | 0.1862 | 0.07535 | 0.0307 |
| 2.79 | 0.5879 | 0.2690 | 14.74 | 6.76 | 0.1819 | 0.0266 | 2670 | 242 | 99.82 | 0.1377 | 0.02056 | 0.03597 |
| 2.98 | 0.4906 | 0.0600 | 11.39 | 1.33 | 0.1683 | 0.00886 | 2541 | 88 | 100.00 | 0.08463 | 0.0155 | 0.02843 |
| 3.16 | 0.4668 | 0.0780 | 11.47 | 1.83 | 0.1782 | 0.0115 | 2636 | 107 | 100.00 | 0.1380 | 0.02046 | 0.02884 |
| 3.35 | 0.6007 | 0.1790 | 15.43 | 4.63 | 0.1863 | 0.00805 | 2710 | 71 | 100.00 | 0.1289 | 0.02766 | 0.03117 |
| 3.53 | 0.5640 | 0.2500 | 15.13 | 6.81 | 0.1945 | 0.0144 | 2781 | 121 | 100.00 | 0.08495 | 0.0603 | 0.02742 |
| 3.72 | 0.7097 | 0.3890 | 16.92 | 9.22 | 0.1729 | 0.0105 | 2586 | 101 | 100.00 | 0.1020 | 0.02284 | 0.03004 |
| 3.91 | 0.7340 | 0.6270 | 17.28 | 14.5 | 0.1707 | 0.0185 | 2565 | 181 | 100.00 | 0.1315 | 0.02348 | 0.0238 |
| 4.09 | 0.7523 | 0.5330 | 19.96 | 13.9 | 0.1924 | 0.0198 | 2763 | 169 | 100.00 | 0.1389 | 0.03504 | 0.02517 |
| 4.28 | 1.0920 | 1.4700 | 28.33 | 37.9 | 0.1881 | 0.0122 | 2726 | 107 | 100.00 | 0.1299 | 0.06184 | 0.02657 |
| 4.47 | 2.1730 | 7.3000 | 59.92 | 201 | 0.2000 | 0.0192 | 2826 | 156 | 99.72 | 0.09989 | 0.03477 | 0.02716 |
| 4.65 | 0.9596 | 0.7520 | 26.25 | 21 | 0.1984 | 0.0159 | 2813 | 131 | 99.80 | 0.1777 | 0.0474 | 0.03106 |
| 4.84 | 2.5190 | 7.9100 | 65.98 | 207 | 0.1900 | 0.0156 | 2742 | 135 | 99.47 | 0.1514 | 0.03568 | 0.02167 |
| 5.02 | 1.0180 | 0.4780 | 29.09 | 13.7 | 0.2072 | 0.0155 | 2884 | 122 | 100.00 | 0.1164 | 0.07906 | 0.02909 |
| 5.21 | 0.8928 | 0.6240 | 26.35 | 18.1 | 0.2140 | 0.0231 | 2936 | 174 | 100.00 | 0.09061 | 0.04691 | 0.01837 |
| 5.40 | 1.1350 | 0.9020 | 36.13 | 29.1 | 0.2308 | 0.0194 | 3058 | 134 | 100.00 | 0.1208 | 0.04202 | 0.01876 |
| 5.58 | 0.6017 | 0.0404 | 19.14 | 1.23 | 0.2307 | 0.00393 | 3057 | 27 | 99.72 | 0.1378 | 0.01427 | 0.03895 |
| 5.77 | 0.6320 | 0.0223 | 20.35 | 0.734 | 0.2335 | 0.0052 | 3076 | 36 | 99.80 | 0.1437 | 0.006118 | 0.03855 |
| 5.95 | 0.6527 | 0.0457 | 21.14 | 1.4 | 0.2350 | 0.0042 | 3086 | 29 | 99.94 | 0.1435 | 0.007995 | 0.03898 |
| 6.14 | 0.6379 | 0.0538 | 20.77 | 1.74 | 0.2362 | 0.00775 | 3094 | 52 | 99.90 | 0.1430 | 0.007933 | 0.0383 |
| 6.33 | 0.6076 | 0.0466 | 19.9 | 1.61 | 0.2375 | 0.0153 | 3103 | 103 | 99.93 | 0.1433 | 0.03324 | 0.03769 |
| 6.51 | 0.6550 | 0.0530 | 22.76 | 1.88 | 0.2520 | 0.0073 | 3197 | 46 | 99.87 | 0.1361 | 0.01298 | 0.03587 |
| 6.70 | 0.6754 | 0.0378 | 24.43 | 1.39 | 0.2623 | 0.00324 | 3261 | 19 | 99.95 | 0.1405 | 0.0086 | 0.03512 |
| 6.88 | 0.6403 | 0.0257 | 23.53 | 1.02 | 0.2666 | 0.00469 | 3286 | 28 | 99.93 | 0.1173 | 0.005545 | 0.03138 |
| 7.07 | 0.6888 | 0.0784 | 26.07 | 3.05 | 0.2745 | 0.0108 | 3332 | 62 | 100.00 | 0.1162 | 0.005439 | 0.02944 |
| 7.26 | 0.7026 | 0.0783 | 26.95 | 2.79 | 0.2781 | 0.00922 | 3353 | 52 | 100.00 | 0.1172 | 0.007693 | 0.0276 |
| 7.44 | 0.7782 | 0.0403 | 31.44 | 1.62 | 0.2930 | 0.00479 | 3434 | 25 | 100.00 | 0.1041 | 0.006938 | 0.0278 |
| 7.63 | 0.6954 | 0.0822 | 28.49 | 3.43 | 0.2971 | 0.0060 | 3455 | 31 | 99.98 | 0.09243 | 0.004893 | 0.02677 |
| 7.81 | 0.7310 | 0.0320 | 30.08 | 1.31 | 0.2985 | 0.00519 | 3462 | 27 | 99.98 | 0.1007 | 0.005117 | 0.02769 |
| 8.00 | 0.7787 | 0.1140 | 32.59 | 4.7 | 0.3035 | 0.00594 | 3488 | 30 | 100.00 | 0.08808 | 0.004821 | 0.02499 |
| 8.19 | 0.7159 | 0.1000 | 30.49 | 4.2 | 0.3089 | 0.0061 | 3515 | 31 | 100.00 | 0.08752 | 0.006129 | 0.02441 |

TABLE A2
*(continued)*

| Depth (μm) | $^{206}Pb^*/^{238}U$ ratio | 1se | $^{207}Pb^*/^{235}U$ ratio | 1se | $^{207}Pb^*/^{206}Pb^*$ ratio | 1se | $^{207}Pb/^{206}Pb$ age (Ma) | 1se | $^{206}Pb^*$ (%) | Th/U | 1se | $^{208}Pb/^{206}Pb$ ratio |
|---|---|---|---|---|---|---|---|---|---|---|---|---|
| 8.37 | 0.7671 | 0.1130 | 32.85 | 4.86 | 0.3105 | 0.0112 | 3524 | 56 | 100.00 | 0.1064 | 0.0131 | 0.02699 |
| 8.56 | 0.6834 | 0.0331 | 29.25 | 1.39 | 0.3104 | 0.0048 | 3523 | 24 | 100.00 | 0.1201 | 0.006448 | 0.02586 |
| 8.74 | 0.6981 | 0.0246 | 30.43 | 1.32 | 0.3162 | 0.00805 | 3551 | 39 | 100.00 | 0.1045 | 0.006069 | 0.02573 |
| 8.93 | 0.6951 | 0.0728 | 30.37 | 3.12 | 0.3169 | 0.0105 | 3555 | 51 | 99.97 | 0.09673 | 0.02049 | 0.03055 |
| 9.12 | 0.7209 | 0.1030 | 31.55 | 4.22 | 0.3175 | 0.00851 | 3558 | 41 | 99.95 | 0.1053 | 0.007667 | 0.02586 |
| 9.30 | 0.6829 | 0.0342 | 29.96 | 1.37 | 0.3182 | 0.00638 | 3561 | 31 | 99.93 | 0.09972 | 0.007213 | 0.02804 |
| 9.49 | 0.7271 | 0.0646 | 32.23 | 2.94 | 0.3215 | 0.00637 | 3577 | 31 | 100.00 | 0.1123 | 0.007275 | 0.02351 |
| 9.67 | 0.6990 | 0.0291 | 30.58 | 1.24 | 0.3173 | 0.00587 | 3557 | 29 | 100.00 | 0.09736 | 0.01793 | 0.02406 |
| 9.86 | 0.6857 | 0.0353 | 30.62 | 1.83 | 0.3238 | 0.00705 | 3588 | 33 | 99.97 | 0.09266 | 0.008599 | 0.01952 |
| 10.05 | 0.7157 | 0.1250 | 32 | 5.57 | 0.3242 | 0.0101 | 3590 | 48 | 99.99 | 0.08303 | 0.01059 | 0.02436 |
| 10.23 | 0.6514 | 0.0380 | 29.82 | 1.67 | 0.3321 | 0.0069 | 3627 | 32 | 99.97 | 0.07161 | 0.009884 | 0.01735 |
| 10.42 | 0.6498 | 0.0370 | 29.68 | 1.67 | 0.3313 | 0.00872 | 3623 | 40 | 100.00 | 0.08591 | 0.006197 | 0.01853 |
| 10.60 | 0.6469 | 0.0318 | 29.44 | 1.43 | 0.3301 | 0.00589 | 3617 | 27 | 100.00 | 0.08889 | 0.005464 | 0.02067 |
| 10.79 | 0.6648 | 0.0403 | 30.26 | 1.84 | 0.3301 | 0.00901 | 3618 | 42 | 100.00 | 0.08019 | 0.008413 | 0.01982 |
| 10.98 | 0.6524 | 0.0378 | 30.02 | 1.49 | 0.3337 | 0.00936 | 3634 | 43 | 99.96 | 0.08844 | 0.0116 | 0.02114 |
| 11.16 | 0.6538 | 0.0340 | 30.41 | 1.6 | 0.3373 | 0.0136 | 3651 | 62 | 100.00 | 0.09903 | 0.02199 | 0.02163 |
| 11.35 | 0.6280 | 0.0288 | 29.04 | 1.59 | 0.3354 | 0.00817 | 3642 | 37 | 99.97 | 0.1006 | 0.00951 | 0.02462 |
| 11.53 | 0.6508 | 0.0233 | 30.72 | 1.08 | 0.3423 | 0.00787 | 3673 | 35 | 99.99 | 0.09838 | 0.007402 | 0.02522 |
| 11.72 | 0.6325 | 0.0560 | 29.93 | 2.6 | 0.3432 | 0.0158 | 3677 | 70 | 99.98 | 0.09657 | 0.0061 | 0.0264 |
| 11.91 | 0.6226 | 0.0318 | 29.09 | 2.27 | 0.3389 | 0.0156 | 3658 | 70 | 100.00 | 0.1032 | 0.02836 | 0.02506 |
| 12.09 | 0.5946 | 0.0431 | 27.78 | 1.91 | 0.3388 | 0.00904 | 3658 | 41 | 100.00 | 0.1153 | 0.008119 | 0.02793 |
| 12.28 | 0.6076 | 0.0313 | 28.78 | 1.5 | 0.3436 | 0.00769 | 3679 | 34 | 99.97 | 0.1123 | 0.006911 | 0.02981 |
| 12.47 | 0.5851 | 0.0269 | 27.37 | 1.12 | 0.3393 | 0.00698 | 3660 | 31 | 100.00 | 0.1244 | 0.009109 | 0.03126 |
| 12.65 | 0.6249 | 0.0359 | 29.6 | 1.66 | 0.3436 | 0.00464 | 3679 | 21 | 99.97 | 0.1069 | 0.00832 | 0.02945 |
| 12.84 | 0.6110 | 0.0516 | 28.39 | 1.83 | 0.3370 | 0.0204 | 3649 | 93 | 100.00 | 0.1135 | 0.008582 | 0.03127 |
| 13.02 | 0.7481 | 0.2350 | 34.32 | 10.7 | 0.3327 | 0.0200 | 3630 | 92 | 100.00 | 0.08763 | 0.01829 | 0.01695 |
| 13.21 | 0.7024 | 0.2350 | 32.72 | 11.2 | 0.3379 | 0.0268 | 3653 | 121 | 100.00 | 0.08778 | 0.0176 | 0.01685 |
| 13.40 | 0.6408 | 0.0999 | 29.03 | 4.58 | 0.3286 | 0.0189 | 3610 | 88 | 100.00 | 0.09187 | 0.0290 | 0.01523 |
| 13.58 | 0.6423 | 0.0798 | 30.53 | 3.81 | 0.3447 | 0.0163 | 3684 | 72 | 99.93 | 0.06934 | 0.01495 | 0.01926 |
| 13.77 | 0.6522 | 0.3620 | 28.7 | 15.7 | 0.3192 | 0.0715 | 3566 | 345 | 99.75 | 0.0918 | 0.03333 | 0.01591 |
| 13.95 | 0.6349 | 0.0907 | 28.87 | 4.27 | 0.3298 | 0.0136 | 3616 | 63 | 100.00 | 0.1214 | 0.02828 | 0.02347 |
| 14.14 | 0.8483 | 0.3210 | 38.32 | 14.4 | 0.3276 | 0.0178 | 3606 | 84 | 100.00 | 0.09152 | 0.0186 | 0.02085 |
| 14.33 | 0.6103 | 0.1070 | 29.39 | 5.56 | 0.3493 | 0.0209 | 3704 | 91 | 100.00 | 0.1144 | 0.03088 | 0.03279 |
| 14.51 | 0.6824 | 0.2560 | 32.09 | 12.1 | 0.3411 | 0.0133 | 3668 | 60 | 100.00 | 0.1207 | 0.04925 | 0.03114 |
| 14.70 | 0.9123 | 0.3580 | 43.4 | 17.9 | 0.3450 | 0.0883 | 3685 | 390 | 100.00 | 0.1118 | 0.02639 | 0.0272 |
| 14.88 | 0.7618 | 0.2680 | 35.02 | 11.9 | 0.3334 | 0.0265 | 3633 | 122 | 100.00 | 0.07906 | 0.02886 | 0.02552 |
| 15.07 | 0.7371 | 0.1440 | 33.23 | 6.68 | 0.3270 | 0.0203 | 3603 | 95 | 100.00 | 0.1131 | 0.02224 | 0.03523 |
| 15.26 | 0.8342 | 0.3280 | 39.22 | 15.5 | 0.3410 | 0.0229 | 3667 | 103 | 100.00 | 0.1520 | 0.05645 | 0.02749 |
| 15.44 | 0.8752 | 0.5680 | 43.95 | 28.6 | 0.3642 | 0.0192 | 3767 | 80 | 100.00 | 0.1394 | 0.05504 | 0.02506 |
| 15.63 | 0.7282 | 0.1870 | 32.65 | 8.34 | 0.3251 | 0.0236 | 3594 | 112 | 100.00 | 0.07701 | 0.07728 | 0.03374 |
| 15.81 | 0.7775 | 0.3560 | 34.46 | 15.9 | 0.3214 | 0.0320 | 3577 | 153 | 100.00 | 0.1319 | 0.04314 | 0.03366 |
| 16.00 | 0.7626 | 0.2580 | 36.02 | 12.1 | 0.3425 | 0.0190 | 3674 | 85 | 100.00 | 0.1522 | 0.02537 | 0.03479 |
| 16.19 | 0.7039 | 0.2230 | 31.78 | 10.1 | 0.3275 | 0.0137 | 3605 | 64 | 100.00 | 0.1161 | 0.02143 | 0.03325 |
| 16.37 | 0.8443 | 0.5120 | 38.46 | 23 | 0.3303 | 0.0187 | 3619 | 87 | 100.00 | 0.1150 | 0.02072 | 0.03786 |
| 16.56 | 1.1860 | 1.7600 | 57.1 | 84.6 | 0.3491 | 0.0243 | 3703 | 106 | 100.00 | 0.07925 | 0.05326 | 0.0421 |

TABLE A2
*(continued)*

| Depth (μm) | $^{206}Pb^*/^{238}U$ ratio | 1se | $^{207}Pb^*/^{235}U$ ratio | 1se | $^{207}Pb^*/^{206}Pb^*$ ratio | 1se | $^{207}Pb/^{206}Pb$ age (Ma) | 1se | $^{206}Pb^*$ (%) | Th/U | 1se | $^{208}Pb/^{206}Pb$ ratio |
|---|---|---|---|---|---|---|---|---|---|---|---|---|
| 16.74 | 0.7877 | 0.0288 | 38.12 | 1.39 | 0.3510 | 0.00863 | 3711 | 37 | 99.90 | 0.1709 | 0.01551 | 0.04337 |
| 16.93 | 0.7795 | 0.0188 | 37.94 | 0.939 | 0.3530 | 0.00637 | 3720 | 28 | 99.99 | 0.1839 | 0.02696 | 0.04292 |
| 17.12 | 0.7856 | 0.0207 | 37.85 | 1.14 | 0.3494 | 0.00795 | 3704 | 35 | 99.93 | 0.1559 | 0.00717 | 0.04273 |
| 17.30 | 0.7721 | 0.0324 | 37.28 | 1.56 | 0.3502 | 0.0117 | 3708 | 51 | 99.93 | 0.1943 | 0.0138 | 0.0415 |
| 17.49 | 0.7867 | 0.0233 | 37.92 | 1.15 | 0.3496 | 0.00801 | 3705 | 35 | 99.93 | 0.1563 | 0.01709 | 0.04189 |
| 17.67 | 0.7909 | 0.0485 | 39.12 | 2.27 | 0.3587 | 0.0152 | 3745 | 64 | 99.93 | 0.1787 | 0.01106 | 0.04728 |
| 17.86 | 0.7704 | 0.0446 | 37.79 | 2.13 | 0.3558 | 0.00932 | 3732 | 40 | 99.94 | 0.1792 | 0.02848 | 0.04428 |
| 18.05 | 0.7507 | 0.0354 | 36.1 | 1.67 | 0.3487 | 0.00842 | 3702 | 37 | 99.92 | 0.1915 | 0.00894 | 0.04504 |
| 18.23 | 0.7553 | 0.0200 | 37.06 | 0.985 | 0.3558 | 0.00527 | 3732 | 23 | 99.96 | 0.1824 | 0.008336 | 0.04749 |
| 18.42 | 0.7700 | 0.0242 | 37.88 | 1.21 | 0.3568 | 0.00855 | 3736 | 36 | 99.97 | 0.1852 | 0.01009 | 0.05021 |
| 18.60 | 0.7664 | 0.0368 | 37.3 | 1.79 | 0.3529 | 0.0152 | 3720 | 66 | 99.92 | 0.1910 | 0.00852 | 0.05057 |
| 18.79 | 0.7469 | 0.0374 | 37.29 | 2.02 | 0.3621 | 0.0107 | 3759 | 45 | 99.83 | 0.2192 | 0.01211 | 0.04456 |
| 18.98 | 0.7596 | 0.0277 | 37.5 | 1.23 | 0.3580 | 0.00813 | 3742 | 35 | 99.91 | 0.1876 | 0.02199 | 0.04963 |
| 19.16 | 0.7534 | 0.0173 | 36.88 | 0.871 | 0.3551 | 0.00648 | 3729 | 28 | 99.89 | 0.2013 | 0.02361 | 0.05179 |
| 19.35 | 0.7426 | 0.0615 | 35.82 | 2.96 | 0.3499 | 0.0152 | 3707 | 66 | 99.85 | 0.2124 | 0.01141 | 0.05333 |
| 19.53 | 0.7184 | 0.0268 | 35.66 | 1.34 | 0.3600 | 0.00508 | 3750 | 22 | 99.86 | 0.2323 | 0.01008 | 0.04851 |
| 19.72 | 0.7521 | 0.0173 | 36.83 | 0.98 | 0.3552 | 0.00695 | 3729 | 30 | 99.83 | 0.1928 | 0.01517 | 0.04953 |
| 19.91 | 0.7135 | 0.0230 | 35.1 | 1.08 | 0.3568 | 0.00759 | 3736 | 32 | 99.94 | 0.2079 | 0.0153 | 0.05062 |
| 20.09 | 0.7161 | 0.0305 | 34.86 | 1.41 | 0.3531 | 0.0133 | 3720 | 57 | 99.94 | 0.2328 | 0.02327 | 0.04875 |
| 20.28 | 0.6991 | 0.0671 | 34.22 | 3.38 | 0.3550 | 0.0192 | 3729 | 82 | 99.92 | 0.2297 | 0.01292 | 0.0529 |
| 20.47 | 0.7195 | 0.0573 | 36.06 | 3.37 | 0.3635 | 0.0147 | 3765 | 61 | 99.76 | 0.3195 | 0.0145 | 0.08514 |
| 20.65 | 0.7004 | 0.1120 | 34.65 | 5.59 | 0.3588 | 0.0104 | 3745 | 44 | 99.89 | 0.3091 | 0.0353 | 0.08653 |
| 20.84 | 0.7669 | 0.0664 | 38.59 | 3.24 | 0.3650 | 0.00863 | 3771 | 36 | 99.98 | 0.3018 | 0.01448 | 0.08857 |
| 21.02 | 0.8496 | 0.1300 | 42.09 | 6.45 | 0.3593 | 0.0170 | 3747 | 72 | 99.62 | 0.2808 | 0.02436 | 0.09126 |
| 21.21 | 0.8505 | 0.0799 | 45.22 | 4.24 | 0.3856 | 0.0082 | 3854 | 32 | 99.80 | 0.2955 | 0.01901 | 0.09113 |
| 21.40 | 0.7481 | 0.1400 | 38.22 | 7.42 | 0.3705 | 0.0102 | 3793 | 42 | 99.66 | 0.2796 | 0.0140 | 0.08796 |
| 21.58 | 0.8869 | 0.0990 | 44.20 | 4.94 | 0.3614 | 0.00878 | 3756 | 37 | 99.67 | 0.2992 | 0.02636 | 0.09608 |
| 21.77 | 0.6401 | 0.0506 | 32.52 | 2.33 | 0.3685 | 0.0100 | 3785 | 41 | 99.49 | 0.3136 | 0.0310 | 0.09343 |
| 21.95 | 0.7589 | 0.0843 | 39.46 | 4.48 | 0.3771 | 0.00939 | 3820 | 38 | 99.74 | 0.2983 | 0.01394 | 0.0963 |
| 22.14 | 0.7774 | 0.0679 | 40.90 | 3.62 | 0.3815 | 0.0107 | 3838 | 43 | 99.73 | 0.3052 | 0.0215 | 0.09066 |
| 22.33 | 0.7885 | 0.1170 | 40.67 | 6.18 | 0.3741 | 0.0181 | 3808 | 73 | 99.48 | 0.2934 | 0.02765 | 0.08675 |
| 22.51 | 0.8822 | 0.0833 | 45.92 | 4.32 | 0.3776 | 0.00945 | 3822 | 38 | 99.75 | 0.2919 | 0.01798 | 0.0901 |
| 22.70 | 0.7766 | 0.0706 | 40.01 | 3.55 | 0.3736 | 0.0081 | 3806 | 33 | 99.63 | 0.2941 | 0.0348 | 0.0943 |
| 22.88 | 0.6392 | 0.0445 | 33.46 | 2.33 | 0.3797 | 0.00852 | 3831 | 34 | 99.77 | 0.3092 | 0.01959 | 0.09327 |
| 23.07 | 0.6682 | 0.1050 | 34.45 | 5.51 | 0.3739 | 0.0147 | 3807 | 60 | 99.60 | 0.2855 | 0.01296 | 0.09104 |
| 23.26 | 0.6491 | 0.0489 | 33.75 | 2.56 | 0.3771 | 0.0098 | 3820 | 39 | 99.74 | 0.3092 | 0.02922 | 0.09285 |
| 23.44 | 0.6736 | 0.0483 | 35.18 | 2.61 | 0.3788 | 0.00999 | 3827 | 40 | 99.86 | 0.2739 | 0.01348 | 0.08482 |
| 23.63 | 0.6663 | 0.0603 | 35.11 | 3.29 | 0.3822 | 0.0111 | 3840 | 44 | 99.80 | 0.2918 | 0.01793 | 0.08707 |
| 23.81 | 0.6755 | 0.0676 | 35.03 | 3.59 | 0.3761 | 0.00665 | 3816 | 27 | 99.90 | 0.2814 | 0.01251 | 0.08929 |
| 24.00 | 0.6408 | 0.0779 | 32.00 | 4.02 | 0.3622 | 0.0118 | 3759 | 50 | 99.38 | 0.3070 | 0.02182 | 0.0906 |
| 24.19 | 0.5861 | 0.0952 | 30.33 | 4.99 | 0.3754 | 0.0184 | 3813 | 74 | 99.71 | 0.3287 | 0.03935 | 0.09302 |
| 24.37 | 0.5810 | 0.0792 | 30.86 | 4.23 | 0.3853 | 0.0131 | 3853 | 52 | 99.91 | 0.3151 | 0.04716 | 0.09402 |
| 24.56 | 0.6071 | 0.0422 | 32.55 | 2.27 | 0.3888 | 0.00948 | 3866 | 37 | 99.94 | 0.2928 | 0.02595 | 0.09367 |
| 24.74 | 0.6357 | 0.0390 | 33.76 | 2.13 | 0.3852 | 0.0069 | 3852 | 27 | 99.75 | 0.2974 | 0.01138 | 0.09317 |
| 24.93 | 0.5832 | 0.0474 | 30.51 | 2.43 | 0.3794 | 0.00967 | 3830 | 39 | 99.76 | 0.3101 | 0.01449 | 0.09228 |

TABLE A2
*(continued)*

| Depth (μm) | $^{206}Pb^*/^{238}U$ ratio | 1se | $^{207}Pb^*/^{235}U$ ratio | 1se | $^{207}Pb^*/^{206}Pb^*$ ratio | 1se | $^{207}Pb/^{206}Pb$ age (Ma) | 1se | $^{206}Pb^*$ (%) | Th/U | 1se | $^{208}Pb/^{206}Pb$ ratio |
|---|---|---|---|---|---|---|---|---|---|---|---|---|
| 25.12 | 0.5530 | 0.0518 | 28.92 | 2.71 | 0.3793 | 0.0072 | 3829 | 29 | 99.87 | 0.3106 | 0.01171 | 0.09462 |
| 25.30 | 0.5690 | 0.0756 | 29.57 | 3.94 | 0.3768 | 0.0214 | 3819 | 86 | 99.73 | 0.3152 | 0.01537 | 0.09429 |
| 25.49 | 0.6149 | 0.0451 | 31.79 | 2.34 | 0.3749 | 0.0105 | 3811 | 42 | 99.73 | 0.2968 | 0.0237 | 0.09622 |
| 25.67 | 0.5373 | 0.0489 | 28.47 | 2.49 | 0.3842 | 0.00903 | 3848 | 36 | 99.66 | 0.3102 | 0.01146 | 0.09594 |
| 25.86 | 0.5063 | 0.0705 | 26.80 | 3.67 | 0.3839 | 0.0123 | 3847 | 48 | 99.63 | 0.3039 | 0.0147 | 0.09275 |
| 26.05 | 0.5322 | 0.0628 | 27.73 | 3.24 | 0.3780 | 0.0131 | 3824 | 52 | 99.80 | 0.3032 | 0.03029 | 0.09277 |
| 26.23 | 0.5274 | 0.0836 | 26.82 | 4.35 | 0.3688 | 0.0181 | 3786 | 74 | 99.82 | 0.3096 | 0.03299 | 0.09229 |
| 26.42 | 0.5019 | 0.0439 | 26.37 | 2.42 | 0.3811 | 0.00758 | 3836 | 30 | 99.90 | 0.3156 | 0.01971 | 0.09855 |
| 26.60 | 0.5137 | 0.0736 | 27.14 | 3.89 | 0.3831 | 0.0182 | 3844 | 72 | 99.87 | 0.3198 | 0.0215 | 0.09314 |
| 26.79 | 0.4931 | 0.0463 | 25.68 | 2.42 | 0.3777 | 0.0108 | 3823 | 43 | 99.72 | 0.3044 | 0.0115 | 0.09263 |
| 26.98 | 0.4700 | 0.0827 | 24.60 | 4.30 | 0.3796 | 0.0259 | 3830 | 103 | 99.80 | 0.3298 | 0.02542 | 0.0882 |
| 27.16 | 0.5004 | 0.0516 | 26.02 | 2.68 | 0.3771 | 0.00583 | 3820 | 23 | 99.87 | 0.3159 | 0.03888 | 0.09175 |
| 27.35 | 0.4953 | 0.0494 | 25.70 | 2.57 | 0.3764 | 0.0107 | 3817 | 43 | 99.91 | 0.2896 | 0.01078 | 0.09449 |
| 27.53 | 0.4850 | 0.0384 | 25.34 | 2.00 | 0.3789 | 0.00753 | 3827 | 30 | 99.89 | 0.3292 | 0.01566 | 0.09077 |
| 27.72 | 0.4516 | 0.0433 | 23.71 | 2.37 | 0.3808 | 0.00777 | 3835 | 31 | 99.81 | 0.3429 | 0.02304 | 0.09526 |
| 27.91 | 0.4540 | 0.0475 | 23.46 | 2.42 | 0.3748 | 0.0148 | 3811 | 60 | 99.96 | 0.3394 | 0.0339 | 0.09762 |
| 28.09 | 0.4407 | 0.0365 | 23.01 | 1.96 | 0.3787 | 0.00834 | 3826 | 33 | 99.87 | 0.3500 | 0.01158 | 0.09943 |
| 28.28 | 0.4324 | 0.0361 | 22.45 | 1.90 | 0.3766 | 0.00911 | 3818 | 37 | 99.77 | 0.3557 | 0.03108 | 0.1005 |
| 28.47 | 0.4559 | 0.0534 | 24.08 | 2.73 | 0.3831 | 0.0201 | 3844 | 79 | 99.89 | 0.3638 | 0.01725 | 0.1032 |
| 28.65 | 0.4451 | 0.0405 | 23.52 | 2.27 | 0.3832 | 0.0077 | 3844 | 30 | 99.93 | 0.3607 | 0.01983 | 0.1055 |
| 28.84 | 0.4487 | 0.0360 | 23.49 | 1.90 | 0.3797 | 0.00573 | 3830 | 23 | 99.86 | 0.3772 | 0.01059 | 0.1044 |
| 29.02 | 0.4475 | 0.0492 | 23.45 | 2.64 | 0.3800 | 0.00741 | 3832 | 29 | 99.90 | 0.3611 | 0.01019 | 0.1091 |
| 29.21 | 0.4487 | 0.0441 | 23.25 | 2.23 | 0.3758 | 0.00992 | 3815 | 40 | 99.91 | 0.3628 | 0.01015 | 0.1066 |
| 29.40 | 0.4356 | 0.0403 | 22.61 | 2.02 | 0.3764 | 0.00702 | 3817 | 28 | 99.94 | 0.3934 | 0.01036 | 0.1077 |
| 29.58 | 0.4228 | 0.0365 | 21.83 | 1.87 | 0.3745 | 0.0081 | 3810 | 33 | 99.92 | 0.3997 | 0.03154 | 0.1141 |

Each depth interval corresponds to mean of 15 analysis cycles. Associated uncertainty in one standard error (se) in the mean. Depths estimated from number of cycles divided by pit depth assuming constant sputtering rate. See figure 3 for sample location.

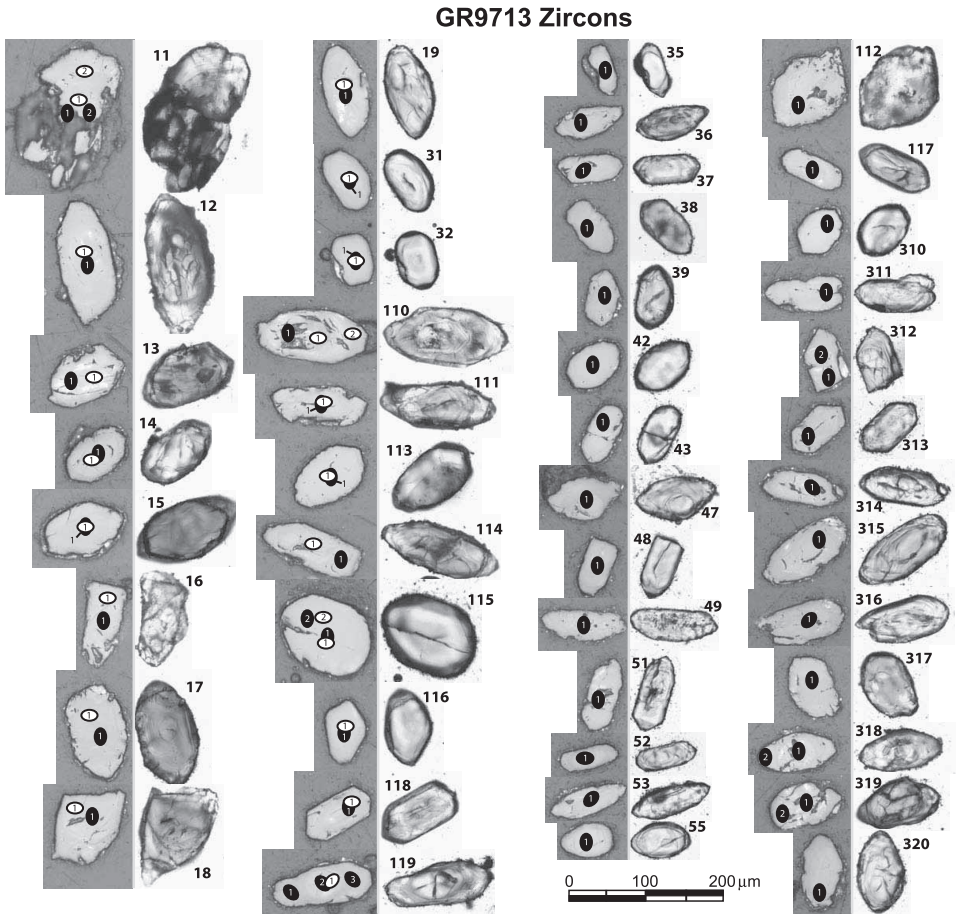


Fig. A1. Zircon analysis locations, *Qp* sample GR9713 (fig. 3). Analyses were collected during two sessions, with repolishing of the sample mount between sessions. Black ovals denote Analysis spots from session 1, whereas white ovals designate analysis spots from session 2. Results of analyses are given in table A1.

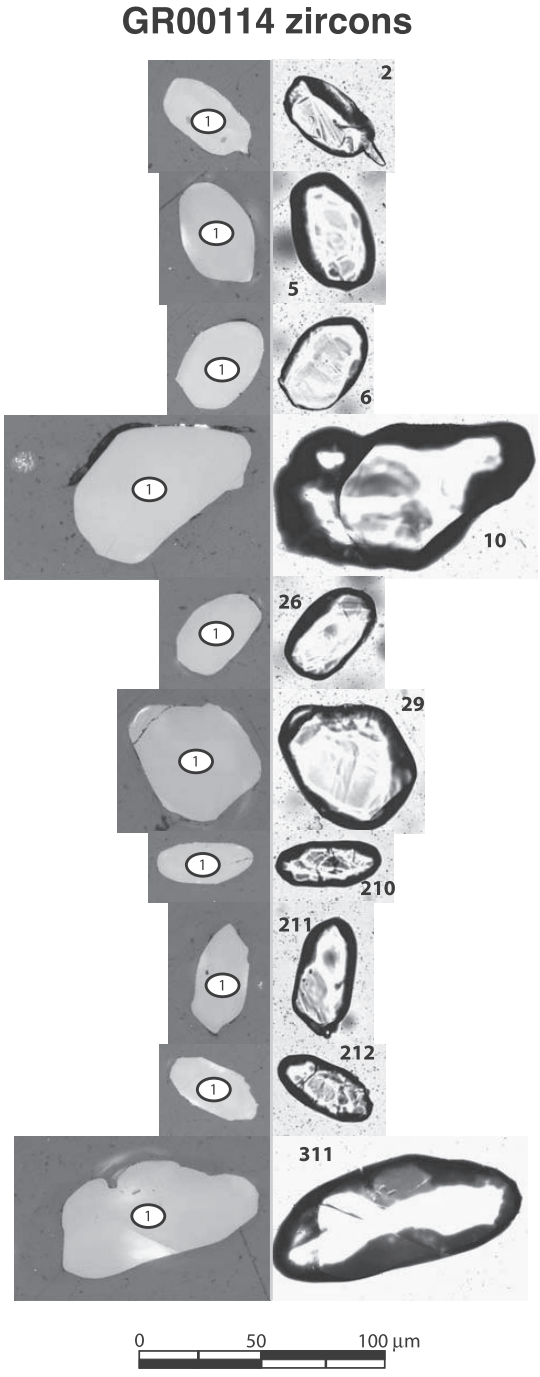


Fig. A2. Zircon analysis locations, metasedimentary(?) anthophyllite-garnet schist sample GR00114 (fig. 3). Ovals denote ion-microprobe spots (table A1).

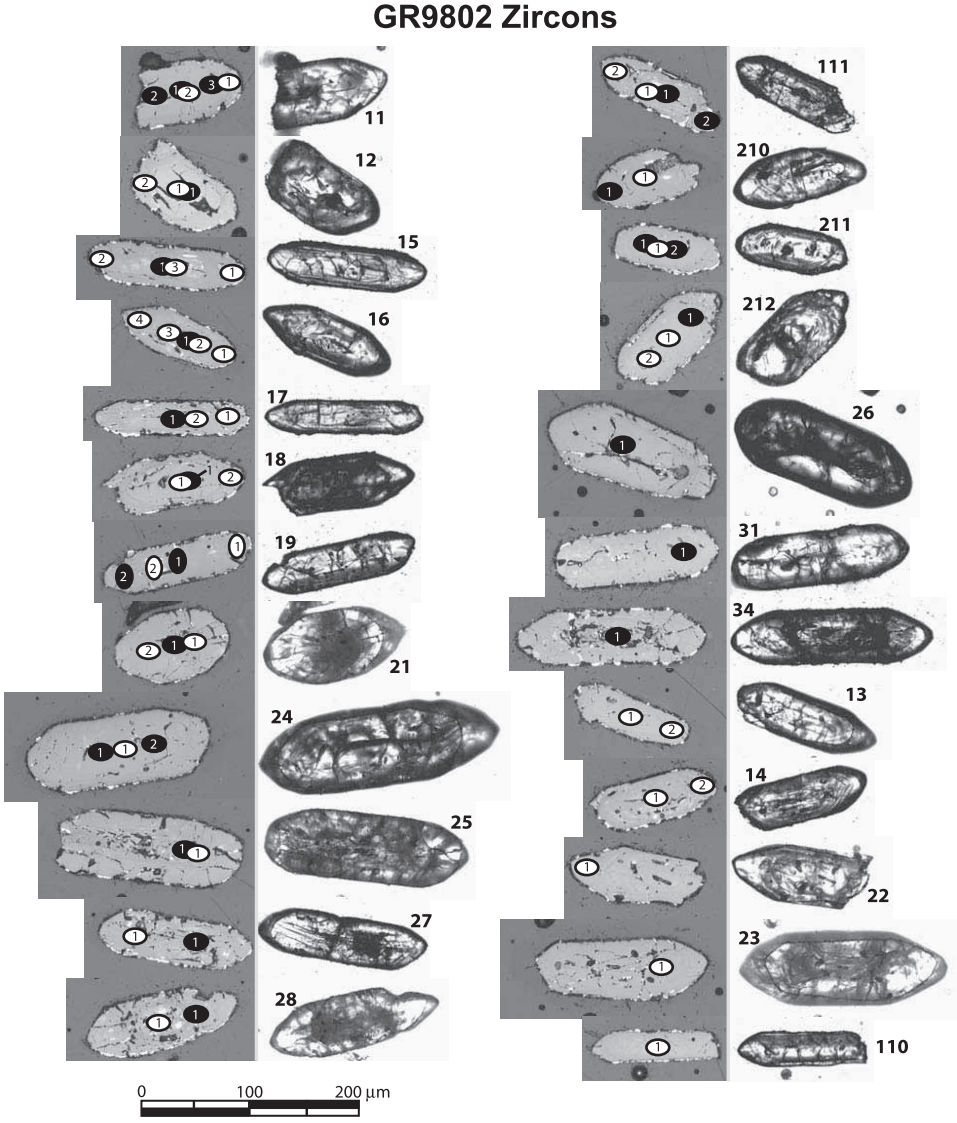


Fig. A3. Zircon analysis locations, *Ogn-1* sample GR9802 (fig. 3). Analyses were collected during two sessions, with repolishing of the sample mount between sessions. Black ovals denote Analysis spots from session 1, whereas white ovals designate analysis spots from session 2. Results of analyses are given in table A1.

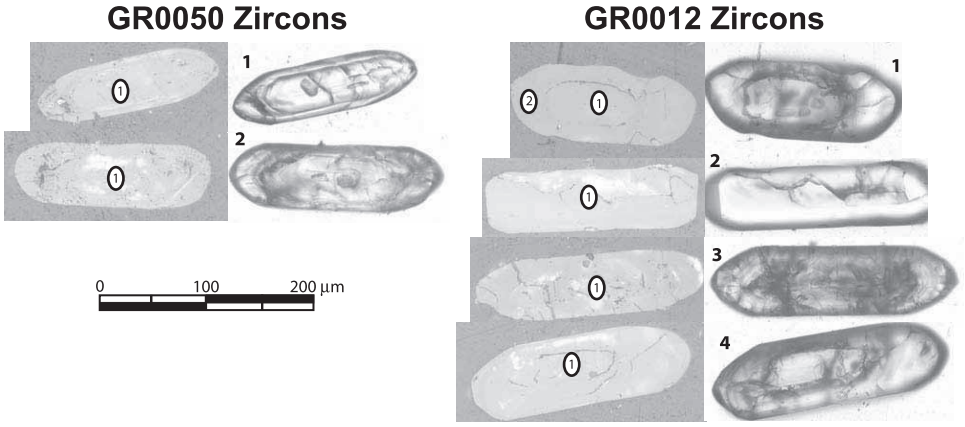


Fig. A4. Zircon analysis locations, *Ogn-1* samples GR0050 and GR0012 (fig. 3). Ovals denote ion-microprobe spots (table A1).

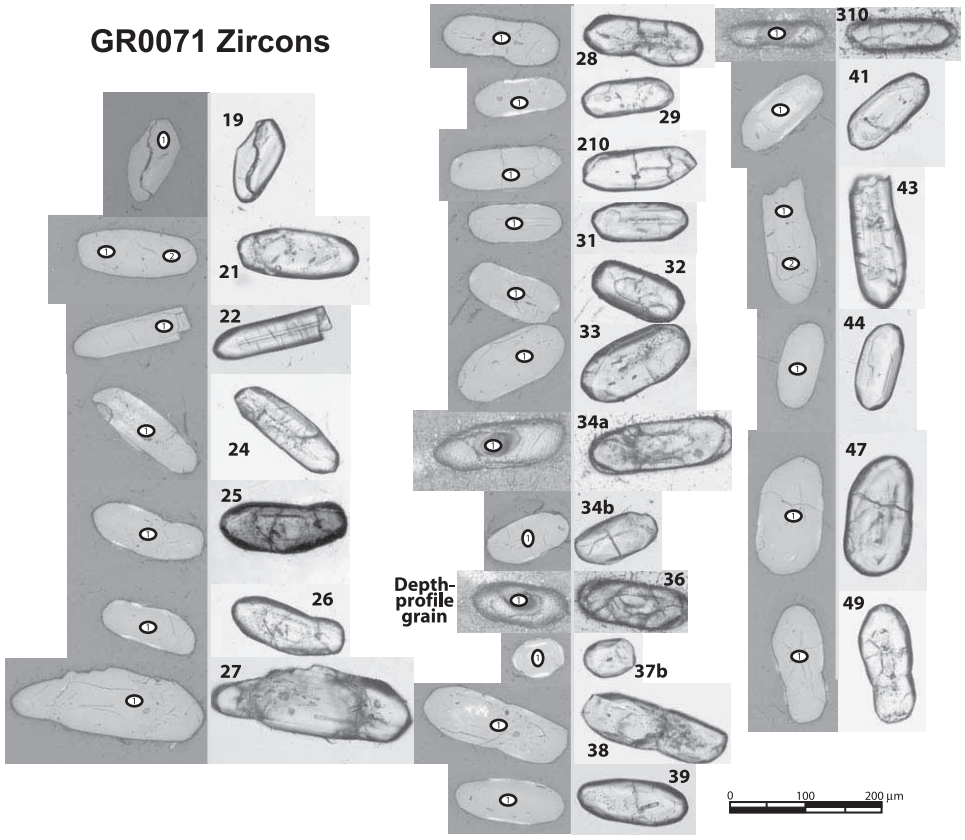


Fig. A5. Zircon analysis locations, *Ogn-2* sample GR0071 (fig. 3). Ovals denote ion-microprobe spots (table A1). Grain 36 was selected for depth-profiling study (see text and table A2).

## References


Anbar, A. D., Zahnle, K. J., Arnold, G. L., and Mojzsis, S. J., 2001, Extraterrestrial iridium, sediment accumulation and the habitability of the early Earth's surface: Journal of Geophysical Research, v. 106, p. 3219–3236.

Anders, E., and Grevesse, N., 1989, Abundances of the elements: meteoritic and solar: Geochimica et Cosmochimica Acta, v. 53, p. 197–214.

André, L., Cardinal, D., Alleman, L. Y., and Moorbath, S., 2006, Silicon isotopes in ~3.8 Ga West Greenland rocks as clues to the Eoarchaean supracrustal Si cycle: Earth and Planetary Science Letters, v. 245, p. 162–173.

Arndt, N. T., 1994, Archean komatiites, *in* Condie, K. C., editor, Archean Crustal Evolution: Amerstdam, Elsevier, p. 11–44.

Baadsgaard, H., 1976, Further U-Pb dates on zircons from early Precambrian of Godthaabsfjord area, West Greenland: Earth and Planetary Science Letters, v. 33, p. 261–267.

Baadsgaard, H., Nutman, A. P., Bridgwater, D., McGregor, V. R., Rosing, M., and Allaart, J. H., 1984, The zircon geochronology of the Akilia association and the Isua supracrustal belt, West Greenland: Earth and Planetary Science Letters, v. 68, p. 221–228.

Barker, F., 1979. Trondhjemite: Definition, environment and hypotheses of origin, *in* Barker, F., editor, Trondhjemites, Dacites, and Related Rocks: Amsterdam, Elsevier, p. 1–12.

Barrett, T. J., Fralik, P. W., and Jarvis, I., 1988, Rare-earth-element geochemistry of some Archean iron formations north of Lake Superior, Ontario: Canadian Journal of Earth Sciences, v. 25, p. 570–580.

Bau, M., 1991, Rare-earth element mobility during hydrothermal and metamorphic fluid-rock interaction and the significance of the oxidation state of europium: Chemical Geology, v. 93, p. 219–230.

——— 1993, Effects of syn- and post-depositional processes on the rare-earth element distribution in Precambrian iron-formations: European Journal of Mineralogy, v. 5, p. 257–267.

——— 1996, Controls on the fractionation of isovalent trace elements in magmatic and aqueous systems: evidence from Y/Ho and Zr/Hf, and lanthanide tetrad effect: Contributions to Mineralogy and Petrology, v. 123, p. 323–333.

Bau, M., and Dulski, P., 1996, Distribution of yttrium and rare-earth elements in the Penge and Kuruman iron-formations, Transvaal Supergroup, South Africa: Precambrian Research, v. 79, p. 37–55.

——— 1999, Comparing yttrium and rare earths in hydrothermal fluids from the Mid-Atlantic Ridge: implications for Y and REE behaviour during near-vent mixing and for the Y/Ho ratio of Proterozoic seawater: Chemical Geology, v. 155, p. 77–90.

Baumgartner, L. P., and Rumble, D., III, 1988, Transport of stable isotopes. I: Development of a kinetic continuum theory for stable isotope transport: Contributions to Mineralogy and Petrology, v. 98, p. 417–430.

Beard, B. L., and Johnson, C. M., 2004, Fe isotope variations in the modern and ancient Earth and other planetary bodies: Reviews in Mineralogy, v. 55, p. 319–357.

Blundy, J., and Wood, B., 1994, Prediction of crystal-melt partition coefficients from elastic moduli: Nature, v. 372, p. 452–454.

Bolhar, R., Kamber, B. S., Moorbath, S., Fedo, C. M., and Whitehouse, M. J., 2004, Characterisation of early Archaean chemical sediments by trace element signatures: Earth and Planetary Science Letters, v. 222, p. 43–60.

Bottinga, Y., and Javoy, M., 1975, Oxygen isotope partitioning among the minerals and triplets in igneous and metamorphic rocks: Reviews of Geophysics and Space Physics, v. 13, p. 401–418.

Bridgwater, D., Keto, L., McGregor V. R., and Myers, J. S., 1976, Archaean Gneiss Complex of Greenland, *in* Escher, A., and Watt, W. S., editors, Geology of Greenland: Copenhagen, Geological Survey of Greenland, p. 18–75.

Brown, M., Friend, C. R. L., McGregor, V. R., and Perkins, W. T., 1981, The Late Archean Qôrqut Granite Complex of southern West Greenland: Journal of Geophysical Research, v. 86, p. 617–632.

Büno, G., and Meisel, T., 1994, Major, trace, noble and rare earth element distribution in polymetamorphic ultramafic rocks: Schweizerische Mineralogische und Petrographische Mitteilungen, v. 74, p. 69–86.

Carson, C. J., Ague, J. J., Grove, M., and Coath, C. D., and Harrison, T. M., 2002, U-Pb isotopic behaviour of zircon during upper-amphibolite facies fluid infiltration in the Napier Complex, east Antarctica: Earth and Planetary Science Letters, v. 199, p. 287–310.

Cates, N. L., and Mojzsis, S. J., 2006, Chemical and isotopic evidence for widespread Early Archean (>3.7 Ga) volcano sedimentary enclaves in southern West Greenland: Geochimica et Cosmochimica Acta, v. 70.

Chadwick, B., 1981, Field relations, petrography and geochemistry of Archaean amphibolite dykes and Malene supracrustal amphibolites, northwest Buksefjorden, southern West Greenland: Precambrian Research, v. 14, p. 221–259.

Chadwick, B., and Coe, K., 1983, Geological map of Greenland, 1:100,000, Buksefjorden, 63 V.2 Nord: Copenhagen, Geological Survey of Greenland, 70 p.

Chadwick, B., and Nutman, A. P., 1979, Archaean structural evolution in the northwest of the Buksefjorden region, southern west Greenland: Precambrian Research, v. 9, p. 199–226.

Coe, K., Compton, P. M., Stainforth, J., Vines, K. J., and Wells, P. R. A., 1976, Investigation of Precambrian rocks in the Buksefjorden region, southern West Greenland: Greenland Geological Survey Report n. 80, p. 77–82.

Condie, K. C., 1993, Chemical composition and evolution of the upper continental crust: Contrasting results from surface samples and shales: Chemical Geology, v. 104, p. 1–37.

Crowley, J. L., 2002, Testing the model of late Archean terrane accretion in southern West Greenland: a comparison of the timing of geologic events across the Qarliit nunaat fault, Buksefjorden region: Precambrian Research, v. 116, p. 57–79.

Cullers, R. L., Medaris, L. G., and Haskin, L. A., 1973, Experimental studies of distribution of rare earths as trace elements among silicate minerals and liquids and water: Geochimica et Cosmochimica Acta, v. 37, p. 1499–1512.
Dauphas, N., van Zuilen, M., Wadhwa, M., Davis, A. M., Marty, B., and Janney, P. E., 2004, Clues from Fe isotope variations on the origin of early Archean BIFs from Greenland: Science, v. 306, p. 2077–2080.
Dymek, R. F., and Klein, C., 1988, Chemistry, petrology and origin of banded iron-formation lithologies from the 3800 Ma Isua supracrustal belt, West Greenland: Precambrian Research, v. 39, p. 247–302.
Dymek, R. R., Brothers, S. C., and Schiffries, C. M., 1988, Petrogenesis of ultramafic metamorphic rocks from the 3800 Isua Supracrustal Belt, west Greenland: Journal of Petrology, v. 29, p. 1353–1397.
Edmonds, H. N., and German, C. R., 2004, Particle geochemistry in the Rainbow hydrothermal plume, Mid-Atlantic Ridge: Geochimica et Cosmochimica Acta, v. 68, p. 759–772.
Farquhar, J., Bao, H., and Thiemens, M., 2000, Atmospheric influences of Earth's earliest sulfur cycle: Science, v. 289, p. 756–758.
Fedo, C. M., and Whitehouse, M. J., 2002a, Metasomatic origin of quartz-pyroxene rock, Akilia, Greenland, and implications for Earth's earliest life: Science, v. 296, p. 1448–1452.
——— 2002b, Origin and significance of Archean quartzose rocks at Akilia, Greenland—Response: Science, v. 298, p. 917a.
——— 2002c, The origin of a most contentious rock—Response: Science, v. 298, p. 961–962.
Ferry, J. M., and Gerdes, M., 1998, Chemically reactive fluid flow during metamorphism: Annual Reviews of Earth and Planetary Sciences, v. 26, p. 255–287.
Floyd, P. A., and Winchester, J. A., 1975, Magma type and tectonic setting discrimination using immobile elements: Earth and Planetary Science Letters, v. 27, p. 211–218.
Fraser, G., Ellis, D., and Eggins, S., 1997, Zirconium abundance in granulite-facies minerals, with implications for zircon geochronology in high-grade rocks: Geology, v. 25, p. 607–610.
Frei, R., Rosing, M. T., Waight, T. E., and Ulfbeck, D. G., 2002, Hydrothermal-metasomatic and tectonometamorphic processes in the Isua supracrustal belt (West Greenland); a multi-isotopic investigation of their effects on the Earth's oldest oceanic crustal sequence: Geochimica et Cosmochimica Acta, v. 66, p. 467–486.
Friend, C. R. L., and Nutman, A. P., 2005a, Complex 3670–3500 Ma orogenic episodes superimposed on juvenile crust accreted between 3850 and 3690 Ma, Itsaq Gneiss Complex, southern west Greenland: Journal of Geology, v. 113, p. 375–397.
——— 2005b, New pieces to the Archaean terrane jigsaw puzzle in the Nuuk region, southern west Greenland: steps in transforming a simple insight into a complex regional tectonothermal model: Journal of the Geological Society of London, v. 162, p. 147–162.
Friend, C. R. L., Nutman, A. P., and McGregor, V. R., 1987, Late-Archaean tectonics in the Færingehavn-Tre Brødre area, south of Buksefjorden, southern west Greenland: London, Journal of the Geological Society, v. 144, p. 369–376.
——— 1988, Late Archaean terrane accretion in the Godthåb region, southern west Greenland: Nature, v. 335, p. 535–538.
Friend, C. R. L., Nutman, A. P., Baadsgaard, H., Kinny, P. D., and McGregor, V. R., 1996, Timing of late Archaean terrane assembly, crustal thickening and granite emplacement in the Nuuk region, southern West Greenland: Earth and Planetary Science Letters, v. 142, p. 353–365.
Friend, C. R. L., Nutman, A. P., and Bennett V. C., 2002a, Origin and significance of Archean quartzose rocks at Akilia, Greenland: Science, v. 298, p. 5595.
Graf, J. L., Jr., 1978, Rare earth elements, iron formations and sea water: Geochimica et Cosmochimica Acta, v. 42, p. 1845–1850.
Griffin, W. L., McGregor, V. R., Nutman, A. P., and Taylor, P. N., 1980, Early Archaean granulite facies metamorphism south of Ameralik, West Greenland: Earth and Planetary Science Letters, v. 50, p. 59–74.
Hanchar, J. M., and Watson, E. B., 2003, Zircon saturation thermometry: Reviews in Mineralogy, v. 53, p. 89–112.
Harrison, T. M., and Watson, E. B., 1983, Kinetics of zircon dissolution and zirconium diffusion in granitic melts of variable water content: Contributions to Mineralogy and Petrology, v. 84, p. 66–72.
James, R. H., Elderfield, H., and Palmer, M. R., 1995, The chemistry of hydrothermal fluids from the Broken Spur site, 29°N Mid-Atlantic Ridge: Geochimica et Cosmochimica Acta, v. 59, p. 651–659.
Jochum, K. P., Arndt, N. T., and Hofmann, A. W., 1991, Nb-Th-La in komatiites and basalts, constraints on komatiite petrogenesis and mantle evolution: Earth and Planetary Science Letters, v. 107, p. 272–289.
Johannesson, K. H., Hawkins, D. L., and Cortes, A., 2006, Do Archean sediments record ancient seawater rare earth element patterns: Geochimica et Cosmochimica Acta, v. 70, p. 871–890.
Johnson, C. M., Beard, B. L., Beukes, J. J., Klein, C., and O'Leary, J. M., 2003, Ancient geochemical cycling in the Earth as inferred from Fe isotope studies of banded iron formations from the Transvaal Craton: Contributions to Mineralogy and Petrology, v. 144, p. 523–547.
Jones, D., and Knauth, L. P., 1979, Oxygen isotopic and petrographic evidence relevant to the origin of the Arkansas novaculite: Journal of Sedimentary Petrology, v. 49, p. 581–598.
Kamber, B. S., and Moorbath, S., 1998, Initial Pb of the Amitsoq gneiss revisited: implications for the timing of early Archaean crustal evolution in West Greenland: Chemical Geology, v. 150, p. 19–41.
——— 2000, Initial Pb of the Amitsoq gneiss revisited: implications for the timing of early Archaean crustal evolution in West Greenland – Reply: Chemical Geology, v. 166, p. 309–312.
Kamber, B. S., Ewart, A., Collerson, K. D., Bruce, M. C., and McDonald, G. D., 2002, Fluid-mobile trace element constraints on the role of slab melting and implications for Archaean crustal growth models: Contributions to Mineralogy and Petrology, v. 144, p. 38–56.
Kamber, B. S., Collerson, K. D., Moorbath, S., and Whitehouse, M. J., 2003, Inheritance of early Archaean Pb-isotope variability from long-lived Hadean protocrust: Contributions to Mineralogy and Petrology, v. 145, p. 25–46.

Kato, Y., Ohta, I., Tsunematsu, T., Watanabe, Y., Isozaki, Y., Maruyama, S., and Imai, N., 1998, Rare earth element variations in mid-Archean banded iron formations: implications for the chemistry of ocean and continent and plate tectonics: Geochimica et Cosmochimica Acta, v. 62, p. 3475–3497.

Kerrich, R., 1987, Stable isotope studies of fluids in the crust, *in* Kyser, T. K., editor, Stable Isotope Geochemistry of Low Temperature Fluids: Mineralogical Association of Canada Short Course Notes, v. 13, p. 258–278.

Kinny, P. D., 1986, 3820 Ma zircons from a tonalitic Amîtsoq gneiss in the Godthab district of southern West Greenland: Earth and Planetary Science Letters, v. 79, p. 337–347.

Klein, C., and Beukes, N. J., 1989, Geochemistry and sedimentology of a facies transition from limestone to iron-formation deposition in the Early Proterozoic Transvaal Supergroup, South Africa: Economic Geology, v. 84, p. 1733–1774.

Knauth, L. P., 1992, Origin and diagenesis of cherts: an isotopic perspective, *in* Clauer, N., and Chaudhuri, S., editors, Isotopic Signatures and Sedimentary Records: Berlin, Springer-Verlag, Lecture Notes in Earth Sciences, v. 43, p. 123–152.

Kolodny, Y., and Epstein, S., 1976, Stable isotope geochemistry of deep sea cherts: Geochimica et Cosmochimica Acta, v. 40, p. 1195–1209.

Krogh, T. E., Kamo, S. L. and Kwok, Y. Y., 2002, An isotope dilution, etch abrasion solution to the Akilia Island U-Pb age controversy: Geochimica et Cosmochimica Acta, v. 64 (S1), p. A419.

Lepland, A., Arrhenius, G., and Cornell, D., 2002, Apatite in early Archean Isua supracrustal rocks, southern West Greenland: its origin, association with graphite and potential as a biomarker: Precambrian Research, v. 118, p. 221–241.

Lepland, A., van Zuilen, M. A., Arrhenius, G., Whitehouse, M. J., and Fedo, C. M., 2005, Questioning the evidence for Earth's earliest life—Akilia revisited: Geology, v. 33, p. 77–79.

Ludden, J., and Gelinas, L., 1982, Trace element characteristics of komatiites and komatiitic basalts from the Abitibi metavolcanic belt of Quebec, *in* Arndt, N. T., and Nisbet, E. G., editors, Komatiites: London, Allen and Unwin, p. 331–346.

Ludden, J., Gelinas, L., and Trudel, P., 1982, Archean metavocanics from the Rouyn-Noranda district, Abitibi greenstone belt, Quebec: 2. Mobility of trace elements and petrogenetic constraints: Canadian Journal of Earth Science, v. 19, p. 2276–2287.

Ludwig, K. R., 2000, ISOPLOT/EX, version 2.2: A Geochronological Toolkit for Microsoft Excel: Berkeley Geochronology Center Special Publication No. 1a, 56 p.

Mahood, G., and Hildreth, W., 1983, Large partition-coeffcients for trace-elements in high-silica rhyolites: Geochimica et Cosmochimica Acta, v. 47, p. 11–30.

Manning, C. E., 1994a, The solubility of quartz in $H_2O$ in the lower crust and upper mantle: Geochimica et Cosmochimica Acta, v. 58, p. 4831–4839.

——— 1994b, Fractal clustering of metamorphic veins: Geology, v. 22, p. 335–338.

Martin, H., 1986, Effect of steeper Archean geothermal gradient on geochemistry of subduction-zone magmas: Geology, v. 14, p. 753–756.

Matsuhisa, U., Goldsmith, J. R., and Clayton, R. N., 1979. Oxygen isotopic fractionation in the system quartz-albite-anorthite-water: Geochimica et Cosmochimica Acta, v. 43, p. 1131–1140.

McGregor, V. R., 1968, Field evidence of very old Precambrian rocks in the Godthåb area West Greenland: Grønlands Geologiske Undersøgelse Rapport, v. 15, p. 31–35.

——— 1973, The early Precambrian gneisses of the Godthåb district, West Greenland: Philosophical Transactions of the Royal Society of London, v. A273, p. 343–358.

——— 1979, Archean gray gneisses and the origin of the continental crust: evidence from the Godthåb region, West Greenland, *in* Barker, F., editor, Trondhjemites, Dacites, and Related Rocks: Amsterdam, Elsevier, p. 169–204.

——— 2000, Initial Pb of the Amitsoq gneiss revisited: implications for the timing of early Archaean crustal evolution in West Greenland—Comment: Chemical Geology, v. 166, p. 301–308.

McGregor, V. R., and Mason, B., 1977, Petrogenesis and geochemistry of metabasaltic and metasedimentary enclaves in the Amîtsoq gneisses, West Greenland: American Mineralogist, v. 62, p. 887–904.

McGregor, V. R., Friend, C. R. L., and Nutman, A. P., 1991, The late Archean mobile belt through Godthåbsfjord, southern West Greenland: a continent-continent collision zone?: Bulletin of the Geological Society of Denmark, v. 39, p. 179–197.

McLennan, S. M., Taylor, S. R., and McGregor, V. R., 1984, Geochemistry of Archean sedimentary rocks from West Greenland: Geochimica et Cosmochimica Acta, v. 48, p. 1–13.

Melcher, F., Grum, W., Thalhammer, T. V., and Thalhammer, O. A. R., 1999, The giant chromite deposits at Kempirsai, Urals: constraints from trace element (PGE, REE) and isotope data: Mineralium Deposita, v. 34, p. 250–272.

Mojzsis, S. J., and Harrison, T. M., 2000, Vestiges of a beginning: Clues to the emergent biosphere recorded in the oldest known sedimentary rocks: GSA Today, v. 10, p. 1–6.

——— 2002a, Establishment of a 3.83-Ga magmatic age for the Akilia tonalite (southern West Greenland): Earth and Planetary Science Letters, v. 202, p. 563–576.

——— 2002b, Origin and significance of Archean quartzose rocks at Akilia, Greenland: Science, v. 298, p. 5595.

Mojzsis S. J., Arrhenius, G., McKeegan, K. D., Harrison, T. M., Nutman, A. P., and Friend, C. R. L., 1996, Evidence for life on Earth before 3,800 million years ago: Nature, v. 384, p. 55–59.

Mojzsis, S. J., Coath, C. D., Greenwood, J. P., McKeegan, K. D., and Harrison, T. M., 2003a, Mass-independent isotope effects in Archean (2.5 to 3.8 Ga) sedimentary sulfides determined by ion microprobe analysis: Geochimica et Cosmochimica Acta, v. 67, p. 1635–1658.

Mojzsis, S. J., Devaraju, T. C., and Newton, R. C., 2003b, Ion microprobe U-Pb age determinations on zircon from the Late Archean granulite facies transition zone of southern Karnataka, India: Journal of Geology, v. 111, p. 407–425.
Mojzsis, S. J., Papineau, D., Adam, J. D., and Harrison, T. M., 2005, Life on Earth before 3.83 Ga? Carbonaceous inclusions from Akilia (West Greenland): Eos, 86(52), Fall Meeting Supplement, Abstract V41F-1537.
Moorbath, S., and Pankhurst, R. J., 1976, Further rubidium-strontium age and isotope evidence for the nature of the Late Archaean plutonic event in West Greenland: Nature, v. 262, p. 124–126.
Moorbath, S., Whitehouse, M. J., and Kamber, B. S., 1997, Extreme Nd-isotope heterogeneity in the early Archaean—fact or fiction? Case histories from northern Canada and West Greenland: Chemical Geology, v. 135, p. 213–231.
Myers, J. S., and Crowley, J. L., 2000, Vestiges of life in the oldest Greenland rocks? A review of early Archean geology in the Godthåbsfjord region, and reappraisal of field evidence for >3850 Ma life on Akilia: Precambrian Research, v. 103, p. 101–124.
Mysen, B. O., 1979, Trace-element partitioning between garnet peridotite minerals and water-rich vapor: experimental data from 5 to 30 kbar: American Mineralogist, v. 64, p. 274–287.
Nabelek, P. I., 1991, Stable isotope monitors: Reviews in Mineralogy, v. 26, p. 395–436.
Newton, R. C., and Manning, C. E., 2000a, Metasomatic phase relations in the system CaO-MgO-$SiO_2$-$H_2O$-NaCl at high temperatures and pressures: International Geology Review, v. 42, p. 152–162.
——— 2000b, Quartz solubility in concentrated aqueous NaCl solutions at deep crust-upper mantle metamorphic conditions: 2-15 kbar and 500-900 °C: Geochimica et Cosmochimica Acta, v. 64, p. 2993–3005.
——— 2002, Solubility of silica in equilibrium with enstatite, forsterite, and $H_2O$ at deep crust/upper mantle pressures and temperatures and an activity-concentration model for polymerization of aqueous silica: Geochimica et Cosmochimica Acta, v. 66, p. 4165–4176.
Nozhkin, A. D., and Turkina, O. M., 1995, Radiogeochemistry of the charnockite-granulite complex, Sharyzhalgay Window, Siberian Platform: Geochemistry International, v. 32(2), p. 62–78.
Nutman, A. P., and Bridgwater, D., 1986, Early Archaean Amitsoq tonalites and granites of the Isukasia area, southern West Greenland: development of the oldest-known sial: Contributions to Mineralogy and Petrology, v. 94, p. 137–148.
Nutman, A. P., McGregor, V. R., Friend, C. R. L., Bennett, V. C., and Kinny, P. D., 1996, The Itsaq Gneiss Complex of southern west Greenland; The world's most extensive record of early crustal evolution (3900–3600 Ma): Precambrian Research, v. 78, p. 1–39.
Nutman A. P., Mojzsis, S. J., and Friend, C. R. L., 1997, Recognition of ≥3850 Ma water-lain sediments in West Greenland and their significance for the early Archaean Earth: Geochimica et Cosmochimica Acta, v. 61, p. 2475–2484.
Nutman, A. P., Bennett, V. C., Friend, C. R. L., and Norman, M. D., 1999, Meta-igneous (non-gneissic) tonalites and quartz-diorites from an extensive ca. 3800 Ma terrain south of the Isua supracrustal belt, southern West Greenland: constraints on early crust formation: Contributions to Mineralogy and Petrology, v. 137, p. 364–388.
Nutman, A. P., Bennett, V. C., Friend, C. R. L., and McGregor, V. R., 2000, The early Archaean Itsaq Gneiss Complex of southern West Greenland: the importance of field observations in interpreting age and isotopic constraints for early terrestrial evolution: Geochimica et Cosmochimica Acta, v. 64, p. 3035–3060.
Nutman, A. P., McGregor, V. R., Shiraishi, K., Friend, C. R. L., Bennett, V. C., and Kinny, P. D., 2002, ≥3850 Ma BIF and mafic inclusions in the early Archaean Itsaq Gneiss Complex around Akilia, southern West Greenland? The difficulties of precise dating of zircon-free protoliths in migmatites: Precambrian Research, v. 117, p. 185–224.
Nutman, A. P., Friend, C. R. L., Barker, S. L. L., and McGregor, V. R., 2004a, Inventory and assessment of Palaeoarchaean gneiss terrains and detrital zircons in southern West Greenland: Precambrian Research, v. 135, p. 281–314.
Nutman, A. P., Friend, C. R. L., Bennett, V. C., and McGregor, V. R., 2004b, Dating of the Ameralik dyke swarms of the Nuuk district, southern west Greenland: mafic intrusion events starting from c. 3510 Ma: London, Journal of the Geological Society, v. 161, p. 421–430.
O'Nions, R. K., and Pankhurst, R. J., 1974, Rare-earth element distribution in Archaean gneisses and anorthosites, Godthåb area, West Greenland: Earth and Planetary Science Letters, v. 22, p. 328–338.
Paces, J. B., and Miller, J. D., 1993, Precise U-Pb ages of Duluth Complex and related mafic intrusions, northeastern Minnesota—geochronological insights to physical, petrogenetic, paleomagnetic and tectonomagmatic processes associated with the 1.1 Ga midcontinent rift system: Journal of Geophysical Research, v. 98, p. 13997–14013.
Palin, J. M., 2002, The origin of a most contentious rock: Science, v. 298, p. 961.
Pearce, J. A., 1975, Basalt geochemistry used to investigate past tectonic environments on Cyprus: Tectonophysics, v. 25, p. 41–67.
Perry, E. C., Jr., Ahmad, S. N., and Swulius, T. M., 1978, The oxygen isotope composition of 3,800 m.y. old metamorphosed chert and iron formation from Isukasia, west Greenland: Journal of Geology, v. 86, p. 223–239.
Polat, A., Hofmann, A. W., Münker, C., Regelous, M., and Appel, P. W. U., 2003, Contrasting geochemical patterns in the 3.7-3.8 Ga pillow basalt cores and rims, Isua greenstone belt, Southwest Greenland: Implications for postmagmatic alteration processes: Geochimica et Cosmochimica Acta, v. 67, p. 441–457.
Pride, C., and Muecke, G. K., 1981, Rare earth element distributions among coexisting granulite facies minerals, Scourian Complex, NW Scotland: Contributions to Mineralogy and Petrology, v. 76, p. 463–471.

Quidelleur X., Grove M., Lovera, O. M., Harrison, T. M., Yin, A., and Ryerson, F. J., 1997, Thermal evolution and slip history of the Renbu Zedong Thrust, southeastern Tibet: Journal of Geophysical Research, v. 102, p. 2659–2679.

Reitan, P. H., Roelandts, I., and Brunfeldt, A. O., 1980, Optimum ionic size for substitution in the M(2)-site in metamorphic diopside: Neues Jahrbuch für Mineralogie, Monatschefte, v. 1980, p. 181–191.

Rollinson, H. R., and Windley, B. F., 1980, Selective elemental depletion during metamorphism of Archean granulites, Scourie, NW Scotland: Contributions to Mineralogy and Petrology, v. 72, p. 257–263.

Rose, N. M., Rosing, M. T., and Bridgwater, D., 1996, The origin of metacarbonate rocks in the Archaean Isua supracrustal belt, west Greenland: American Journal of Science, v. 296, p. 1004–1044.

Rosing, M. T., 1999, $^{13}$C-depleted carbon microparticles in >3700-Ma sea-floor sedimentary rocks from West Greenland: Science, v. 283, p. 674–676.

Rosing, M. T., Rose, N. M., Bridgwater, D., and Thomsen, H. S., 1996, Earliest part of Earth's stratigraphic record: A reappraisal of the >3.7 Ga Isua (Greenland) supracrustal sequence: Geology, v. 24, p. 43–46.

Schidlowski, M., 1988, A 3,800-million-year isotopic record of life from carbon in sedimentary rocks: Nature, v. 333, p. 313–318.

Schiøtte, L., and Compston, W., 1990, U-Pb age pattern for single zircons from the early Archean Akilia Association south of Ameralik Fjord, southern West Greenland: Chemical Geology, v. 80, p. 147–157.

Schiøtte, L., Compston, W., and Bridgwater, D., 1988, Late Archaean ages for the deposition of clastic sediments belonging to the Malene supracrustals, southern West Greenland: evidence from an ion probe U-Pb zircon study: Earth and Planetary Science Letters, v. 87, p. 45–58.

Schuhmacher, M., de Chambost, E., McKeegan, K. D., Harrison, T. M., and Migeon, H, 1994, In situ dating of zircon with the CAMECA ims 1270, *in* Benninghoven, A., and others, editors, Secondary Ion Mass Spectrometry SIMS IX: Chichester, United Kingdom, Wiley, p. 919–922.

Schmitt, A. K., Grove, M., Harrison, T. M., Lovera, O. M., Hulen, J., and Waters, M., 2003, The Cobb Mountain-Geyser's magma system, California (Part 1): U-Pb zircon ages, conditions of crystallization, and magma residence times: Geochimica et Cosmochimica Acta, v. 67, p. 3423–3442.

Snoke, A. W., and Calk, L. C., 1978, Jackstraw-textured talc-olivine rocks, Preston Peak area, Klamath Mountains, California: Geological Society of America Bulletin, v. 89, p. 223–230.

Sun, S. S., and Nestbitt, R. W., 1979, Petrogenesis of Archean ultrabasic rocks and basic volcanics: evidence from rare earth elements: Contributions to Mineralogy and Petrology, v. 65, p. 301–325.

Taylor, H. P., 1977, Water-rock interactions and the origin of $H_2O$ in granitic batholiths: London, Journal of the Geological Society, v. 133, p. 509–588.

Taylor, S. R., Rudnick, R. L., McLennan, S. M., and Eriksson, K. A., 1986, Rare earth element patterns in Archean high-grade metasediments and their tectonic significance: Geochimica et Cosmochimica Acta, v. 50, p. 2267–2279

Ueno, Y., Yurimoto, H., Yoshioka, H., Komiya, T., and Maruyama, S., 2002, Ion microprobe analysis of graphite from ca. 3.8 Ga metasediments, Isua supracrustal belt, West Greenland: Relationship between metamorphism and carbon isotopic composition: Geochimica et Cosmochimica Acta, v. 66, p. 1257–1268.

Valley, J. W., 1986, Stable isotope geochemistry of metamorphic rocks: Reviews in Mineralogy, v. 16, p. 445–489.

van Zuilen, M., Lepland, A., and Arrhenius, G., 2002, Reassessing the evidence for the earliest traces of life: Nature, v. 418, p. 627–630.

Watson, E. B., and Harrison, T. M., 1983, Zircon saturation revisited: temperature and composition effects in a variety of crustal magma types: Earth and Planetary Science Letters, v. 64, p. 295–304.

Wenner, D. B., and Taylor, H. P., Jr., 1971, Temperatures of serpentinization of ultramafic rocks based on $^{18}O/^{16}O$ fractionations between coexisting minerals and magnetite: Contributions to Mineralogy and Petrology, v. 32, p. 165–185.

White, R. V., Crowley, J. L., and Myers, J. S., 2000, Earth's oldest well-preserved mafic dyke swarms in the vicinity of the Isua greenstone belt, southern West Greenland: Geology of Greenland Survey Bulletin, v. 186, p. 65–72.

Whitehouse, M. J., and Fedo, C. M., 2003, Deformation features and critical field relationships of early Archaean rocks, Akilia, West Greenland: Precambrian Research, v. 126, p. 259–271.

Whitehouse, M. J., and Kamber, B. S., 2002, On the overabundance of light rare earth elements in terrestrial zircons and its implication for Earth's earliest magmatic differentiation: Earth and Planetary Science Letters, v. 204, p. 333–346.

——— 2003, A rare earth element study of complex zircons from early Archean Amîtsoq gneisses, Godthåbsfjord, south-west Greenland: Precambrian Research, v. 126, p. 363–377.

——— 2005, Assigning dates to thin gneissic veins in high-grade metamorphic terranes: a cautionary tale from Akilia, southwest Greenland: Journal of Petrology, v. 46, p. 291–318.

Whitehouse, M. J., Kamber, B. S., and Moorbath, S., 1999, Age significance of U-Th-Pb zircon data from early Archaean rocks of West Greenland—a reassessment based on combined ion-microprobe and imaging studies: Chemical Geology, v. 160, p. 201–224.

——— 2001, Age significance of U-Th-Pb zircon data from early Archaean rocks of west Greenland—a reassessment based on combined ion-microprobe and imaging studies—reply: Chemical Geology, v. 175, p. 201–208.

Whitehouse, M. J., Kamber, B. S., Fedo, C. M., and Lepland, A., 2005, Integrated Pb- and S-isotope investigation of sulphide minerals from the early Archean of southwest Greenland: Chemical Geology, v. 222, p. 112–131.

Wyllie, P. J., Wolf, S. R., and van der Lann, S. R., 1997, Conditions for the formation of tonalites and trondjemites: magma sources and products, *in* de Wit, M. J., and Ashwal, L. D., editors, Greenstone Belts: Oxford, Oxford University Press, p. 256–265.